

9th INTERNATIONAL
100% RENEWABLE
ENERGY CONFERENCE



IRENEC 2019

PROCEEDINGS

24 - 26 APR 2019

RENEWABLE ENERGY
ASSOCIATION



Editors

Tanay Sıdkı Uyar

Alper Saydam

Publishing Date September 2019

ISBN 978-605-62511-5-3

Copyright © 2019 Renewable Energy Association of Turkey (EUROSOLAR Turkey)

All rights reserved. No part of this book may be reproduced in any form or by any electronic or mechanical means, including information storage and retrieval systems, without permission in writing from the publisher.

No responsibility is assumed by the publisher for any injury and/or damage to persons or property as a matter of products liability, negligence or otherwise or from any use or operation of methods, products, instructions or ideas contained in the material here in.

Dear Participants,

In our journey of promoting 100% Renewable Energy, we have arrived the 8th stop where we shall again share our research results and other achievements.

Every day we are discovering and practicing the good quality of renewable energies. The genie is out of the bottle. It is time to use the good quality of human beings to guide this opportunity effectively to the destination. The qualities of human beings can play its role if the individuals and countries talk together and define problems correctly and find solutions that can be implemented.

Renewable energy resources at each corner of the atmosphere are ready to be converted to electricity and process heat locally when needed. Kinetic energy of the moving air, chemical energy stored in biomass, heat and light of the sun and geothermal resources are available all over our planet earth free of charge. As the main energy source of living space on earth, sun and its derivatives were available before, are available today and will be available in the future.

Global support provided for the renewable energy made the market penetration of renewables possible. Today wind and solar energy became the cheapest way of producing electricity in many parts of the World.

Cities and countries who are trying to reach 100% renewable energy mix are working on preparing the infrastructure necessary to be able to supply more renewable energy for industry, transportation and buildings by smart grids and renewable energy storage systems.

Since renewable energy is available at every corner of our atmosphere, Community Power (the involvement of the local people individually or through their cooperatives and municipalities in the decision making process and ownership of their energy production facilities) is becoming the most effective approach for transition to 100% renewable energy future.

During IRENEC2019 we shall share and learn from the global experiences on difficulties, barriers, opportunities and solutions for transition to 100 % renewable energy societies and make our contribution to Global Transition to 100% Renewable Energy.

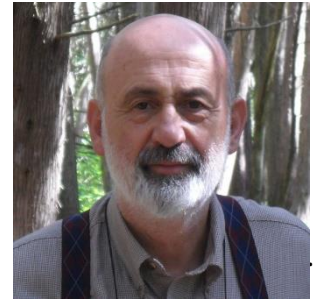
Best Regards,

Tanay Sıdkı Uyar

Conference Chair, IRENEC2019

President, Renewable Energy Association of Turkey

(EUROSOLAR Turkey)



Conference Chair,
IRENEC2019



Organization

Organizing Committee

Conference Chair

Tanay Sıdkı Uyar

Marmara University, TR

Conference Co-Chairs

İbrahim Dinçer

University of Ontario Institute of Technology, CA

Remigijus Lapinskis

President of World Bioenergy Association, LT

Wolfgang Palz

EU Commission Official (ret.)

Local Organizing Committee (Administrative)

Erhan Çakar

Başak Gündüz

Ahmet Özer Kaliber

Turgut Okkaya

Serdar Tan

Işıl Uyar

Local Organizing Committee (Academic)

Alper Saydam

Doğancan Beşikci

Uğur Baş

Ahmet Erkoç

Ozan Özmen Eren Şat

Anıl Türkünoğlu

Tanay Sıdkı Uyar

Program Committee (Research Papers)

Saka, Kenan	Bursa Uludag University, TR
Kahraman, Huseyin	Sakarya University, TR
Uslu, Salih Güvenç	Marmara University, TR
Basyooni, Mohammed Ali	University of Konya, TR
Meşe, Emine	University of Durham, UK
Beşikci, Doğançan	Marmara University, TR
Sarı, Alperen	National Defense University, TR
Zorlu, Salih Korhan	National Defense University, TR
Köker, Utku	Suleyman Demirel University, TR
Ersoy, Gizem	Marmara University, TR
Leblebicioğlu, Emre	Marmara University, TR
Şerifoğlu Akyürek, B. Özge	University of California, USA
Doğan, Reyhane	Erciyes University, TR
Konde, Arcell Lelo	Cyprus International University, CY

Scientific Advisory Committee

Houri, Ahmad F.	Lebanese American University, LB
Ragnarsson, Árni	Iceland GeoSurvey, IS
Dinçer, İbrahim	University of Ontario, CA
Yıldız, İlhami	Dalhousie University, CA
Sulukan, Egemen	National Defense University, TR
Sağlam, Mustafa	Marmara University, TR
Osman Benchikh	Ex-Head of Energy Programme, UNESCO

Contents

Full Research Papers

An Investigation on Hydrogen Production Capacity of a PV Power Plant in Bursa, Turkey.....	3
<i>Kenan Saka</i>	
Analysis and Modeling of Gaskets, End Plates and Current Collectors in a Proton Exchange Membrane Fuel Cell	16
<i>Kenan Saka, Mehmet F. Orhan and Huseyin Kahraman</i>	
The Conversion of a Residential Building into a Net Zero Energy Building	32
<i>Salih GüvençUslu and Tanay Sıdkı Uyar</i>	
The synthesis of TiO ₂ /TiO _x NY Mushrooms-Like Nanocomposites Based on Nanoporous Anodic Aluminum Oxide Template for Hydrogen Generation.....	45
<i>Mohamed Rabia, Mohamed A. Basyooni, Sodky H. AboLaila, Huaping Zhou, Mohamed Shaban, Yong Lei, Ashour M. Ahmed</i>	
Theoretical Model to Relate Morphology to Device Efficiency	55
<i>Emine Meşe and Nigel Clarke</i>	
Potential Analysis of Manure Based Biogas to Electricity Generation: Case Study of Burdur	64
<i>Doğancan Beşikci, Egemen Sulukan and Tanay Sıdkı Uyar</i>	
Transition to a Low Carbon Future in Maritime Fleet for Climate Change.....	72
<i>Alperen Sarı, Egemen Sulukan, Doğuş Özkan, Tanay Sıdkı Uyar</i>	
A Residential Energy Simulation Tool Design	83
<i>Salih Korhan Zorlu, Egemen Sulukan, Doğuş Özkan, Tanay Sıdkı Uyar</i>	
Calculating the Levelized Cost of Electricity by an Urban Scaled Simulation Approach	92
<i>Utku Köker, Halil İbrahim Kuruca, Egemen Sulukan, Tanay Sıdkı Uyar</i>	
Designing Onshore Wind Farm for Marmara University Following the Global Experience.....	104
<i>Gizem Ersoy, Tanay Sıdkı Uyar</i>	

User-Focused Designing and Pricing of An Off-Grid Photovoltaic Solar Energy System	120
<i>Emre Leblebicioğlu</i>	
Investigation of Engine Performance and Emission Parameters of Ethanol-Acetylene Mixture in an SI Engine at Partial Load	132
<i>Reyhane Doğan, Mehmet İlhan İlhak, Selahaddin Orhan Akansu, Sebahattin Ünalın</i>	
Decentralization of The Power Sector in The City-Province of Kinshasa For Achieving the Vision 100% Renewable Electricity By 2050	140
<i>Arcell Lelo Konde and. Tanay Sidki Uyar</i>	
A Comprehensive Sustainability Investigation of Solar Hydrogen Production Options	153
<i>Canan Acar</i>	

An Investigation on Hydrogen Production Capacity of a PV Power Plant in Bursa, Turkey

Kenan SAKA^[0000-0002-2296-894X]

¹Bursa Uludağ University Vocational School of Yenisehir Ibrahim Orhan, PO Box: 16900,
Bursa, Turkey
kenansaka@uludag.edu.tr

Abstract. Hydrogen utilization as an energy carrier is expected to increase in the future. However, it does not exist in nature in its elemental form so it must be produced from water using various energy sources. Renewable energy sources such as solar are the best option for clean and sustainable hydrogen production. Soğuksu photovoltaic solar power plant is the first large scale power plant with 7 MW peak capacity and located in Bursa, Turkey. In this study, hydrogen production capacity of the power plant is evaluated. Daily, monthly and annual electricity generation values of Soğuksu photovoltaic solar power plant were recorded under actual operating conditions in the data library of the power plant. These values have been used here to investigate hydrogen production from Proton Exchange Membrane (PEM) electrolyzer. Results show that the maximum mass flow of hydrogen production is $0.0625 \text{ kgs}^{-1}\text{H}_2$ at peak load. Also, total annual electricity generation of the power plant is 10.7 GWh that result in an annual hydrogen production of 344 tons.

Keywords: Hydrogen Production, PEM Electrolyzer, Solar Energy, PV Power Plant

1 Introduction

Energy in all its forms plays critical roles in human life. It has a direct impact on every sector of the economy and social life. Renewable energy sources have been utilized by mankind since ancient time. Recently, the energy demand has increased due to high population and risen life standard. Also, environmental concerns, due to pollution of fossil fuel based sources, have resulted in an ongoing effort to increase the capacity of sustainable and clean renewable sources to answer the global increasing energy demand.

For instance, according to Kaygusuz [1] Turkey's economy continues to rapidly expand, which results in a growing energy demand. Turkey has to install approximately between 35 and 60GW of additional power generation capacity to meet its electricity demand by 2020. It is also emphasized that, beside hydropower generation, most of the Turkish electricity is based on thermal power plants, and natural gas is by far the most important fuel for power generation.

On the other hand, in the coming years, it is expected that Turkey will continue to depend mainly on coal and natural gas as fossil based energy source in the power sector. It is also predicted that natural gas, wind and nuclear power capacities should increase in the near future [1]. Renewable energy sources are divided into two main groups as intermittent and non-intermittent sources. Common intermittent renewable sources are wind and solar, while non-intermittents are hydro, biomass and geothermal. As an intermittent renewable energy, solar utilization is classified into heating, process heat and electricity. To improve its energy security, Turkey is increasing its renewable energy production capacity. In this regard, potential of renewable energy in electricity production for sustainable development of Turkey has been investigated by Benli [2], including its energy policies. Many studies are presented in the literature on photovoltaic solar technologies and their suitability for electricity generation in many countries such as Jordan, Morocco, Serbia, Iran and India [3-7]. Also, Sharaf and Orhan [8] have studied thermodynamic analysis and optimization of densely-packed receiver assembly components in high-concentration concentrated photovoltaic thermal solar collectors. Their results have showed the existence of optimum geometrical design vectors ensuring that the system-level performance of a concentrated photovoltaic thermal solar collector employing the optimized components is maximized. Incekara and Ogulata [9] have presented a mathematical energy model for Turkey's energy planning considering global environmental concerns. They have reported that the usage of energy sources are as follows by the year 2023. In high-demand scenario; solar power plants rank first (25.9%), wind power plants are second (24.0%) and natural gas power plants rank third (23.1%). Especially in 2030, solar power plants rank first (20.7%), wind power plants are second (19.1%), natural gas power plants rank third (18.6%) and hydroelectric power plants rank fourth (14.7%). PV power generation is becoming the main process for utilizing solar energy as its efficiency increases while its cost drops [9].

Hydrogen as an energy carrier can be utilized in a clean manner including its conversion to electricity with no CO₂ emission. It can also be stored and transported over long distances with lower loss compared to electricity. Hydrogen can be produced efficiently with very low emissions from various renewable energy sources such as wind, solar, biogases, industrial waste streams and geothermal energy. Kanoglu et al. [10] have developed four models for the use of geothermal energy for hydrogen production. It is reported that the use of renewable energy resources such as geothermal will likely continue to increase and diversify, especially for suitable applications [10]. Orhan et al. [11] have presented an integrated system to couple nuclear and renewable energy sources for hydrogen production. Several possible applications involving nuclear independent and nuclear assisted renewable hydrogen production have been proposed. Some of the considered options include storage of hydrogen and its conversion to electricity by fuel cells when needed [11]. Yuksel and Ozturk [12] have conducted a study on energy and exergy analyses of a geothermal based multi-generation of electricity, hydrogen, domestic hot water, heating and cooling. The system employs a Proton Exchange Membrane (PEM) electrolyzer for hydrogen production. It was observed that when electrical power generation of the system is increased from 4 MW to 8.5 MW, the hydrogen production rises from about 0.030 kgs⁻¹ to 0.075 kgs⁻¹ [12]. Cilogullari et al. [13] have investigated hydrogen production performance of a Proton Exchange

Membrane electrolyzer powered by a Photovoltaic and Thermal System (PV/T) with a surface area of 1.28m². They have observed that 0.018 kg hydrogen can be produced by using a single PV/T panel on a summer day. Koponen et al. [14] have used a 5 kWp fixed installation solar power plant as a power reference for a commercial PEM water electrolyzer. They have reported that in a PEM water electrolysis system without separate post-electrolysis compression, the real hydrogen production will be maximized by controlling the stack hydrogen outlet pressure as close to the storage pressure as possible. Ebaid et al. [15] have designed a PV-hydrogen gas turbine hybrid power plant to generate 100 MW electrical loads. It is reported that the price of the electricity produced is 0.12 \$/kWh for average case scenario and 0.16 \$/kWh for the worst case scenario [15]. Boudries et al. [16] have carried out a study to show that a two-axis tracking system could slash the cost hydrogen production by almost a half. Hydrogen production options have investigated using solar energy available in Biskra region in the east of Algeria by the Proton Exchange Membrane electrolyzer [17]. It was concluded that Biskra is one of the most appropriate region for hydrogen production, not only in Algeria but also in North Africa.

In this study, our objectives are to investigate the daily, monthly and annual hydrogen production capacity of a proton exchange membrane electrolyzer using actual electricity generation values of the Soğuksu solar power plant in Bursa, Turkey. To carry out a parametric study to optimize the operating conditions, and maximize the efficiency and hydrogen production capacity with allocate energy losses and evaluate their impact on the overall performance.

1.1 System description

A schematic diagram of the system under investigation in this study is given in Fig. 1. The overall system consists of three main subsections. Each of these subsections will be explained here in detail. The first and the most important subsection is the Soğuksu solar power plant, where necessary electricity is generated to produce hydrogen. The power station is also grid connected and therefore the electricity is generated in AC phase. However, the PEM electrolyzer operates with electricity in DC phase, which adds an extra AC-DC converter to the system.

Soğuksu solar power plant consists of seven units of 1 MWe capacity. Each unit has 20 inverters that connect 10 lines. Each line consists of 22 photovoltaic panels connected in series. The properties of the solar panels from manufacturer are given in Table 1. The panels are made of polycrystalline silicone and each panel house 60 cells. Also, each panel can produce 270 W powers with 16.6% efficiency, which is not the most efficient type in the market but selected due to its easy and ready availability. The characteristics of the power plant and its coordinates from satellite images are shown in Table 2. The power plant was installed on 170,000 m² area with 30,800 panels.

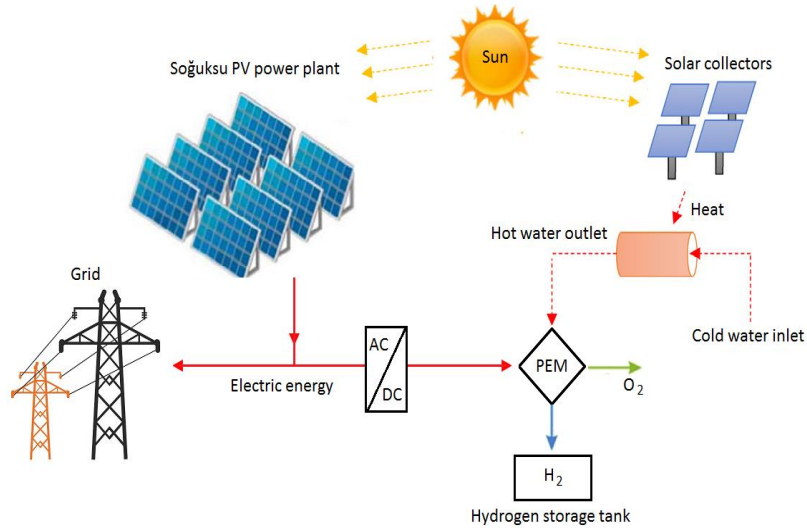


Fig. 1. PV power plant aided hydrogen production system

In Fig. 2, the map shows the location of the power plant in Bursa, Turkey and its satellite image. The location of the power plant has the advantage of natural ventilation as it is situated on a high hill.

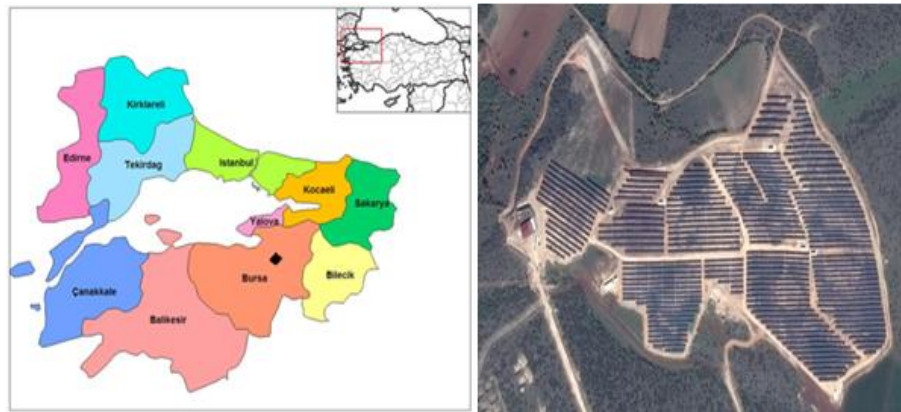


Fig. 2. Satellite view and location of Soğuksu solar power plant on the map

Theoretically, the amount of electricity generated by a solar power plant is estimated as a function of the panel surface area, the number of production days, efficiencies of the panels and inverters, and global solar radiation values. Also, electricity generation is directly related to the energy carried by the sunrays coming onto the surface of panels under overcast weather conditions.

The global solar radiation value is helpful to approximate the generation capacity and can give an idea about a region for potential of solar energy but not an exactly generation value. Fig. 3 shows the global solar radiation values of Yenişehir, Bursa and Turkey.

Table 1. Properties of PV solar panels used in Soğuksu solar power plant

Model of the Panel	UP-M270P
Type	Polycrystalline Silicone
Power Rating	270 Watt
Peak Efficiency	16.6%
Number of Cells	60
Dimension of the Cells	156 mm X 156 mm
Length	1640 mm
Width	992 mm

Table 2. General characteristics of Soğuksu solar power plant

Area where the power plant is installed	170,000 m ²
Number of panels used	30,800
Total panel surface area	50,108 m ²
Total cell surface area	44,972.9 m ²
Plant Power	7 MWp
Inverter Efficiency	95% - 97%
Generation Commencement Date	20 th March 2017
Plant Coordinates	40° 12' 57'' N 29° 25' 50'' E

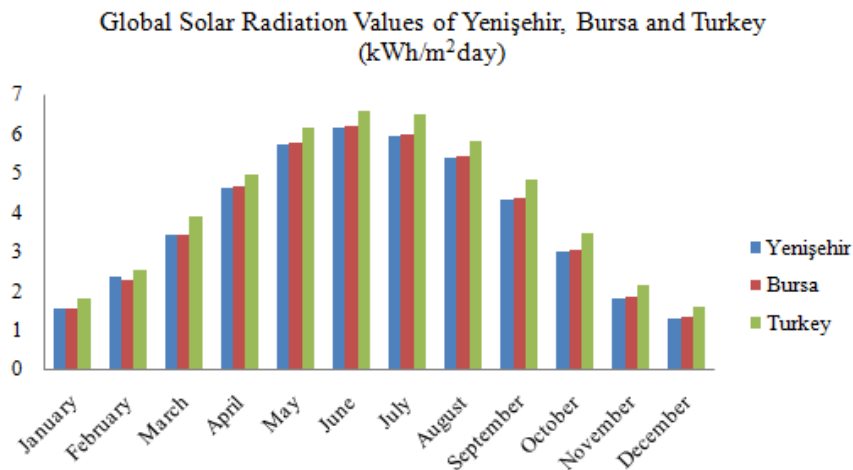


Fig. 3. Global solar radiation values of Yenişehir, Bursa and Turkey

The second subsection of the system is the PEM electrolyzer where the water is split and hydrogen is produced. The produced hydrogen is then sent to a storage tank. The electrolyzer is built around a proton conductive polymer electrolyte to split up water. Different PEM electrolyzer models can be designed depending on operating conditions. In this study, the model in [18] is used at 80 °C operation temperature. Higher temperatures of electrolysis increases hydrogen production rate and decreases electricity consumption. With the model used in this study at 80 °C operating temperature, hydrogen can be produced at a rate of 0.0340 kg/s by using 3810 kW electricity power. This result agrees with 0,054 kg/s of hydrogen production rate by using 6 MW of electrical power in [12].

In the electrolyzer section, liquid water is fed to the preheater at the environment temperature and is heated by the solar collectors. Then, electricity and preheated water are supplied to the PEM electrolyzer to drive the electrochemical reactions. Generated H₂ (hydrogen) from the cathode dissipates heat and cool down to the reference environment temperature.

The last subsection consists of solar collectors and water heater system. This section has importance because the water to be electrolyzed is preheated to 80 °C before entering to PEM electrolyzer. As previously mentioned, water can be fed to the electrolyzer at any temperature. However, a preheating process is necessary to increase the efficiency of electrolysis process. There is no available hot water or waste heat at the plant, therefore the water can be preheated by three ways. One way is to use electrical heaters. This method is simple and easy but electrical heaters will add parasitic load and use about %2 of the generated electricity. The other method is to heat the water by using it as the coolant for solar panels. Efficiency of the panels and the electricity production will increase as a result of this method. However, it will add more complexity to the system and might not sufficiently heat the water. The last method is to use separate thermal solar collectors to heat the water. This method was selected to provide sufficient heating without affecting the electricity production rate. Soğuksu photovoltaic power plant was established as a grid connected plant. Therefore, the last phase of the electricity is AC before transmitted to grid. However, the electrolyzer uses the electricity in DC phase. Thus, an AC-DC converter is added to the system as shown in Fig. 1.

2 Energy Analysis

As detailed above, the plant in investigation consists of three main sections. A comprehensive energy analysis of each section will be presented here. For the power plant, the electricity generation is defined as,

$$E_G = N_p E_S \eta_P \eta_{inv} \eta_{los} \quad (1)$$

Where, N_p is the total number of panels and E_S is the incident solar radiation on the panel's active surface area that varies daily and hourly. Active surface area of the panels is lower than the total panel area due to their frames.

Panel conversion efficiency, η_p , is given as;

$$\eta_p = \frac{E_{el}}{E_s} \quad (2)$$

where, E_{el} is the electricity generated by panels. η_{inv} is the inverter DC to AC conversion efficiency between 95% - 97%.

There are many losses associated with the solar plant. The losses are usually caused by module mismatches, temperature effects, dust or snow on the panels, conduction losses, wiring, humidity, wind speed, and soiling. η_{los} shows the total efficiency accounting for the losses. To maximize the electricity production by the photovoltaic power plant, the losses should be minimized. The results presented in this study, account for all the losses since they are obtained using the actual production data.

Electrical properties of photovoltaic panels at standard test conditions (STC) can be defined with Eq. (3). Standard test conditions are 1000 W/m² solar irradiance and 25 °C cell temperature.

$$E_{el} = I_{dc}V_{dc} \quad (3)$$

where, I_{dc} is the current and V_{dc} is the voltage of the panels in DC phase. The maximum voltage and current values are 31.4 V and 8.6 A, respectively.

The second section of the system is the Proton Exchange Membrane (PEM) electrolyzer with an acid polymer membrane electrolyte made of Nafion. This membrane, acts also as a gas separator. Water is decomposed into oxygen and hydroxonium ion (H₃O⁺) in the anode. Hydroxonium ion migrates through the acid membrane to the cathode where hydrogen and water are formed. The acceptable operation temperature range is between 25 – 80 °C and the current density range is between 0 – 10,000 A/m² [18]. The maximum operating temperature, current density and efficiency can be as high as 150 °C, 1600 mA/cm² and 70%, respectively [16].

Analysis of the electrolyzer below assumes all the gases involved in the process as ideal gases. Also, any side reaction or mixing is neglected. Electrolysis of water as an electrochemical process operating at constant pressure and temperature, the maximum possible useful work is equal to the change in Gibbs energy. Theoretically, the energy required for water electrolysis is given by the change in the enthalpy of reaction ΔH . The global reaction during water electrolysis is,



The feed water is in liquid state and according to the thermodynamic laws; the theoretical energy necessary for this reaction to take place is given by,

$$\Delta H = \Delta G + T\Delta S \quad (5)$$

where, ΔG is the required electrical energy and $T\Delta S$ is the thermal energy demand. ΔG represents the reversible part of the process while $T\Delta S$ represents the irreversible part

of the process. Also, the electrical energy involved in the Proton Exchange Membrane electrolysis process can be determined by the following electrochemical model,

$$\dot{W}_{electricity} = I_e V_e \quad (6)$$

where, V_e is the necessary cell voltage for the startup of electrolysis operation, I_e is the current density and $\dot{W}_{electricity}$ is the electrical power consumption in electrolysis.

The last section is the solar aided water preheater system with solar collectors. The thermal energy of the solar collectors is,

$$\dot{E}_{th} = \dot{m}_w c_p (T_{out} - T_{in}) \quad (7)$$

where, \dot{m}_w is the water mass flow, c_p is the specific heat of the water. Also, T_{out} and T_{in} are the output and input water temperature, respectively.

3 Results and discussion

Distribution of the electrical power generated by the solar power plant on a clear summer day is given in Fig. 4. A summer day with clear skies can be regarded as the perfect day for solar harvesting and therefore there is no disconnection between production values throughout the day. On a perfect day, with the sun rising, the power plant wakes up with a slight production. Gradually increasing the production capacity during the day until it reaches a peak value at midday. Then, the production decreases through afternoon and reaches to zero as the sun sets.

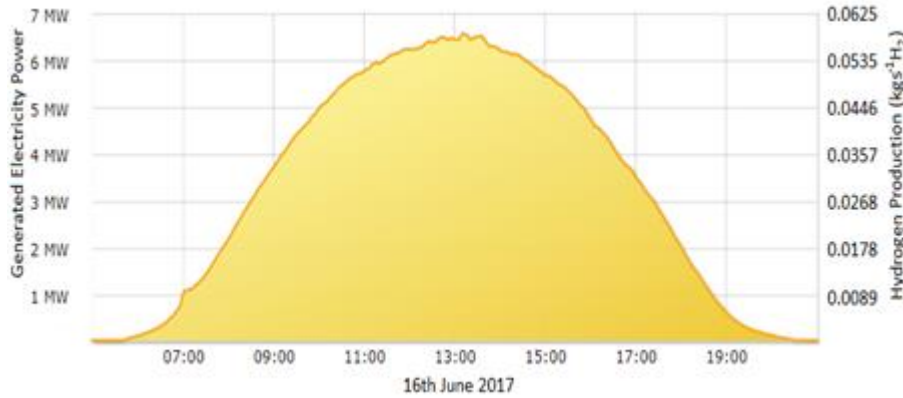


Fig. 4. Distribution of the power with hydrogen production capacity on a clear summer day

In the distribution given in Fig. 4, the electricity generated in the power plant in June 16, 2017 is shown. Distribution behaviour of the figure is very close to a perfect day. The power plant started to wake up after 6:00 am in the morning. Just after 1:00 pm, the peak power generation reaches to about 6.8 MW, which result in a hydrogen generation rate of about 0.06 kg/s. It should be noted that the maximum hydrogen production rate can reach to $0.0625 \text{ kgs}^{-1}\text{H}_2$ at peak loads. Electricity generation continues until

8:00 pm harnessing a total solar energy value of 53.15 MWh throughout the day. This daily electrical power can produce 1707.5 kg/day of hydrogen by electrolysis process.

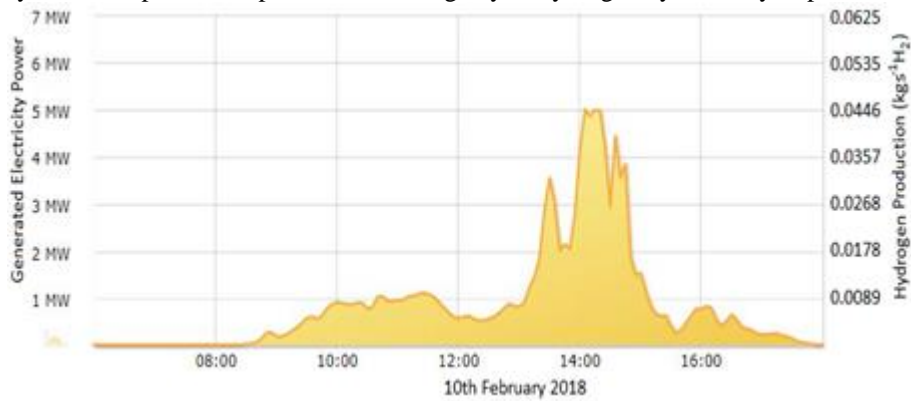


Fig. 5. Distribution of the power with hydrogen production capacity on a winter day

The daily electrical power generation distribution in Fig. 4 is not always available as it is not always a perfect solar day, especially in winters. Fig. 5 presents the daily electricity generation distribution of a winter day with the hydrogen production capacity. The figure shows the effect of overcast weather on electricity generation distribution throughout a winter day of February 10, 2018. The weather conditions have a significant impact on electrical power production. On a normal winter day the peak power is 5 MW that result in 10.28 MWh of electricity production throughout the day. In terms of hydrogen production, the electrolyzer can produce 330.25 kg hydrogen in this day, comparing to 1707.5 kg/day of a summery day.

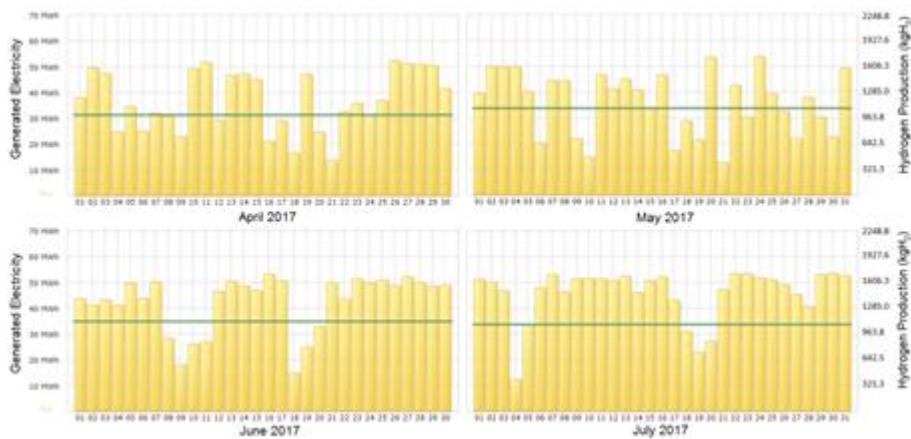


Fig. 6. Daily electricity generation values from April to July in Soğuksu solar power plant

The daily values of electricity transmitted to the grid with hydrogen production capacity between April and July in the Soğuksu solar power plant is given in Fig. 6.

Monthly generation values are obtained by adding daily generation quantities. The straight lines shown on the figure indicate the generation values targeted during the plant design process.

As it is observed from Fig. 6; the number of days, in which the electricity generation values are below the specified target, are nine during the month April. 1100 MWh of electricity is produced in total during this month that result in a hydrogen production capacity of 35338.6 kg/month. In May, monthly hydrogen production capacity is more than April even though the number of days, in which electricity generation is below the specified target, are twelve. Total electricity generation of May is 1120 MWh with 35981.1 kg/month hydrogen production capacity. In June, the number of days, in which electricity generation is below the specified target, is only seven. Monthly total electricity generation is 1270 MWh and hydrogen production capacity is 40800 kg in this month. The best month of the year is July in terms of electricity generation. The number of days, in which electricity generation is below the specified target, is only four and monthly total electricity generation is 1410 MWh with 45300 kg hydrogen production capacity.

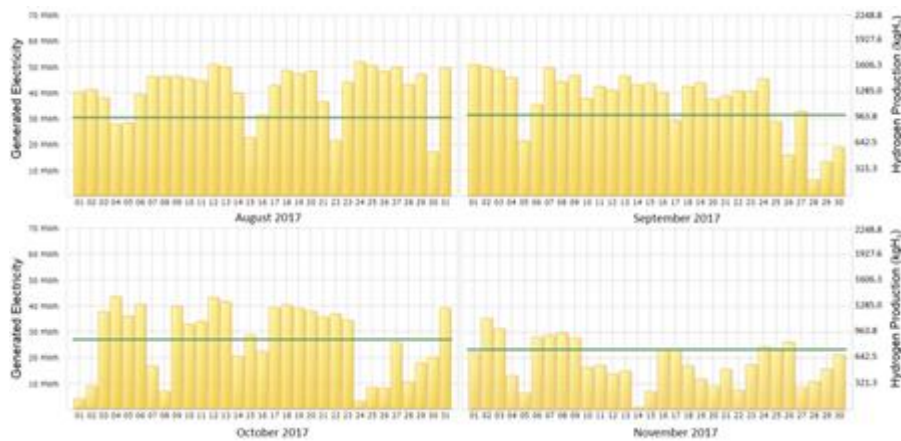


Fig. 7. Daily electricity generation values from August to November in the solar power plant

The generated electricity that was transmitted to the grid between August and November in the Soğuksu solar power plant is given in Fig. 7, with hydrogen production capacity. Looking at the last days of September, it can be seen that the power plant starts to be affected by the arrival of autumn.

Also, the generated electricity with hydrogen production capacities between August and November is given in Fig. 8. The minimum monthly electricity generation of the year is 370.18 MWh in December, since daily productions are very low with only seven days close to the targeted value. In March, the power plant escapes from the effect of the winter by a power generation value of approximately twice in February.

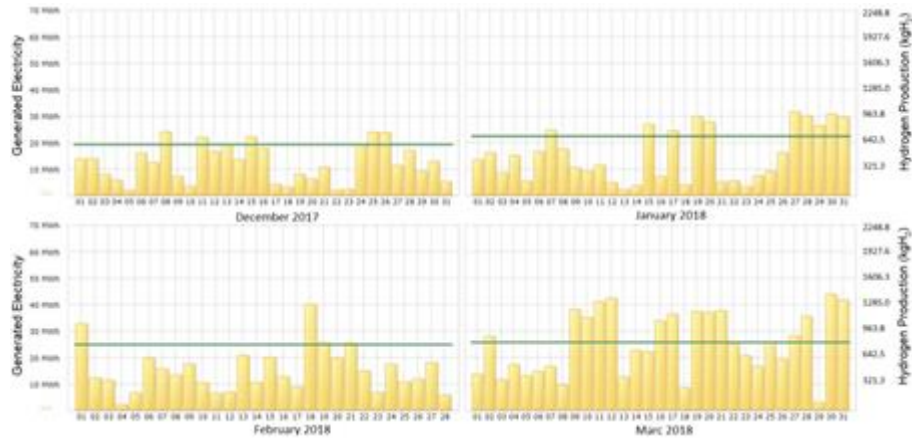


Fig. 8. Daily electricity generation values from December to March in the solar power plant

In Table 3, monthly electricity generation and hydrogen production capacity in Söğüksu solar power plant for a year is given. Total annual electricity generation of the plant is 10.7 GWh. The maximum electricity generation was observed in July with %13.3 and the minimum electricity generation was observed in December with %3.5. The investigated annual hydrogen production capacity of the power plant is 344020.5 kg.

Table 3. Electricity generation values and hydrogen production capacity by months

Months	Generated Electricity (MWh)	%	Hydrogen Production (kg)
April, 2017	1100	10.3	35338.6
May, 2017	1120	10.5	35981.1
June, 2017	1270	11.9	40800.0
July, 2017	1410	13.2	45297.6
August, 2017	1280	12.0	41121.3
September, 2017	1110	10.4	35659.8
October, 2017	838.29	7.8	26930.9
November, 2017	539.37	5.0	17327.8
December, 2017	370.18	3.5	11892.4
January, 2018	468.22	4.4	15042.0
February, 2018	419.04	3.9	13426.1
March, 2018	783.38	7.3	25166.9

4 Conclusions

In this study, a comprehensive investigation on hydrogen production capacity of a photovoltaic solar power plant was performed by using a Proton Exchange Membrane (PEM) electrolyzer. The analyses are carried out based on actual electricity generation values of a year from April 2017 to March 2018. The power plant is located in Bursa, Turkey. The plant is grid connected and it is the first solar power plant installed in the region with 7 MW peak power capacity. It can be concluded from the study that, the maximum mass flow rate of hydrogen production is $0.0625 \text{ kgs}^{-1}\text{H}_2$ during the peak load. However, this production rate can drop sharply, especially in winters, due to the effect of cloudy and rainy weather on the power plant. The power plant has a capacity to generate over 50 MWh electricity on a clear sunny day, which will result in 1700 kg/day of hydrogen production. During the year, the minimum electricity generation was obtained in December with % 3.5. While, the maximum electricity generation was obtained in July with % 13.2 of the year. The total annual electricity generation of the plant is 10.7 GWh with annual hydrogen production capacity of 344020.5 kg.

5 References

1. Kaygusuz K. Prospect of concentrating solar power in Turkey: The sustainable future. *Renewable and Sustainable Energy Review* 2011; 15:808-814.
2. Benli H. Potential of renewable energy in electrical energy production and sustainable energy development of Turkey: Performance and policies. *Renewable Energy* 2013; 50:33-46.
3. Hrayshat E. S. Viability of solar photovoltaics as an electricity generation source for Jordan. *International Journal of Sustainable Engineering* 2009; 2:1,67-77.
4. Merrouni AA., Mezrhab A, Mezrhab A. PV sites suitability analysis in the Eastern region of Morocco. *Sustainable Energy Technologies and Assessments* 2016; 18:6-15.
5. Doljak D, Popovic D, Kuzmanovic, D. Photovoltaic potential of the City of Požarevac. *Renewable Sustainable Energy Review* 2017; 73:460-467.
6. Edalati S, Ameri M, Iranmanesh M, Sadeghi Z. Solar photovoltaic power plants in five top oil-producing countries in Middle East: A case study in Iran. *Renewable Sustainable Energy Review* 2017; 69:1271-1280.
7. Kumar B.S. Sudhakar K. Performance evaluation of 10 MW grid connected solar photovoltaic power plant in India. *Energy Reports* 2015; 1:184-192.
8. Sharaf O Z, Orhan M F. Thermodynamic analysis and optimization of densely-packed receiver assembly components in high-concentration CPVT solar collectors. *Energy Conversion and Management* 2016; 121:113-144.
9. Incekara C O, Ogulata S N, Turkey's energy planning considering global environmental concerns. *Ecological Engineering* 2017; 102:589-595.
10. Kanoglu M, Bolatturk A, Yilmaz C. Thermodynamic analysis of models used in hydrogen production by geothermal energy. *International journal of hydrogen energy* 2010; 35:8783-8791.
11. Orhan M F, Dincer I, Rosen M A, Kanoglu M. Integrated hydrogen production options based on renewable and nuclear energy sources. *Renewable and Sustainable Energy Review* 2012; 16:6059-6082.

12. Yuksel E Y, Ozturk M. Thermodynamic and thermo economic analyses of a geothermal energy based integrated system for hydrogen production. *International Journal of Hydrogen Energy* 2017; 42:2530-2546.
13. Cilogullari M, Erden M, Karakilcik M, Dincer I. Investigation of hydrogen production performance of a Photovoltaic and Thermal System, *International Journal of Hydrogen Energy* 2017; 42:2547-2552.
14. Koponen J, Kosonen A, Ruuskanen V, Huoman K, Niemela M, Ahola J. Control and energy efficiency of PEM water electrolyzers in renewable energy systems. *International Journal of Hydrogen Energy* 2017; 42:29648-29660.
15. Ebaid M S Y, Hammad M, Alghamd T. Thermo economic analysis of PV and hydrogen gas turbine hybrid power plant of 100 MW power output. *International Journal of Hydrogen Energy* 2015; 40:12120-12143.
16. Boudries R, Khellaf A, Aliane A, Ihaddaden L, Khida F. PV system design for powering an industrial unit for hydrogen production. *International Journal of Hydrogen Energy* 2014; 39:15188-15195.
17. Saadi A, Becherif M, Ramadan H. S. Hydrogen production horizon using solar energy in Biskra, Algeria. *International Journal of Hydrogen Energy* 2016; 41:21899-21912.
18. Yilmaz C, Kanoglu M. Thermodynamic evaluation of geothermal energy powered hydrogen production by PEM water electrolysis. *Energy* 2014; 69:592-602.
19. Saka K. Seasonal generation of a grid connected PV power plant. The 6th European conference on renewable energy systems. Istanbul Turkey 25-27 June 2018, 77-82.

Analysis and Modeling of Gaskets, End Plates and Current Collectors in a Proton Exchange Membrane Fuel Cell

Kenan Saka¹ Mehmet F. Orhan² and Huseyin Kahraman³

¹Vocational School of Yenisehir Ibrahim Orhan, Bursa Uludag University, PO Box: 16900, Yenisehir, Bursa, Turkey

²Department of Mechanical Engineering, American University of Sharjah, P.O. Box: 26666, Sharjah, United Arab Emirates

³Department of Mechanical Education, Technical Education Faculty, Sakarya University, P.O. Box: 54187, Sakarya, Turkey

Emails: kenansaka@uludag.edu.tr, morhan@aus.edu, huseyink@sakarya.edu.tr

Abstract. A single proton exchange membrane (PEM) fuel cell is composed of several components such as gaskets, end plates and current collectors. These crucial components should be modeled and diagnosed properly for a higher overall efficiency. The gasket is very essential for the cell as a barrier to leakages. Also, the end plates assure a uniform distribution of clamping pressure along all the components. On the other hand, the current collectors can be made of various materials and should carefully be selected. In this study, a model for the gaskets, end plates and current collectors has been created in terms of heat conduction. A nodal analysis has been used to evaluate the variation in temperature due to heat conduction of different end plate materials and gasket thicknesses. The current collector materials and their impact to the cell performance have also been investigated. The results show that as the hard rubber gasket layer thickness increases, the temperature takes longer time to reach a steady state. The current collector plates made of grafiol show the best performance at various current density loads.

Keywords: Fuel cell, proton exchange membrane (PEM), gaskets, end plates, current collectors

1 Introduction

One of the major difficulties that face the designer of a proton exchange membrane fuel cell (PEMFC) is to prevent any gas leakage between the cells in the stack design. In order to preserve the reactant gases in their regions, certain electrometric gaskets must be comprised in each cell. Since gaskets cause to experience different factors like acidic

environment, humid air, hydrogen, and mechanical compressive load, they might upon it material age or simply fail. Especially in PEM fuel cells. Those factors would make the gasket to lose its elasticity and ability of sealing compactly, in consequence, a leakage or an unintentional mix between the reactant gases might happen. Beside the significant drop in the performance of the PEM fuel cell, the issue raises series safety concern [1]. However, gas tightness can be improved by increasing stack compression and/or by finding a better gasket material. Many types of gasket materials can be used in fuel cell stacks. For example some researchers use various materials tested are copolymeric resin, liquid silicone rubber, fluorosilicone rubber, ethylene propylene diene monomer rubber, and fluoroelastomer copolymer [2].

There are many reports accentuation the thermal and irradiative behaviors of various gasket materials in literature [3-5]. Although there are only a few substantial literatures discussing chemical degradation of elastomeric gasket materials in PEM fuel cell environment. Schulze et al. [6] investigated the degradation of seals in PEM fuel cells during fuel cell operation. Tan et al. [7-9] studied the chemical and mechanical degradation of Silicone rubber exposed to a high concentration PEM fuel cell solution in accelerated tests. Lee et al. [10] studied the effects of compression and gas diffusion layers on the performance of a PEM fuel cell.

As a contribution to the ongoing efforts, in this study we aim to analyze, design, and optimize various models of gaskets, end plates and current collectors. To use a nodal analysis and evaluate the variation in temperature due to heat conduction of different end plate materials and gasket thicknesses. To investigate various current collector materials and their impact to the cell performance. To conduct extensive parametric studies that illustrate the complex relations between cell components and variables, and measure the effects of different parameters on the cell performance.

2 System Description

Some of the considerations when selecting the appropriate gasket material should be:

- Chemically stable for long term use.
- Avoid mixing the reactant gases.
- Avoid releasing the reactant gases to the environment.
- Act as a vibration and shock absorbent.
- Electrically separate the cell components.
- Minimal mechanical and thermal mismatch stresses.
- Mechanically stable over the required temperature range.
- Low-cost.
- Good sealing capability.
- Low-cost stacks manufacturing methods.
- Prevent mechanical bonding of components (for certain fuel cell types).

As observed in Table (1) a list of common materials which used for the fabrication process of gaskets. These materials are distinguished with their reasonable prices, and

easy manufacturing [11]. In choosing a soft gasket material, silicon has showed an impressive airtight sealing especially in small stacks at ambient temperature. Upon experience, it was noticed that that gasket material in PEM and DMFCs has an identical thickness to the (MEA). Thus, that gasket may experience deformation in shape due to compression and that might cause blocking the gas flow. This obstacle can be prevented either by using more rigid gasket material, covering the flow channels with bridge pieces, or machining the flow channels to a deeper width and depth.

Table 1. Types of gaskets and advantages/disadvantages

Gasket type	Advantage/disadvantage
Silicon	<ul style="list-style-type: none"> • Good gas tightness • Available in several thicknesses • May deform and obstruct gas flow
EPDM rubber	<ul style="list-style-type: none"> • Good gas tightness • Thin sheets may not be readily available
PTEF	<ul style="list-style-type: none"> • Difficult to make gas tight
PTEF coated glass fiber thread	<ul style="list-style-type: none"> • Easy to handle • Available in several thicknesses • Requires more compression for gas tightness
EPDM/ PTEF	<ul style="list-style-type: none"> • Available in several thicknesses

When we talk about a stack configuration, we talk about more than one cell being assembled together with many components. In order to assure a uniform distribution of clamping pressure along all the components of the fuel cell, end plates with bolts attached are used. Especially in the GDL, since its features are dependent on the compression pressure. As the pressure on the GDL is inversely related to the thermal and electric contact resistances on the GDL electrode and GDL flow field plate interfaces, a compression pressure of 10 Bars is sufficient for low contact losses. After all, its effect on the contact resistances is trivial. In contrast, increasing the compression pressure will lower the GDL porosity and accordingly raise mass transfer limitations. In which will drop the performance of the fuel cell significantly. The optimum pressure is dependent on the gas diffusion material and some parameters in the fuel cell such as temperature and humidity of the inlet gas. The local (under ribs and channels) and regional

(whole cell area) pressure distributions on the MEA and GDL are influenced by factors such as the dimensions, the geometrical shape, and the chosen material of the stack components. In terms of regional pressure distribution, end plates have been considered as the most influential component in the cell. The end plates should have a comparatively high rigidity in order to maintain an even distribution of pressure across the complete regional area. In order to satisfy the rigidity, the thick endplates have been employing. But they are not only heavy, but also have high thermal conductivity and thermal inertia, which deteriorate the cold-start characteristics of fuel cell stack, a new development of the endplate with light weight and better thermal properties is necessary [12]. Table (2) lists some properties of the end plates [13].

Table 2. Properties of End Plates (Adapted from Fu et al, 2007; Karvonen et al, 2008)

Function	Property	Comments
To maintain low contact resistance between different components by withstanding high pressures	Enough rigidity and strength	This should be attained in the operational temperature, operational pressure, and humidity ranges
Serves as a universal inlet and outlet for the fuel, oxidant, and coolant	Chemical and electro-chemical stability	-
Aids in preventing the membrane from dehydrating and flooding	The endplates are prone to corrosion in the two-phase flows	Especially in acidic media
Ensures startup from freezing, glycol antifreeze is often added to the cooling water	Exhibit high chemical stability in glycol solution	-
The high-power PEMFC stacks consisting of over 100 single cells have a very high output voltage	Good electrical insulation to ensure safety	-

End plates should have some specific properties because of their functions. The most important function that end plates do is that they supply the stack with enough pressure to maintain low resistance between different components in the stack. As a result, the end plate should have enough rigidity and strength to supply this force without deforming. The second function is that the end plate serves as the universal inlet and outlet for the fuel, oxidant, and coolant. Those reactants have special chemical, electrical and

mechanical properties. Some of them may react with the end plate if the end plate does not have enough mechanical and chemical stability. Also, the membrane should be mentioned at a pressure that prevents dehydrating or flooding. This pressure is obtained from the end plate and it may happen that water may flow in both opposite direction and in two phases depending on the situation “dehydrating or flooding”. As a result, these different directions of flow and different phases may lead to cause corrosion for the end plates. As a result, the end plate should be anti-corrosion. Most of the times, glycol antifreeze is added to the cooling water to prevent it from freezing. Most materials and especially end plate materials are sensitive to glycol. So we should be careful when we choose the end plate material to be sure that it is not sensitive to glycol. A lot of stacks generate high electrical power as we increase the number of cells. Finally, the end plate should be well insulated to ensure safety that when someone touches the end plate, he/she does not get electrified. Those properties are summarized with their related function in Table (2).

From a perspective on industry, the rigidity of the material depends on thickness, thus a high rigid material, would simply mean a thicker plate (larger in mass and volume). This solution would not be practical, particularly in portable and automotive applications. Therefore it was innovated to manufacture so called a ribbed-structure, which is a thin plate with ribs fixed to the surface. This configuration has managed to lower the weight of the stack significantly, and achieve higher rigidity [13].

In summary an end plate should provide below requirements:

- Provide even pressure distribution to the stack with small mass.
- Improve the cold-start characteristics.
- Increase the corrosion resistance of the surface of the endplate.

For satisfy these requirements well, design parameters below should be considered:

- High specific flexural stiffness with a clamping device
- Thermal properties of the endplate material
- Suitable materials for high corrosion resistance

A good end plate material has a high Young’s modulus and a low density [13]. There are many materials currently used for end plates, which can be classified into two types. The first is non-metallic materials, which includes engineering plastics, polysulfone, etc. However, the thermal stability of engineering plastics and polysulfone is not satisfactory as they tend to degenerate under PEMFC operating temperatures. The second type of endplate material is metals, which includes aluminum alloy, titanium, stainless steel, and so on. Metals have a high mechanical strength, but their corrosion resistance and electrical insulation should be considered. There are two ways to achieve the desired properties: one is to put an additional insulating plate between the current collector and the endplate, which makes the stack more complicated, another is to make a surface modification [14]. According to Spiegel [11], some of the materials that are being used for the end plates are:

- Graphite.

- Stainless steel.
- Aluminum.
- Titanium.
- Nickel.
- Metal foams.
- PVC.
- Polycarbonate.
- Polyethylene.
- Various other polymers.

Table 3. Specifications of Some Materials Used for Current Collectors)

Material	Specifications	Comment
Gold-Plated Aluminum	Made from aluminum and coated with gold	Gold may degrade and move to the membrane
Stainless Steel	Inexpensive, robust, and easily-fabricated	Dense, thus, the gravimetric power density suffers as a result
Titanium	Lightweight, rugged, easily-machined, good electrical conductivity	Needs some etching and coating on the surface, which may cause voltage losses
Poco™ graphite	Good electrical conductivity, lightweight, chemically inert,	It is not mechanically robust stack built from this material would have to be protected from impact.

Current collectors can be fabricated out of a variety of conductive materials such as tin, brass, aluminum and many others. They are usually placed on the end plates for the job of collecting electrons [15]. Most current collectors are made out of metallic materials because they have high electrical conductivity “electrical conductor” related to other materials. These materials with their specifications are summarized in Table (3) [16]. However, Figure (1) compares different materials to the current density loads that they can have. It is clear that grafiol material is one of the best materials [15].

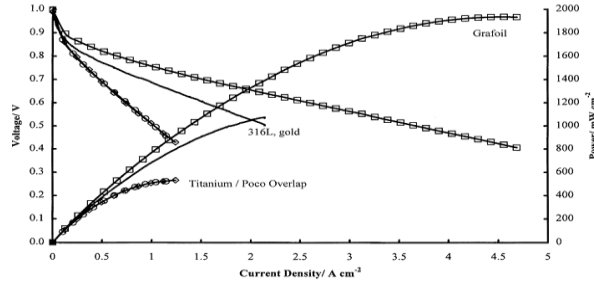


Fig. 1. Performance Comparison of Different Current Collector Materials [15] (Hentall et al, 1999)

3 Analysis

There are two important parameters that characterize the work mechanism for the end plate and the gasket. Those two parameters are the clamping pressure and the temperature. For the temperature change due to the heat conduction, we will derive a set of equations that describe the heat conduction through the gasket and the end plate.

For end plates and gaskets, they are subjected to one dimensional heat transfer conduction from two sides as the heat conduction and convection through the thickness is neglected because the thickness is small compared to the height and width. Figure (2) illustrates this idea.

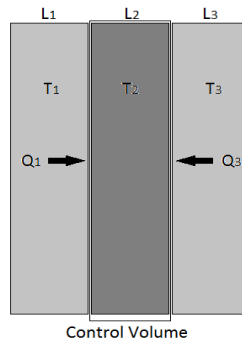


Fig. 2. Energy Balance Around Layer (2)

The general energy balance for the end plate, contact, and GDL layers can be written as:

$$\left(\rho_{\text{Layer2}} A_{\text{Layer2}} t_{\text{Layer2}} c_{p_{\text{Layer2}}}\right) \frac{dT_{\text{Layer2}}}{dt} = Q_{\text{Layer1}} + Q_{\text{Layer3}} \quad (1)$$

where ρ_{Layer2} is the density of Layer2, A_{Layer2} is the area of Layer2, $c_{p_{\text{Layer2}}}$ is the specific heat capacity of Layer2, Q_{Layer1} is the heat flow from Layer1, Q_{Layer3} is the

heat flow from Layer3. The derivative on the left side is the rate of change of control volume temperature of the layer. The heat flow from Layer1 to Layer2 is:

$$Q_{\text{Layer1}} = U_{\text{Layer1}}A(T_{\text{Layer1}} + T_{\text{Layer2}}) \quad (2)$$

where U_{Layer1} is the overall heat transfer coefficient for Layer1, A is the area of the layer, and T is the temperature of the layer. The heat flow from Layer3 to Layer2 can be expressed as:

$$Q_{\text{Layer3}} = U_{\text{Layer3}}A(T_{\text{Layer3}} - T_{\text{Layer2}}) \quad (3)$$

If the heat is coming from the surroundings, the overall heat transfer coefficient can be calculated by:

$$U_{\text{surr}} = \frac{1}{\frac{t_{\text{Layer2}}}{k_{\text{Layer2}}} + \frac{1}{h_{\text{surr}}}} \quad (4)$$

Where:

t_{Layer2} is the thickness of Layer (2).

k_{Layer2} is the thermal conductivity of Layer (2).

h_{surr} is the convective loss from the stack to the air.

The overall heat transfer coefficient for the heat coming from Layer (1) is:

$$U_{\text{Layer1}} = \frac{1}{\frac{t_{\text{Layer2}}}{k_{\text{Layer2}}} + \frac{t_{\text{Layer1}}}{k_{\text{Layer1}}}} \quad (5)$$

The overall heat transfer coefficient for the heat coming from Layer (3) is:

$$U_{\text{Layer1}} = \frac{1}{\frac{t_{\text{Layer3}}}{k_{\text{Layer3}}} + \frac{t_{\text{Layer2}}}{k_{\text{Layer2}}}} \quad (6)$$

If the layer conducts electricity (such as the contact layer), then there is an additional heat generation in Layer (2) ($Q_{\text{res_Layer2}}$) due to electrical resistance, which can be calculated as:

$$Q_{\text{res_Layer2}} = (iA)^2 \frac{\rho_{\text{res_Layer2}} t_{\text{Layer2}}}{A} \quad (7)$$

Where:

i is the current density.

A is the area of the layer.

$\rho_{\text{res_Layer2}}$ is the specific resistance of the material.

t_{Layer2} is the thickness of the layer.

We will use nodal analysis to solve for the temperature change. This is illustrated in Figure (3).

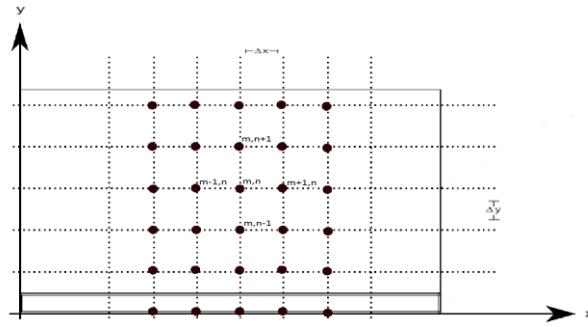


Fig. 3. Two Dimensional Conduction with Nodal Analysis

For the uniform distribution of nodes that us shown in Figure (3), the location of each node (x_i) is:

$$x_i = \frac{(i-1)}{(N-1)}L \text{ for } i = 1 \dots N \quad (8)$$

Where:

N is the number of nodes used for the simulation.

The distance between adjacent nodes (Δx) is:

$$\Delta x = \frac{L}{N-1} \quad (9)$$

Energy balances have been defined around each node (control volume). The control volume for the first, last, and arbitrary. Each control volume has conductive heat transfer with each adjacent node in addition to energy storage:

$$\dot{q}_{LHS} + \dot{q}_{RHS} = \frac{dU}{dt} \quad (10)$$

Each term in Equation (8) must be approximated. The conduction terms from the adjacent nodes are modeled as:

$$\dot{q}_{LHS} = \frac{kA(T_{i-1} - T_i)}{\Delta x} \quad (11)$$

$$\dot{q}_{RHS} = \frac{kA(T_{i+1} - T_i)}{\Delta x} \quad (12)$$

Where:

A is the area of the plate.

The rate of energy storage is the product of the time rate of change of the nodal temperature and the thermal mass of the control volume:

$$\frac{dU}{dt} = A\Delta x\rho c \frac{dT_i}{dt} \quad (13)$$

Substituting Equations (6) through (11) leads to:

$$A\Delta x\rho c \frac{dT_i}{dt} = \frac{kA(T_{i-1}-T_i)}{\Delta x} + \frac{kA(T_{i+1}-T_i)}{\Delta x} \quad (14)$$

Solving for the time rate of the temperature change:

$$\frac{dT_i}{dt} = \frac{k}{\Delta x^2\rho c} (T_{i-1} + T_{i+1} - 2T_i) \text{ for } i = 2 \dots (N - 1) \quad (15)$$

The control volumes on the edges must be treated separately because they have smaller volume and experience different energy transfers. The control volume for the node located at the outer surfaces (node N) has the following the energy balance:

$$\frac{dU}{dt} = \dot{q}_{LHS} + \dot{q}_{conv} \quad (16)$$

or

$$\frac{A\Delta x\rho c}{2} \frac{dT_N}{dt} = \frac{kA(T_{N-1}-T_N)}{\Delta x} + hA(T_f - T_N) \quad (17)$$

Solving for the time rate of temperature change for node N:

$$\frac{dT_N}{dt} = \frac{2k}{\rho c\Delta x^2} (T_{N-1} - T_N) + \frac{2h}{\Delta x\rho c} (T_f - T_N) \quad (18)$$

4 Results and Discussion

Dealing with gaskets and end plates, one of the most important parameters that affects the stack performance is the heat conduction through the end plate and the gaskets in the fuel cell stack. In this study, a model has been created for the end plate and gasket in terms of heat conduction.

We used a nodal analysis with 10 nodes to get the change in temperature because of the heat conduction in different end plates materials because of air flow rate. Figures (4) through (5) compare a polymer end plate with aluminum end plate and polycarbonate end plate at different times. Table (4) show the parameters used for polymer, aluminum and polycarbonate end plates, respectively. Also, Equations (1 – 18) were used to generate these figures.

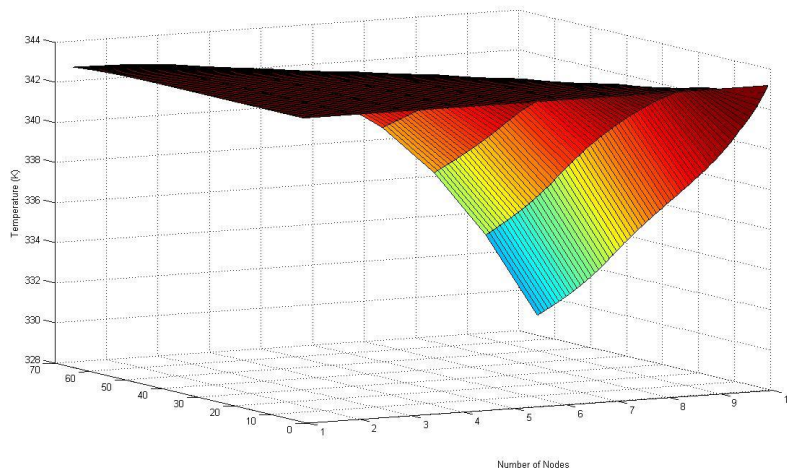


Fig. 4. Polymer End Plate Heat Conduction after 120 seconds time Simulation

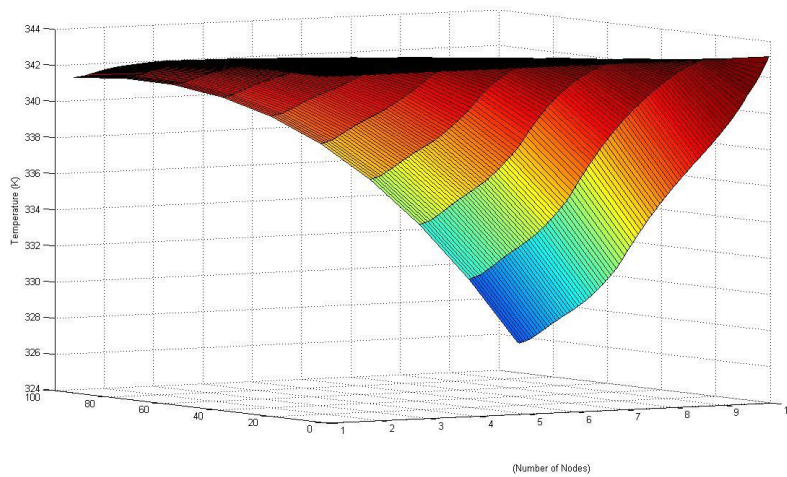


Fig. 5. Polycarbonate End Plate Heat Conduction after 120 seconds Time Simulation

Table 4. Parameters of Aluminum End Plate Heat Conduction for (t = 60, 120, 7000 seconds) Simulation

Parameter	Value	Unit
L	0.01	m
k	220	W/m. K
ρ	2700	kg/m ³
c_p	900	J/kg. K
T_{in}	343.15	K
T_f	280	K
h	17	W/m ² . K
N	10	—

End plate materials are divided into two main categories: nonmetallic materials such as engineering plastics, polysulfons, etc. and metallic materials such as steel, aluminum and titanium. The nonmetallic materials have not sufficient thermal stability and may be damaged at operational temperature. Differ from former group, the metallic materials have high mechanical properties and thermal stability. To make it clear Figures (6) through (7) shows the temperature as a function of time for polymer, aluminum and polycarbonate end plate. It is commonly known that a fuel cell operating at the high current densities or the electrochemical reaction rate increases as the temperature increases. As a consequent, the temperature of the fuel cell should be increased as fast as possible during the cold start allowing the fuel cell to generate power at the rate required. To shorten the temperature rise time required to produce enough power under cold environment, endplates are required to have both low specific heat and low thermal

conductivity. According to the results polycarbonates are much superior to those of conventional metallic and polymer materials for their properties.

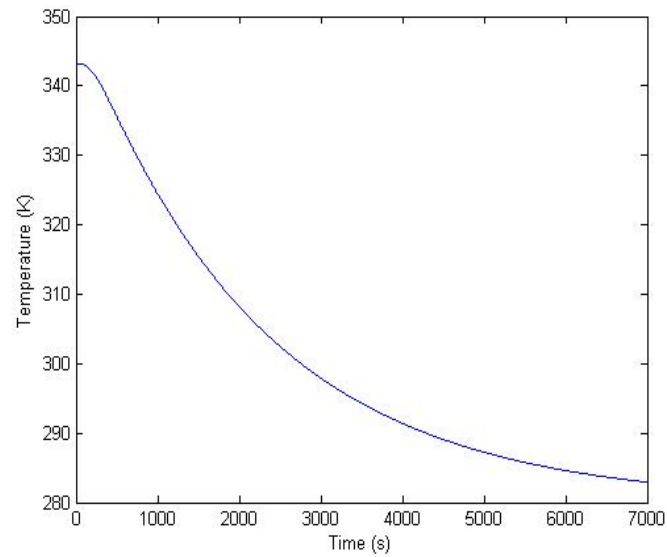


Fig. 6. Change Temperature at Different Time for Polymer End Plate

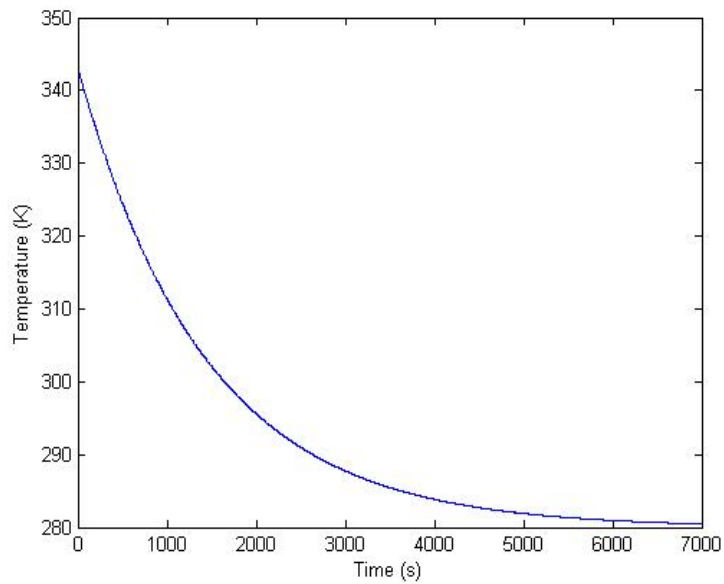


Fig. 7. Temperature Change at Different Time for Aluminum End Plate

While the fuel cell starts up at the cold environment, the temperature in the cell should increase to the operating temperature. The heat loss during energy conversion to electrical energy, heat generates, which is used to increase the temperature in a cell or stack. However, by heat transfer through endplates some portion of the heat is dissipated to the low temperature environment, which should be minimized to decrease cold starting time. Consequently, to shorten the starting-up time that is required to increase temperature to operating temperature, the portion of heat that is required to increase the temperature of endplates and dissipated through the endplates by conduction, should be minimized.

In gasket modeling, we used a nodal analysis with 5 nodes to get the change in temperature because of the heat conduction in a gasket material with different thicknesses because of conduction between the gasket and end plate from one side, and gasket and bipolar plate from the other side.

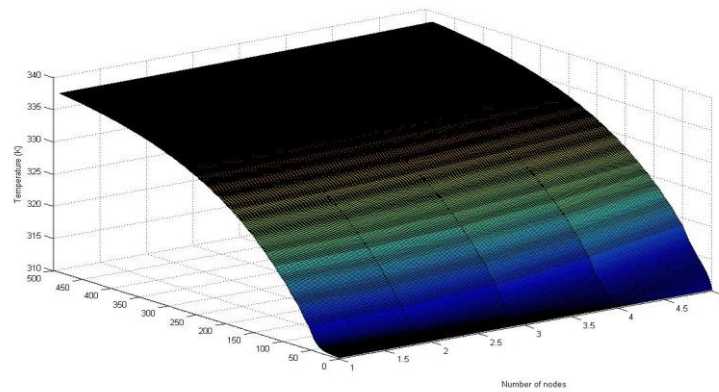


Fig. 8. Hard Rubber Gasket with Thickness of 0.003

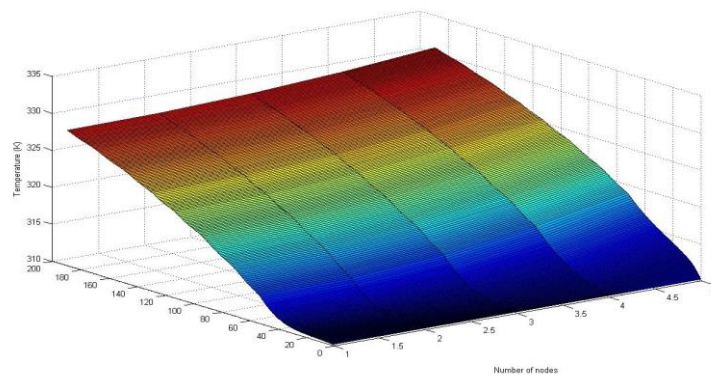


Fig. 9. Hard Rubber Gasket with Thickness of 0.005

Also, as the thickness increases, the temperature takes longer time to reach to steady state. This is illustrated in Figures (8) through (9).

5 Conclusion

In conclusion, the most important parts of the PEM fuel cell are the gasket, end plates and the current collector. These parts should be analyzed and modeled for the purpose of increasing efficiency under different conditions such as varying humidity, temperature and clamping pressure. For example, the gasket should provide correct compression for the system to reach high efficiencies. End plates must provide an adequate distribution of clamping pressure. The design depends on material selection, which leads to more life and durability under different conditions. Since fully humidified fuel/oxidant and the harsh acidic (In the PEMFC working environment, pH is in the range 0~3.5 [17]) environment in the fuel cell, the end plate material should be bearable to corrosion. Additionally, the high power stacks produce high output voltage; so, the end plates should have been insulated properly to ensure safety. Therefore, the ideal materials used in the end plates should have properties such as low density, high rigidity and enough electrochemical stability. Stack configuration is a set of cells being assembled together with many components. Finally, the current collector, which collects electrons from the cells, is an important part of the fuel cell and special consideration especially in terms of material selection for more efficient output.

6 References

1. Li, G., J. Tan, and J. Gong, Degradation of the elastomeric gasket material in a simulated and four accelerated proton exchange membrane fuel cell environments. *Journal of Power Sources*, 2012. **205**(0): p. 244-251.
2. Lin, C.-W., et al., Dynamic mechanical characteristics of five elastomeric gasket materials aged in a simulated and an accelerated PEM fuel cell environment. *International Journal of Hydrogen Energy*, 2011. **36**(11): p. 6756-6767.
3. Bhowmick, A.K., et al., Surface properties of EPDM, silicone rubber, and their blend during aging. *Journal of Applied Polymer Science*, 1995. **57**(5): p. 631-637.
4. Ghanbari-Siahkali, A., et al., Investigation of the hydrothermal stability of cross-linked liquid silicone rubber (LSR). *Polymer Degradation and Stability*, 2005. **90**(3): p. 471-480.
5. Chaudhry, A.N. and N.C. Billingham, Characterisation and oxidative degradation of a room-temperature vulcanised poly(dimethylsiloxane) rubber. *Polymer Degradation and Stability*, 2001. **73**(3): p. 505-510.
6. Schulze, M., et al., Degradation of sealings for PEFC test cells during fuel cell operation. *Journal of Power Sources*, 2004. **127**(1-2): p. 222-229.
7. Tan, J., et al., Degradation of elastomeric gasket materials in PEM fuel cells. *Materials Science and Engineering: A*, 2007. **445-446**(0): p. 669-675.
8. Tan, J., et al., Degradation of silicone rubber under compression in a simulated PEM fuel cell environment. *Journal of Power Sources*, 2007. **172**(2): p. 782-789.

9. Tan, J., et al., Assessment of mechanical properties of fluoroelastomer and EPDM in a simulated PEM fuel cell environment by microindentation test. *Materials Science and Engineering: A*, 2008. **496**(1–2): p. 464-470.
10. Lee, W.-k., et al., The effects of compression and gas diffusion layers on the performance of a PEM fuel cell. *Journal of Power Sources*, 1999. **84**(1): p. 45-51.
11. Spiegel, C., *Designing and building fuel cells*. 2007: Mcgraw-hill New York, NY, USA.
12. Yu, H.N., et al., Axiomatic design of the sandwich composite endplate for PEMFC in fuel cell vehicles. *Composite Structures*, 2010. **92**(6): p. 1504-1511.
13. Karvonen, S., et al., Modeling of Polymer Electrolyte Membrane Fuel Cell Stack End Plates. *Journal of Fuel Cell Science and Technology*, 2008. **5**(4): p. 041009-041009.
14. Fu, Y., et al., Research progress of aluminium alloy endplates for PEMFCs. *Journal of Power Sources*, 2007. **166**(2): p. 435-440.
15. Daniels, F.A., et al., Current collector design for closed-plenum polymer electrolyte membrane fuel cells. *Journal of Power Sources*, 2014. **249**(0): p. 247-262.
16. Hentall, P.L., et al., New materials for polymer electrolyte membrane fuel cell current collectors. *Journal of Power Sources*, 1999. **80**(1–2): p. 235-241.

The Conversion of a Residential Building into a Net Zero Energy Building

M.Sc. Salih Güvenç Uslu¹, Prof. Dr. Tanay Sıdkı Uyar¹

¹Mechanical Engineering Department/Faculty of Engineering/University of Marmara,
Kadıköy/İstanbul/Turkey

Emails: salihguvencuslu@gmail.com

Abstract. Zero energy building concept has gained popularity significantly lately due to the enhanced greenhouse effect and the stringent regulations. The present study exemplifies an integrated approach to convert a 2-floor-residential house into a positive net zero energy building using DesignBuilder, EnergyPlus and Radiance. The study takes into account two study cases. The first case integrates a HVAC system including ground source heat pumps, a ground heat exchanger, an air handling unit (AHU) and heated floors to the actual building air conditioning system plus heated internal floors with upgraded composition and upgraded domestic hot water system to the actual building. The second case, addition to the first case, considers a grid-tied solar system including external wall –and roof-mounted photovoltaic (PV) panels. The results consist of dynamic thermal simulations using EnergyPlus, illumination maps using Radiance solver embedded on DesignBuilder and a steady-state, isothermal, external CFD analysis in the district where the studied building is located. The study as a whole provides a wide outlook over zero energy building concept.

Keywords: Positive Net Zero Energy Building, Ground Source Heat Pump, Heated Floors.

1 Introduction

Zero energy building (ZEB) concept has not been precisely defined. However, across all net zero energy building (NZEB) definitions and classifications, one design rule remains constant that energy demand is to reduce to the lowest possible level first, then to address energy supply, [1].

Igor et al. in 2010, Carlo and Guido in 2015, the National Institute of Building Sciences (NIBS) in 2015, the American Institute of Building Sciences (AIA) in 2016 handled this concept. Igor et al. described NZEB as that is a building whose total amount of energy used on an annual basis is roughly equal to the amount of renewable energy created on the site, [2]. The balance suggested by Igor et al. is represented graphically in Fig.1. In addition to Igor et al., NIBS presented a definition for ZEB that is an energy-

efficient building where, on a source energy basis, the actual annual delivered energy is less than or equal to the on-site renewable exported energy, [3]. AIA handled the concept with their own definitions. Their approach was based on very first statement that was net zero indicates you are living within your means, net positive means a shift to giving back, [4]. The institute described net positive term as a building that produces more than 100% of its energy needs from on-site renewable resources, net zero energy term as a building that uses the same amount of energy that is produced on site on an annual basis.

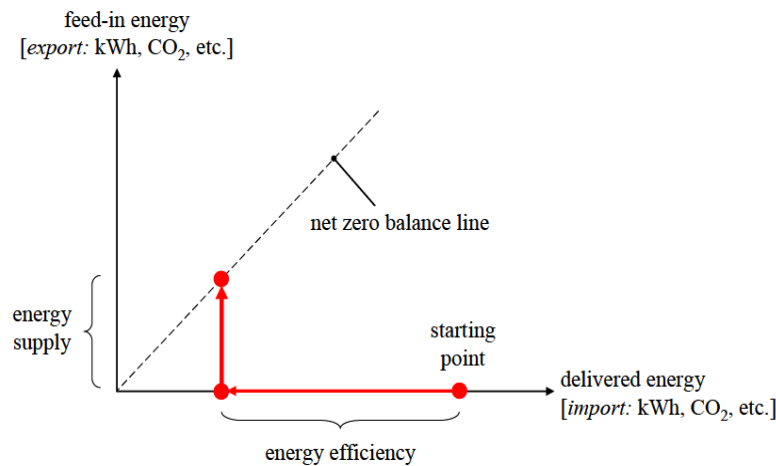


Fig. 1. Net zero balance line [2]

Vancouver City Council published a passive design toolkit in 2009, [5]. The toolkit characterized the passive design of a building step by step. It, first, focused on passive solar power and solar access to the building. Orientation of the building, its shape, its elevation and landscaping, its interior layout including mechanical and plumbing equipment, came after. The steps regarding insulation, glazing, lighting, ventilation, thermal mass and residential density followed the initial steps on the road to improve the passive performance of a building.

2 The Studied Building

The building that is analyzed to be converted into a net zero energy building is located in Beylerbeyi district in Istanbul, Turkey. The current outlook of the building can be seen in Fig.2-1. The final appearance of the building is in Fig.2-2. There are three floors including the basement in the building. The ground floor is several decimeters higher than the ground. A portion of the basement is sunk into the ground and there is around 1m-wall on the southern façade. This wall belongs to the open area next to the building. The ground soil and the wall can also be seen in Fig.2-2.

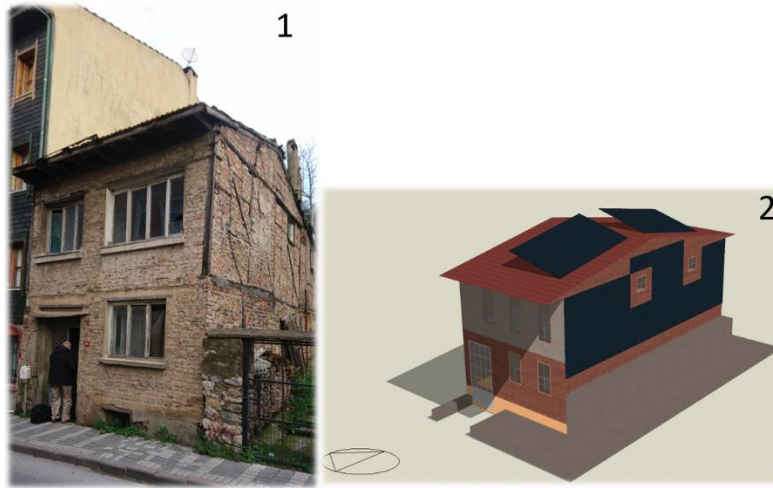


Fig.2. 1-The actual building that is converted, 2-The last outlook of the building on Design-Builder

3 HVAC System and On-Site Electricity Generation

The study takes into account two study cases. The first case, Case 1, integrates the HVAC system depicted in Fig.3 plus heated floors with upgraded composition and domestic hot water system to the actual building. The second case, Case 2, addition to the first case, considers a grid-tied solar system including external wall –and roof-mounted photovoltaic, PV, panels.

The HVAC system handled in the study, Fig.3, involves a condenser loop, a hot water loop, a chilled water loop, an air handling unit, AHU, a zone group where the floors are heated up with upgraded composition, Fig.4. These sub-systems include ground source heat pumps, a ground heat exchanger. The study exemplifies a method for choosing these components. In addition to the HVAC system, hot water is provided by a hot water unit whose energy source is instantaneous electricity.

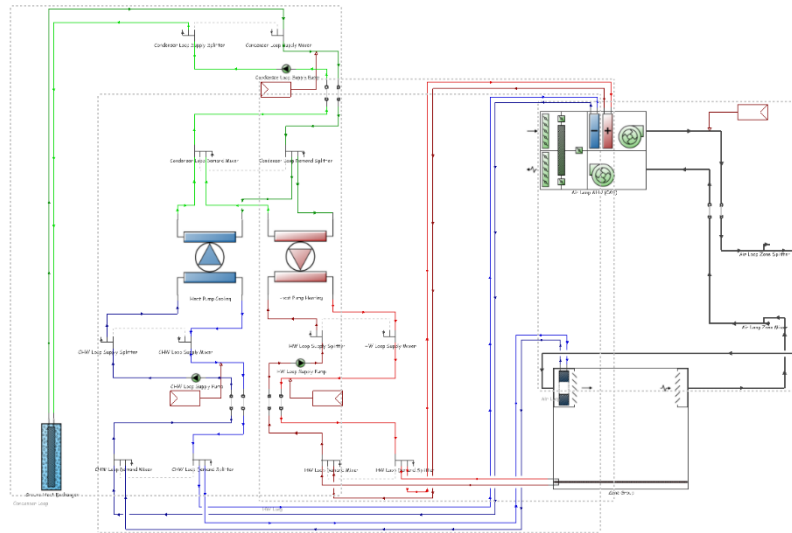


Fig. 3. The whole HVAC system set in the building

The heat pumps and the ground heat exchanger are selected considering the total design heating and cooling capacities. The total design heating capacity calculated through heating design calculation is 4.85 kW. This capacity includes 1.25 design margin that a safety factor. The total design heating and cooling capacities are the same for both of the cases. The total design cooling capacity including 1.15 design margin is 6.6 kW. Carrier 50PSW036 heat pump is selected for the heating purpose in the hot water loop. The rated heating capacity of this pump is 12.6 kW. This value is sufficiently greater than the total design heating capacity. The rated load side flow rate of the pump is $0.000570 \text{ m}^3/\text{s}$. Carrier 50PSW036 heat pump is also selected for the cooling purpose in the chilled water loop. The rated cooling capacity of this pump is 10.8 kW. This value is sufficiently higher than the total design cooling capacity calculated through cooling design calculation. The rated load side flow rate of the pump is $0.000570 \text{ m}^3/\text{s}$.

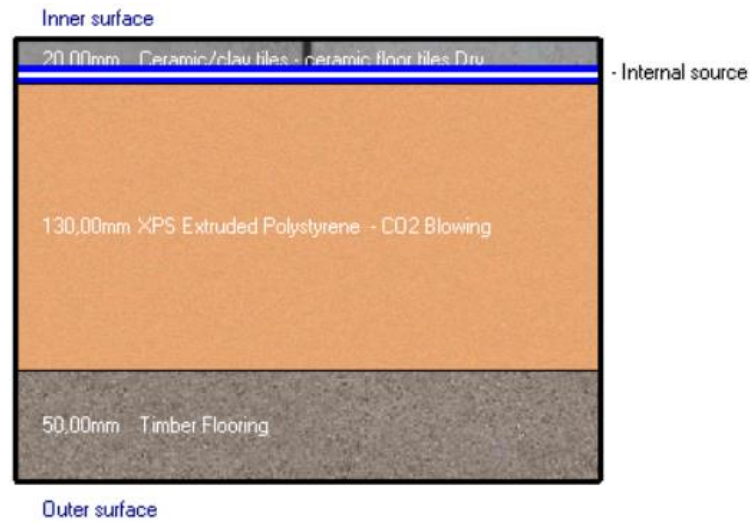
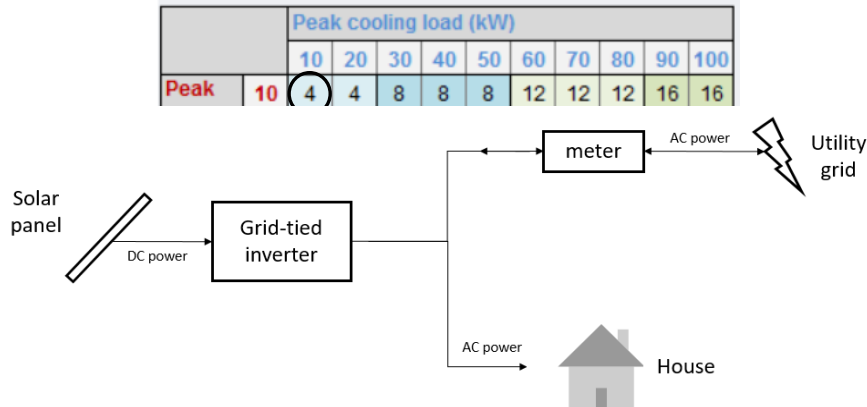


Fig. 4. The cross-section of the internal floor

The ground heat exchanger which belongs to the condenser loop is selected taking into account Tab.1. The most appropriate heat exchanger is the U-tube 76m 4-boreholes one. The procedure of selecting the heat exchanger starts with performing heating/cooling design calculations to obtain peak heating and cooling loads in kW. The apse and the ordinate of Tab.2 demonstrate these peak loads. The minimum borehole number for the model is determined accordingly. The maximum flow rate for the ground heat exchanger should normally be entered as the sum of the rated flow rates for all connected heat pumps including those for heating and cooling. The current HVAC system has one heat pump for heating purpose, one heat pump for cooling purpose. The sum of their rated flow rates is $0.00114 \text{ m}^3/\text{s}$. This value is entered as both the design flow rate and the maximum flow rate of the ground heat exchanger.

Table 4. Ground heat exchanger minimum borehole number selection, [6]

The electric load center in the study includes constant-efficiency PV panels which



are mounted on a façade and on the roof. An inverter in the grid-tied solar system converts DC power generated by the panels into AC power utilized in the house or sent back to the utility grid in case. The simplified solar system is depicted in Fig.5.

Fig. 5. The grid-tied solar system

4 Results

Tab.2 lists the annual site and source energy calculated through dynamic thermal calculations by EnergyPlus. It should be noted that Case 2 is the only one which benefits from solar power. Tab.3 lists the electric loads satisfied in Case 2. Net source energy in Case 2 is lower than zero. Therefore, it can be stated that the configuration in this case makes the building a positive net zero energy building. The generated solar power, electricity over-production etc. in Case 2 is shown in Tab.3.

Table 5. The annual site and source energy

	Case 1	Case 2
Total Site Energy	5236.5	5223.9
Net Site Energy	5236.5	-2567.8
Total Source Energy	16584.0	16544.0
Net Source Energy	16584.0	-8132.3

The study also demonstrates monthly changes on annual basis. Fig.6-7 show the monthly change of net source energy in the cases. The less this parameter is, the more NZEB characteristic is achieved. In Case 1, this parameter cumulatively positive because there is no on-site electricity generation by renewables each month to outweigh

the electricity supplied from the utility grid. Therefore, in Case 1, the balance of the net source energy keeps rising. In Case 2, starting from March to November, the net source energy keeps decreasing. The highest monthly decreases are in summer due to the availability of sunlight. The highest increase is in December due to the deficiency of sunlight. In the end of the year, the balance of the net source energy in Case 2 is around -8000 kWh. The total source energy of Case 2 is approximately 16500 kWh as depicted in Tab.2. The half of this parameter is almost the same as the net source energy obtained in Case 2. This is one of the purposes of the study and it is met. Since the net source energy of Case 2 is below zero, the building is a positive net energy building. It is another purpose of the study and it is met, too.

Table 6. Electric loads satisfied in Case 2

Case 2		
	Electricity [kWh]	Electricity [%]
Photovoltaic Power	8201.9	157.0
Power Conversion	-410.1	-7.9
Total On-Site Electric Sources	7791.7	149.2
Electricity Coming From Utility	3713.4	71.1
Surplus Electricity Going To Utility	6281.3	120.2
Net Electricity From Utility	-2567.8	-49.2
Total On-Site and Utility Sources	5223.9	100.0
Total Electricity End Uses	5223.9	100.0

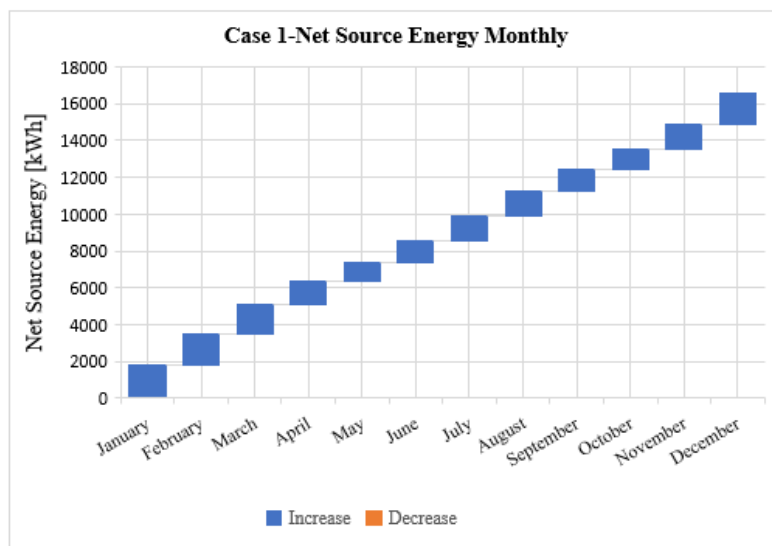


Fig. 6. Case 1- Net source energy monthly

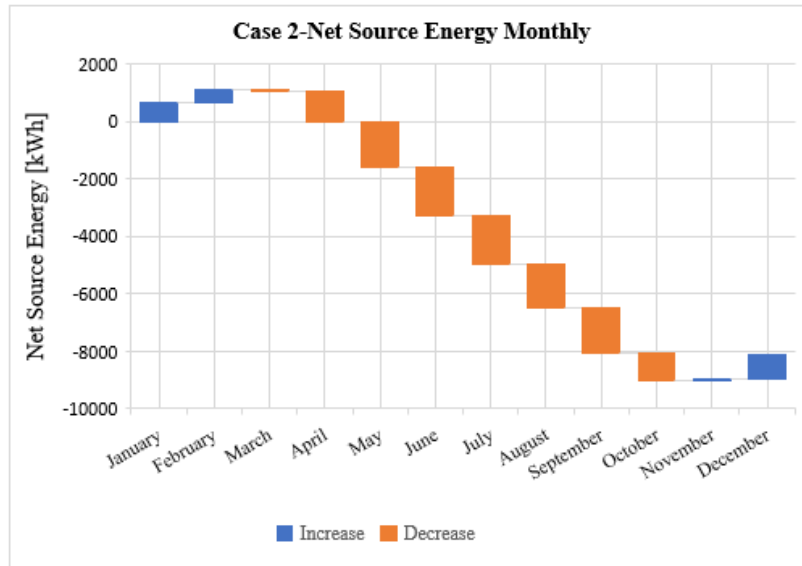


Fig. 7. Case 2- Net source energy monthly

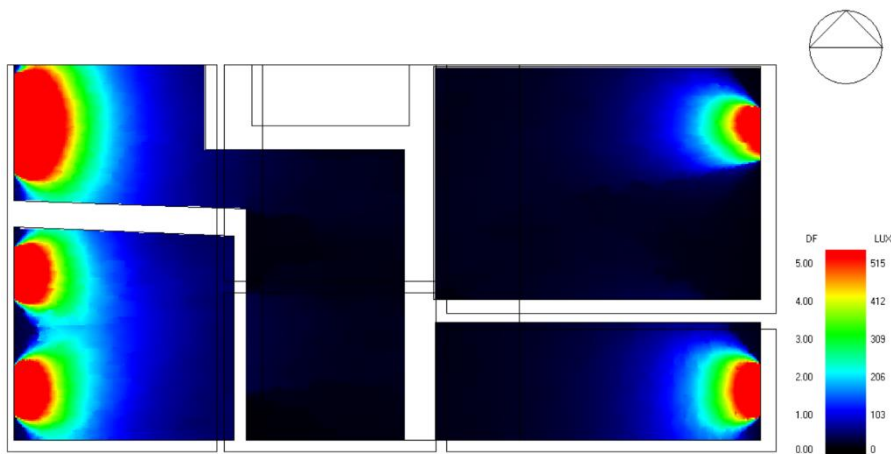


Fig. 8. The ground floor daylight illuminance map

The illuminance map of the ground floor is seen in Fig.8. The scale varies from 0 to 515 lux. According to Fig.7, the brightest domains are by the windows which are located mostly on the west and the eastern façades. The central domain where the dining table is put has no window in the south wall and the holes in the other directions are too far from the windows. Therefore, the sunlight cannot penetrate enough to light up the domain above 50 lux. The domain by the external main door is brighter and wider than the parts. This is because the door is made up of two sections, i.e. the upper part acts as

a windows which has frames on it, the lower part acts as an opaque metal door. The more the window has area which transmits the natural light, the more the light brightens the related zone. The scale is limited by 5% daylight factor in order to study the distribution explicitly. There is neither window shading nor local shading on the external windows.

Table 7. Recommended indoor light levels [6]

	Illumination [lux, lumen/m ²]
Dining area	175
Kitchens	500
Bedroom	250
Stair way	75
Bathroom	200

The General Services Administration, GSA, recommends the indoor light level depicted in Tab.4. The building consists of a dining room and a bathroom, a living room, a domestic circulation zone and two bedrooms. There are domains in the dining rooms where the illumination is lower than 175 lux. Most of the dining room on the working plane has an illumination which is lower 500 lux. This situation is not recommended by GSA. Moreover, the circulation area is too dark. Obviously, their illumination is lower than 200 lux. This is another unsuggested issue by GSA. The kitchen is partially satisfied in terms of illuminance distribution. The interior part of the kitchen is too dark. The illuminance is in this part is around 300 lux which is lower than suggested 500 lux. The average illuminance in the bathroom seems to be around 150 lux. This value is quite close to the recommended level which is 200 lux. The average illuminance in the stair way between the ground floor and the first floor is not obvious. The recommended value is 75 lux as shown in Tab.4. In order to clarify the distribution at low illuminance, the maximum density factor could be decreased, thus shrinking the scale. The average illuminance in the bedroom in the first floor seems to be 250 lux which satisfies the recommended value.

The exposure area of the studied building is roughly drawn to analyse the movement of air by the building considering regional, statistical wind direction and velocity already defined on DesignBuilder. Fig.9 demonstrates the velocity vectors on the selected plane. The wind runs into one façade of the building creating a positive gauge pressure region while a recirculation zone is created in the downstream of the house. The scale is from 0 m/s to 6.8 m/s.

The external CFD results can be beneficial further to assess the pedestrian comfort, to position the natural ventilation openings and to arrange the facilities in the site. The external vents regulate the external ventilation. The outside air enters and leaves the

house through these vents. Therefore, their position on the external walls and on the roof are important. These external boundaries are surrounded with regions whose pressure levels differentiate. According to the results obtained by this study demonstrate that the vents that intend letting the outside air in should be positioned on the eastern façade where the pressure reaches up to 8 Pa. The inside air tend to get out of the house through the external ventilation and infiltration. The external vents not only take the role of getting the outside air in but also getting it out. A suction zone is created in the downstream of the house. The air tends to move from low-pressure zone to high-pressure zone. If the external vents are also positioned on the western façade, the inside air can leave the house feasibly.

Some regions are exposed to high-velocities, some are exposed to low-velocities in the computational domain. It would be wise to construct parks, bus stations, restaurants with outdoor seating etc. in the low-velocities regions. The high-velocities can be beneficial to generate electricity via small wind turbines.

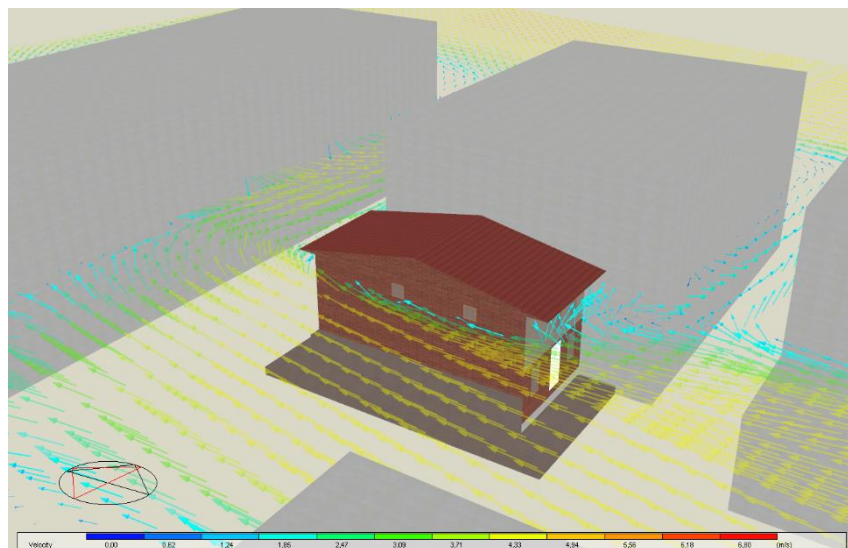


Fig. 9. Velocity vectors on the plane which is horizontally at 3.6 m from the ground

5 Conclusion

The study presents an overall look at the net zero energy building concept providing an example of conversion of a residential building. In order to perform the conversion in detail, a capable software is needed. For this purpose, DesignBuilder V5.5.2.007 is selected. Designbuilder offers an advanced user interface to EnergyPlus, the industry standard building energy simulation tool. EnergyPlus provides advanced dynamic thermal simulation. It reports solar gains, surface temperatures, it assesses passive

performance, thermal mass and it sizes heating and cooling system. EnergyPlus 8.6.0.001 version is used in the study. In addition to EnergyPlus, Radiance software is used for daylighting textures. It provides a detailed multi-zone physics-based calculation of illumination levels on the working place of a building using fixed static external lighting conditions and sky distributions. Radiance and EnergyPlus both are embedded to DesignBuilder.

There are two cases in the study. Both the cases are different from the actual building from constructional point of view. In reality, the internal floors are not heated, the positions and the dimensions of the external windows are different from those built in the model and the HVAC system built in the model has not been installed yet. Case 1 takes into account the revised external windows and the internal floors including the heating tubes in them. Case 2, additionally, considers the on-site electricity generation. For this purpose, an electric load center is built in the model. The southern façade is coated with photovoltaic panels. Two more PV panels are mounted on the roof.

The net source energy in Case 2 is lower than zero kWh and sufficiently low. The passive performance is improved compared to the initial condition thanks to the heated floors and the new internal floors.

The daylighting results are partially satisfactory. The dining room is too dark, particularly its interior part while the other zones meet the minimum requirements. A window could be added to the dining room on the southern façade. On the other hand, this addition would contradict the original house plan and it would reduce the available area on the southern façade where the PV panels are installed.

The external CFD analysis provide an idea on the air movement by the house. The analysis is not confined only with the space in the vicinity of the house, it also considers the other blocks in the region that surround the building. The other blocks are roughly positioned and drawn but their existence in the study improves the analysis, they strengthen the results.

The study could be enriched with more precise sketching of the district where the house is located. The external CFD analysis is isothermal and steady-state. The analysis could be transient so that the air distribution could be observed importing the results at the instants of time. A transient solution is not a must-have but it would help the researcher to figure out the movement of flow with time. Streamlines could be defined in the analysis. They help the researcher to see the trajectories of the flow. Each streamline represents a particle. Once a streamline is defined, a particle is put at the start of one path-line, then the particle flows through the computational domain as indicated by the trajectory. Therefore, streamlines would be helpful to analyze the movement of air in the domain. The computational domain could be enlarged with other blocks in the district. It would broaden the point of view of the researcher as commented on the CFD results. However, each complication brings an uncertainty and increases the computational time. An internal CFD analysis is not performed in the study. A thermo-fluid

analysis would be helpful to measure the performance of the HVAC system, more specifically air handling unit.

The solar system of the building is on-grid. For this purpose, an inverter is used. The system could be off-grid with an addition of batteries and a Diesel generator as an auxiliary energy source. The battery bank requires a more capable inverter. The inverter in the study is obliged to cope with the DC power coming from the solar panels and the AC power from the utility grid. The voltage of the batteries is likely to be different from that in the DC transmission line between the panels and the on-grid inverter. The batteries should be coupled with a charge controller that drops the voltage to that of the batteries in case a battery bank is added to the solar system. Moreover, the charge controller controls the charge of the batteries. In short, the grid-tied solar system could be switched to either an off-grid solar system or a hybrid solar system.

The domestic hot water system extracts instantaneous electricity to heat up the water for end-use. This energy source could increase the electricity coming from the grid. If there was a solar thermal panel in the water heating system, the DHW system could be less costly as the water in the water tank would be heated up through solar energy and stored. Without the solar thermal panel, particularly at nighttime, instantaneous electricity is supplied from the grid.

The study further could be enriched with a parametric solution between defined parameters in a range. For this purpose, wall-to-window ratio, the collecting area of PV panels, set point and setback temperatures in the building level could be design variables to figure out the optimal total energy consumption, total carbon dioxide consumption, heating or cooling load. Apart from the parametric solution, an optimization could be implemented to minimize the carbon dioxide emission or the discomfort in the building level. Moreover, different energy codes could be studied and they could be compared. The positioning of PV panels on the roof or on the external walls, the use of storage, different HVAC and domestic hot water systems with different sources could be studied additionally. However, there are restrictions faced due the original plan of the building once a change is intended making. The studied HVAC system, the heated floors are of the constraints appointed by the householder. Finally, the study does not involve a cost analysis. It is because the green technologies, particularly PV panels, get more affordable with time with no doubt and DesignBuilder is a British software, thus the costs the software provide are not trustable considering that the studied building is in Istanbul. The local Turkish technology suppliers could provide cheaper or more expensive products.

References

1. Building Design & Construction Magazine, Zero and net-zero energy buildings, <https://www.bdcnetwork.com/sites/bdc/files/Zero%20and%20Net-Zero%20Energy%20Buildings%20%2B%20Homes.pdf>, last accessed 2011/03/01.
2. Sartori, I., Pless, S., Marszal, A., Voss, K., “Criteria for definition of net zero energy buildings”, EuroSun 2010, January 2010.
3. The National Institute of Building Sciences, “A common definition for zero energy buildings”, September 2015.
4. The American Institute of Architects, AIA, Net-zero energy design and the living building challenge, https://www.bdcuniversity.com/sites/sgc-university/files/BDC_AIA_BDCSept2016.pdf, last accessed 2016/09/01.
5. Vancouver City Council, Passive design toolkit for homes, <https://vancouver.ca/files/cov/passive-home-design.pdf>, last accessed 2019/01/05.
6. DesignBuilder user manual, GSHP study case, <https://designbuilder.co.uk/helpv4.5/Content/GSHPCaseStudy.htm>, last accessed 2018/08/22.

The Synthesis of TiO₂/TiO_xN_y Mushrooms-Like Nanocomposites Based on Nanoporous Anodic Aluminum Oxide Template for Hydrogen Generation

Mohamed Rabia¹, Mohamed A. Basyooni² Sodky H. AboLaila³, Huaping Zhou⁴, Mohamed Shaban¹, Yong Lei^{*1}, Ashour M. Ahmed¹

¹Nanophotonics and Applications Lab, Physics Department, Faculty of Science, Beni-Suef University, Beni-Suef 62514, Egypt

²Department of Nano Science and Nano Engineering, Institute of Science and Technology, University of Necmettin Erbakan, Konya 42060, Turkey

³Physics Department, Faculty of Science, Sohag University, Sohag 82524, Egypt

⁴Institute of Physics & IMN Macronano®, Ilmenau University of Technology, Ilmenau 98693, Germany

Abstract. TiO₂/TiO_xN_y hollow mushrooms-like nanocomposite photocatalyst was prepared using atomic layer deposition (ALD) and reactive direct current magnetron sputtering, respectively. The preparation process depends on the aluminum oxide template (AOT) that was fabricated using the two-step anodization process after the Ni imprinting process. The chemical, morphological, and optical properties were recorded using different analyses such as XRD, SEM, EDX, and UV-Vis. From the SEM analyses, the AOT pore size increases from 177 to 305 nm after the pore widening process in H₃PO₄. The diameter of the TiO₂ in the upper part is 352 nm, while the diameter of the TiO₂/TiO_xN_y composite is 355 nm in the upper part. The estimated band gap values of TiO₂ and TiO₂/TiO_xN_y are 3.1 and 2.25 eV, respectively. From the values of band gaps, there is a clear enhancement in the optical absorption of the nanocomposite bilayers. The photoelectrochemical (PEC) behaviors of the TiO₂/TiO_xN_y electrodes supported in Au/Ni metal thin film was measured in 1M NaOH as scarifying reagent. The thermodynamic parameters were calculated, in which ΔE , ΔH^* , and ΔS^* values are 16.75 kJmol⁻¹, -15.87 kJmol⁻¹ and 115.65 kJmol⁻¹K⁻¹, respectively.

Keywords: TiO₂/TiO_xN_y nanocomposite, band gap, hydrogen generation

1 Introduction

The usage of solar energy for water splitting to hydrogen and oxygen has been considered as an ultimate process to solve energy and environmental crises. Many works have been done to catalyze the evolution of H₂ from aqueous solutions with and without sacrificial reagents [1-5]. One of the most favorable catalysts is TiO₂ because of its photocatalytic performance, availability, long-term stability, unique physical and chemical properties, and nontoxicity [5,6]. In recent years, the research on preparation and characterization of TiO₂ nanoparticles have more attention due to its massive uses

in photocatalysis, gas sensors, quantum dot and dye-sensitized solar cell, energy storage materials, and degradation of dye pollutants [7-14]. TiO_2 have two common polymorphism rutile and anatase [15-17]. It possesses a wide band gap ($E_g \sim 3.0$ eV for rutile and ~ 3.2 eV for anatase) which induces the low photocatalytic performance for using solar energy. Besides, the high rate of electron-hole recombination moderates the photocatalytic performance of TiO_2 .

For photocatalytic enhancement performance, many techniques such as chemical synthesis and ion implantation have been used to extend the photocatalytic response of TiO_2 to the visible light range [18-20]. One of the essential techniques is to deposited metals on the surface of TiO_2 which can produce traps in its energy gap to capture the photo-induced electrons or holes, leading to the reduction of electron-hole recombination in photocatalytic processes and the increase in the absorption capability for visible light of TiO_2 particles. Although many researchers had tried to improve photocatalytic capabilities of TiO_2 , till now, there is no efficient way to reduce the rate of electron-hole recombination. Jieun Kim et al. [28] used TiO_2 -loaded spherical ZnS nano/micro-composites for high hydrogen production from methanol/water solution photo-splitting. Elies Molins et al. [29] used sol-gel synthesis and characterization of TiO_2 decorated with Au nanoparticles for hydrogen production. Islam et al. [30] used hydrazine-based synergistic Ti(III)/N doping of surfactant-templated TiO_2 thin films for enhanced visible light photocatalysis.

Recently, titanium nitride (TiN) has been intensively studied as an alternative plasmonic material, because it can overcome most of the drawbacks of conventional plasmonic metals [31]. TiN has a bright metallic golden color with good optical and hardness properties. Moreover, its high electronic and thermal conductivities are appealing to plasmonic applications. The optical properties of TiN are essential to its plasmonic performance [32].

On the basis of the established concepts and ideas, a strategy on the new material structure and design are highly desirable to boost the catalytic performance via the surface modification of the TiO_2 [33-34]. As a strong candidate, TiO_xN_y is an n-type semiconductor that shows unique physicochemical properties and large-scale applicability in various fields, including nanoelectronics, catalysis, sensors, photonics, biomaterials, and biomedicine [35]. To the best of our information, no relevant research combining TiO_2 nanotubes (TNR) arrays and TiO_xN_y has been reported for PEC water oxidation. Therefore, the formation of a heterojunction ($\text{TiO}_2/\text{TiO}_x\text{N}_y$) based on the oxynitride and TNR arrays can overcome the drawbacks of the TNR array with coupling to the favorable features of TiO_xN_y nanoparticles having a size of ~ 15 nm, contributing to the increase of PEC performance.

In this research, $\text{TiO}_2/\text{TiO}_x\text{N}_y$ hollow mushrooms-like nanocomposite photocatalyst was prepared using atomic layer deposition (ALD) and reactive direct current magnetron sputtering, respectively. The chemical, morphological, and optical properties were recorded using different analyses. The photoelectrochemical (PEC) behaviors of the $\text{TiO}_2/\text{TiO}_x\text{N}_y$ electrodes supported in Au/Ni metal thin film was recorded on the electrochemical station.

2 Experimental part

2.1 Synthesis of aluminum oxide template (AOT)

The preparation of AOT was carried out using the Ni imprinting method [36]. Firstly, the aluminum foil was electropolished using a mixture of $\text{HClO}_4:\text{C}_2\text{H}_5\text{OH}$ (1:1) for 3 min at 2°C . Ni imprinting molds with a hexagonal order nanopillar array which was previously prepared from a Si master mold with 400 nm spacing shallow array. The Ni imprinting mold was used for the imprinting process on Al foil. Typically, the imprinted Al foil with 400 nm spacing nano shallow array was obtained by applying a pressure of $\sim 10\text{ kN cm}^{-2}$ for 3 min using an oil pressing system. After that, the first anodization step on the imprinted Al foil at 160 V in a mixture solution of $\text{H}_2\text{O}:\text{H}_3\text{PO}_4$: ethylene glycol (1:200:100) at 2°C . Secondly, the chemical etching process for the patterned oxide layer was carried out using a mixture of H_2CrO_4 (1.5 wt %) and H_3PO_4 (6 wt %) at 60°C for 12 h. After that, the second anodization step was carried out for 2 h using the same conditions of the first anodization step. Finally, the pore widening process was carried out from 6 wt.% H_3PO_4 [37].

2.2 Synthesis of $\text{TiO}_2/\text{TiO}_x\text{N}_y$

$\text{TiO}_2/\text{TiO}_x\text{N}_y$ hollow mushrooms-like nanocomposite photocatalyst was prepared using atomic layer deposition (ALD) and reactive direct current magnetron sputtering, respectively. TiO_2 closed nanotubes were synthesized on the previously prepared AOT. All the reactions were carried out in Picosun SUNALE R150 ALD System at 300°C . Titanium (IV) chloride and distilled-water (H_2O) were used as the precursors of Ti and O, respectively, in which the preparation process carried out for 300 cycles.

The TiO_xN_y was prepared using the DC sputtering (sputtering LA440S Ardenne). Sputtering was achieved from Ti metallic target (99.9%) using a mixture of N_2 and Ar with 75 sccm to 25 sccm, respectively. Sputtering was started after reaching a base pressure of 6.7×10^{-7} mbar, while the working pressure was 1.3×10^{-2} mbar. The sputtering rate was 6 nm/min. After getting the multilayer system out of the chamber, the combustion process was carried out in atmospheric air at 300°C and for 2 h. From this combustion process, the oxidation of TiN to TiO_xN_y occurs.

2.3 Characterization and Measurement

Surface morphologies of nanomaterials were examined by SEM (Auriga Zeiss FIB) at an accelerating voltage of 5 kV. EDAX analysis was carried out using a unit attached to the SEM. X-ray diffraction (XRD) pattern was obtained by Bruker/Siemens D5000 diffractometer. The optical behaviors of the samples were examined using UV-Vis double beam spectrophotometer (Perkin Elmer Lambda 950).

2.4 Hydrogen generation process

The photoelectrochemical (PEC) behaviors of the $\text{TiO}_2/\text{TiO}_x\text{N}_y$ photoelectrode supported in Au/Ni metal thin film were recorded on the electrochemical station (CHI660E, USA). The Photoelectrochemical system consists of a three-electrode

system with the $\text{TiO}_2/\text{TiO}_x\text{N}_y$ as photoanode (a cyclic shape with a diameter of 1 cm), Ag/AgCl reference electrode, and a Pt plate as the counter electrode. 1 M NaOH was used as an electrolyte. 400 W Xe lamp (Newport) was used for light illumination during the measurement with a power density of 100 mW cm^{-2} .

3 Results and discussion

3.1 SEM, EDAX, and XRD analyses

The SEM image of the template is shown in Figure 1(A). From this Figure, the template pores are about 177 nm in diameter (before widening). After pore widening using H_3PO_4 at 60 min for 20 min, the pore of AOT increase to 305 nm (Figure 1B). Figure 1C, shows clearly demonstrate the long-range and perfect ordering of TiO_2 nanotubes that prepared inside the AOT using the ALD. These TiO_2 closed nanotubes are appeared after the template removal using NaOH solution.

A mixture of 20 nm Au and Ni metals are used as a supporter of TiO_2 nanotubes after the template removal. The diameter of these TiO_2 closed nanotubes (upper part) is about 352 nm. The inset cross section Figure shows the hollow nanotubes. After DC sputtering of TiN and heat treated at 300°C , the hollow mushrooms-like nanocomposite photocatalyst is consisted, with the diameter of the nanocomposite size of 355 nm. In which the chemical composition for the composite after combustion in the air environment is $\text{TiO}_2/\text{TiO}_{2.22}\text{N}_{0.28}$ as revealed by EDAX analysis, Figure 2A.

The XRD pattern of $\text{TiO}_2/\text{TiO}_x\text{N}_y$ nanocomposite is shown in Figure 2B. All peaks are indexed to anatase TiO_2 phase [JCPDS card no.: 01-089-4921]. No other peaks belonging to titanium oxynitride or titanium nitride phases are seen. This specifies that nitrogen atoms may occupy the locations of oxygen atoms in TiO_2 crystal lattice or they are positioned at the grain boundaries and form amorphous portions.

3.2 Optical absorption and bandgap calculation

The study of the optical absorption of the prepared $\text{TiO}_2/\text{TiO}_x\text{N}_y$ hollow mushrooms-like nanocomposite photocatalyst is important for the application of these films in the photocatalytic H_2 generation. The absorption of the TiO_2 and $\text{TiO}_2/\text{TiO}_x\text{N}_y$ composite is shown in Figure 3A. The absorption intensity of TiO_2 increase after the addition of TiO_xN_y coating. This is attributed to the narrower bandgap of TiO_xN_y comparing with TiO_2 [38]. The absorption spectrum of the $\text{TiO}_2/\text{TiO}_x\text{N}_y$ nanocomposite shows a sharp increase starting around 600 nm, after which a peak in the UV region at 290 nm is observed which is attributed to $\Pi-\Pi^*$ transitions from the titanium ions. Based on the direct allowed transition type, the optical band gap (E_g) of all samples is estimated using Tauc's equation [39];

$$\alpha h\nu = \beta(h\nu - E_g)^{1/2} \quad (1)$$

Here α is the absorption coefficient, β is a constant, h is the Planck constant, and ν is the light frequency. The absorption coefficient (α) depends on the absorbance (A) and is given by [40], where d is the thickness:

$$\alpha = \left(\frac{2.303}{d}\right) A \quad (219)$$

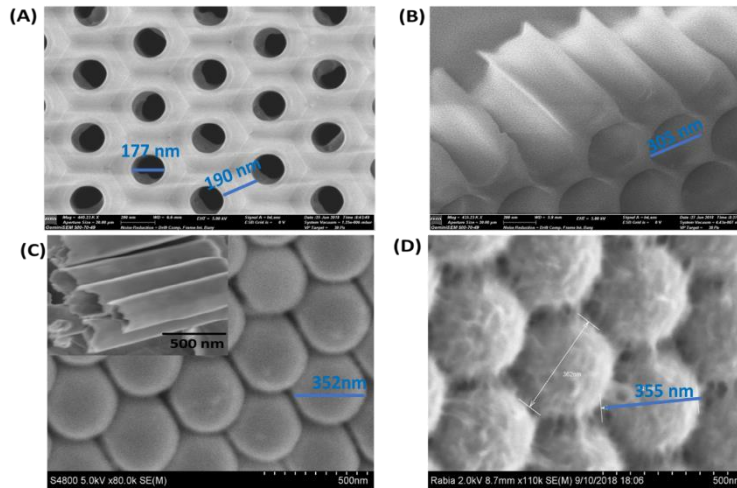


Fig. 1. The SEM image of the AOT (A) before and (B) after pore-widening. (C) closed nanotubes of TiO₂, the inset is the cross section of the closed tubes, and (D) TiO_xN_y coated the TiO₂.

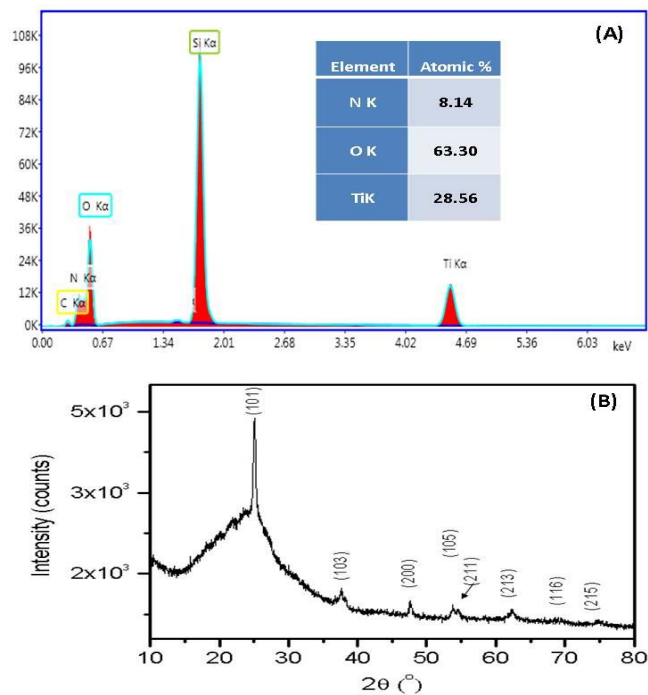


Fig. 2. (A) EDAX spectrum of TiO_xN_y film prepared by deposition of TiN layer Si substrate and heat treated at 300 °C for 2 h and (b) XRD of TiO₂/TiO_xN_y.

The band gap values are estimated by extrapolating the linear part of the $(\alpha h\nu)^2$ versus $h\nu$ curve to intercept with the $h\nu$ axis as shown in Figure 3B. From Figure 3B, the estimated band gap values of TiO₂ and TiO₂/TiO_xN_y are 3.1 and 2.25 eV, respectively.

From the values of band gaps, there is a clear enhancement in the optical absorption of the nanocomposite bilayers. So, $\text{TiO}_2/\text{TiO}_x\text{N}_y$ electrode can be suitable for application in H_2 generation systems.

3.3 H_2 generation

The PEC measurements of the $\text{TiO}_2/\text{TiO}_x\text{N}_y$ electrode were taken in 1 M NaOH solution at room temperature with a sweep rate of 20 mV/s.

The measurements were taken place in dark and under illumination of 400 W Xenon lamp without an optical filter for several times as shown in Figure 4. The photocurrent density (I) values in dark and light are 3.25 and $7.43 \pm 0.3 \text{ mA}\cdot\text{cm}^{-2}$, respectively. The high value of the photocurrent density in light is a pre-indicator for the efficient PEC water splitting. The significant dark current is ascribed to the charge transfer that promoted by ionic currents come from NaOH source electrolyte [41]. Also, the photocurrent density increased by increasing the applied voltage under illumination of a 400 W Xenon lamp due to an increase in the tunneling mechanism.

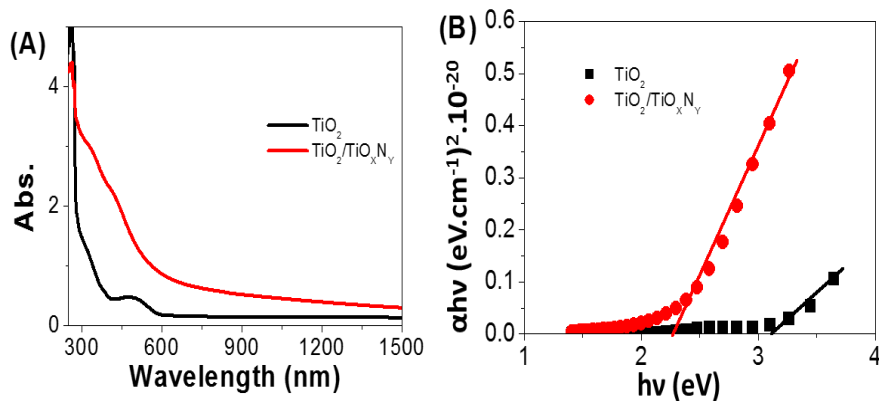


Fig. 3. (A) Optical absorbance spectra and (B) band gaps values for TiO_2 and $\text{TiO}_2/\text{TiO}_x\text{N}_y$ nanocomposite.

The stability of the $\text{TiO}_2/\text{TiO}_x\text{N}_y$ photoanode is investigated for a long time and shown in Figure 5A. During these experiments, a small bias voltage of 1 V is applied. From Figure 5A, the J_{ph} values are decreased in the first period and then remain constant at nearly $1.8 \text{ mA}/\text{cm}^2$ due to the increase in the accumulation of the ionic charges. This result suggests that the $\text{TiO}_2/\text{TiO}_x\text{N}_y$ has high chemical stability and a longer lifetime for solar hydrogen production from water. To investigate the PEC performance of $\text{TiO}_2/\text{TiO}_x\text{N}_y$, the incident-photon-to-current conversion efficiency (IPCE) was measured under monochromatic illumination conditions, as shown in Figure 5B.

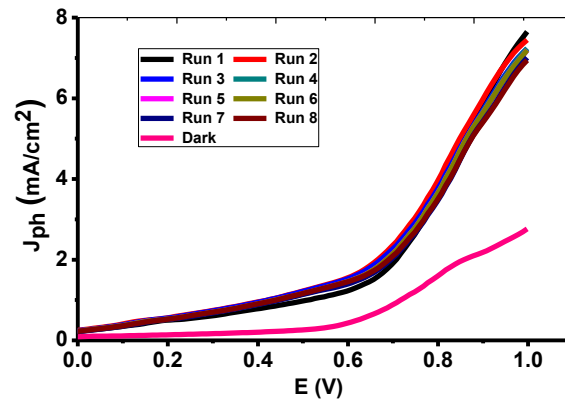


Fig. 4. The PEC behaviors for the TiO₂/TiO_xN_y photoanode in dark and under white light illumination at room temperature.

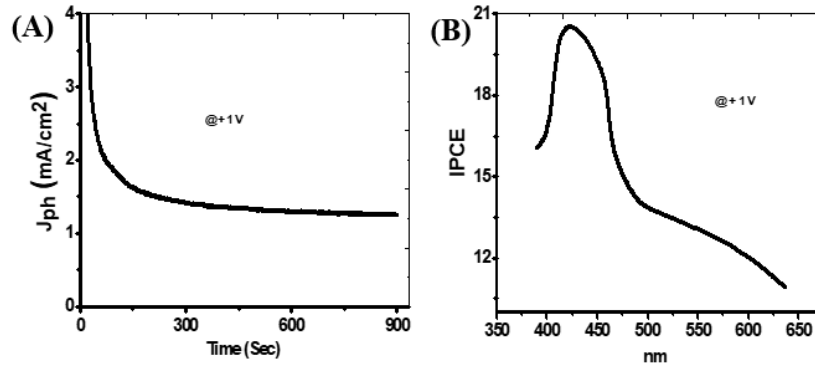


Fig. 5. (A) Current - time characteristic under white light illumination, (A) IPCE % as a function of the wavelength for the TiO₂/TiO_xN_y photoanode

The IPCE is a measure of the ratio of the number of photogenerated electrons taking part in the redox reactions to the number of incident monochromatic photons as a function of the wavelength. The IPCE was calculated at an applied potential of 1 V from equation (3)

$$\text{IPCE} = \frac{1240}{\lambda \text{ (nm)}} \frac{J_{\text{ph}} \text{ (mA/cm}^2\text{)}}{P_{\text{light}} \text{ (mW/cm}^2\text{)}} \times 100 \text{ (\%)} \quad (3)$$

where J_{ph} is the photocurrent density at that particular wavelength of incident light; λ is the wavelength of the illuminating monochromatic light and P_{light} is the illuminating light power density. The optimum IPCE% value of TiO₂/TiO_xN_y photoelectrode is 20.4% at 420 nm as a result of high absorption of light.

The effect of temperature from 20-55° C on TiO₂/TiO_xN_y electrodes for H₂ generation is shown in Figure 6A. From this Figure, the J_{ph} values increase with temperature. The

increase in photocurrent values under the temperature is due to the increase of the ions mobility with temperature. So, the rate of H₂ generation under different temperatures can be replaced by the I value.

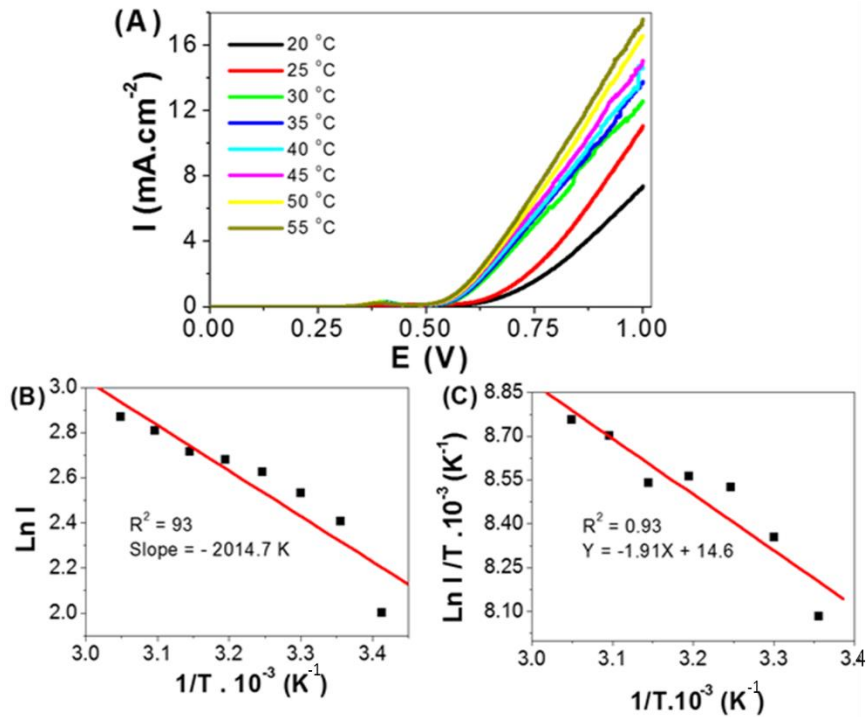


Fig. 6. (A) The effect of temperature on H₂ generation process, (B) plot of the current density against reciprocal of temperature, and (C) plot of current density/T against reciprocal of temperature.

The activation energy (E_a) of the reaction can be calculated using the following Arrhenius equation 3:

$$k = A e^{\frac{-E_a}{RT}} \quad (4)$$

Here k is the rate constant, R is universal gas constant, and T is the absolute temperature. The relation between reciprocal of temperature and $\ln(I)$ values (rate of reaction) is presented in Figure 6B. From the slope value, the E_a is found to be 16.75 kJ mol⁻¹. This value is small, so the prepared TiO₂/TiO_xN_y electrode is very efficient for H₂ generation reaction. In addition, the enthalpy ΔH^* and entropy ΔS^* for the H₂ generation reaction can be calculated from Figure 6C using Eyring equation:

$$k = \frac{T \cdot k_B}{h} e^{\frac{\Delta S^*}{R}} e^{\frac{-\Delta H^*}{RT}} \quad (5)$$

Here k_B is Boltzmann's constant and h is Planck's constant. The plot of $\frac{1}{T}$ versus $\ln \frac{k}{T}$ gives a straight line. From the slope and intercept values of this line, the ΔH^* and ΔS^* values are $-15.87 \text{ kJmol}^{-1}$ and $115.65 \text{ kJmol}^{-1}\text{K}^{-1}$, respectively.

4 Conclusions

$\text{TiO}_2/\text{TiO}_x\text{N}_y$ hollow mushrooms-like nanocomposite photocatalyst was prepared through AOT. The AOT was prepared using a Ni imprinting process, then two-step anodization method. From the SEM analyses, the AOT is formed in a very order semi-cylindrical shape. The diameter of the TiO_2 in the upper part is 352 nm, while the diameter of the $\text{TiO}_2/\text{TiO}_x\text{N}_y$ composite is 355 nm in the upper part. From the EDAX, chemical composition for the nanocomposite after combustion in the air environment is $\text{TiO}_2/\text{TiO}_{2.22}\text{N}_{0.28}$. From the optical analyses, the absorption intensity of TiO_2 increase after the addition of the TiO_xN_y coating. The estimated band gap values of TiO_2 and $\text{TiO}_2/\text{TiO}_x\text{N}_y$ are 3.1 and 2.25 eV, respectively. The application of $\text{TiO}_2/\text{TiO}_x\text{N}_y$ electrode for H_2 generation systems takes place using scarifying reagent NaOH. The current density values in dark and light are 3.25 and 7.43 mA.cm^{-2} , respectively. The thermodynamic parameters were calculated, in which ΔE , ΔH^* , and ΔS^* values are 16.75 kJmol^{-1} , $-15.87 \text{ kJmol}^{-1}$ and $115.65 \text{ kJmol}^{-1}\text{K}^{-1}$, respectively.

Acknowledgments. This research is a part of a project that supported from the Science Technology, Development Fund (STDF), Egypt, (short term fellowship) that obtained by Dr. Mohamed Rabia.

References.

1. M. Rabia, H.S.H. Mohamed, M. Shaban, S. Taha, *Sci. Report.* **8**, 1107 (2018)
2. K. Maeda, K. Domen, *J Phys.Chem. C* **111**, 7851 (2007).
3. K. Maeda, K. Domen, *J Phys.Chem. Lett.* **1**, 2655 (2010).
4. W. Fan, Q. Lai, Q. Zhang, Y. Wang, *J Phys.Chem. C* **115**, 10694 (2011).
5. A.L. Linsebigler, G. Lu, J.T. Yates Jr, *Chem. Rev.* **95**, 735 (1995).
6. J. Zhang, Q. Xu, Z. Feng, M. Li, C. Li, *Angewandte Chemie International Edition* **47**, 1766 (2008).
7. C.A. Linkous, G.J. Carter, D.B. Locuson, A.J. Ouellette, D.K. Slattery, L.A. Smitha, *Environmental Science & Technology* **34** 4754 (2000).
8. J.-K. Yang, A.P. Davis, *Environ. Sci. Technol.* **34**, 3796 (2000).
9. I. Hayakawa, Y. Iwamoto, K. Kikuta, S. Hirano, *Sensors and Actuators B: Chemical* **62**, 55 (2000).
10. Y. Zhu, J. Shi, Z. Zhang, C. Zhang, X. Zhang, *Anal. Chem.* **74**, 120 (2002).
11. M. Kouhnavard, S. Ikeda, N.A. Ludin, N.A. Khairudin, B. Ghaffari, M. Mat-Teridi, M.A. Ibrahim, S. Sepeai, K. Sopian, *Renewable and Sustainable Energy Reviews* **37**, 397 (2014).
12. M. Adachi, Y. Murata, J. Takao, J. Jiu, M. Sakamoto, F. Wang, *J. Am. Chem. Soc.* **126**, 14943 (2004).
13. T. Tatsuma, S. Saitoh, P. Ngaotranwiwat, Y. Ohko, A. Fujishima, *Langmuir* **18**, 7777 (2002).
14. G. Liu, T. Wu, J. Zhao, H. Hidaka, N. Serpone, *Environmental science & technology* **33**, 2081 (1999).
15. W. Xue-Wei, W. Da-Jian, L. Xiao-Jun, *Chinese Physics Letters* **26**, 077809 (2009).
16. M. Weissmann, L.A. Errico, *Physica B: Condensed Matter* **398**, 179 (2007).
17. M.Y. Manuputty, J.A.H. Dreyer, Y. Sheng, E.J. Bringley, M.L. Botero, J. Akroyd, M. Kraft, *Chem. Sci.* **10**, 1342 (2019).

18. Z. Jiang, Y. Liu, T. Jing, B. Huang, Z. Wang, X. Zhang, X. Qin, Y. Dai, *Applied Catalysis B: Environmental* **200**, 230 (2017).
19. R. Bacsa, J. Kiwi, T. Ohno, P. Albers, V. Nadtochenko, *J Phys.Chem. B* **109**, 5994 (2005).
20. R. Asahi, T. Morikawa, T. Ohwaki, K. Aoki, Y. Taga, *Science* **293**, 269 (2001).
21. G. Zhao, H. Kozuka, T. Yoko, *Thin Solid Films* **277**, 147 (1996).
22. J.-M. Herrmann, H. Tahiri, Y. Ait-Ichou, G. Lassaletta, A. Gonzalez-Elipe, A. Fernandez, *Applied Catalysis B: Environmental* **13**, 219 (1997).
23. J.-W. Yoon, T. Sasaki, N. Koshizaki, E. Traversa, *Scripta materialia* **44**, 1865 (2001).
24. A. Scalfani, J.-M. Herrmann, *Journal of Photochemistry and Photobiology A: Chemistry* **113**, 181 (1998).
25. V. Vamathevan, R. Amal, D. Beydoun, G. Low, S. McEvoy, *Journal of Photochemistry and Photobiology A: Chemistry* **148**, 233 (2002).
26. B. Xin, L. Jing, Z. Ren, B. Wang, H. Fu, *J Phys. Chem. B* **109**, 2805 (2005).
27. X.S. Li, G.E. Fryxell, C. Wang, M.H. Engelhard, *Microporous and Mesoporous Materials* **111**, 639 (2008).
28. J.-E. Kim, M.-S. Kang, *Bulletin of the Korean Chemical Society* **33**, 2133 (2012).
29. E. Molins, M. Benito, I. Mata, L. Martínez, L. Soler, J. Llorca, *MRS Advances* **2**, 3499 (2017).
30. S.Z. Islam, S.E. Rankin, *Mater. Chem. Phys.* **182**, 382 (2016).
31. P. Patsalas, N. Kalfagiannis, S. Kassavetis, *Materials* **8**, 3128 (2015).
32. Z. H. Cen, B.X. Xu, J.F. Hu, R. Ji, Y.T. Toh, K.D. Ye, Y.F. Hu, *J. Phys. D: Appl. Phys.* **50**, 075105 (2017).
33. M. Arunachalam, G. Yun, K. Ahn, W. Seo, D.S. Jung, S.H. Kang, *International journal of hydrogen energy*, **43**, 16458 (2018).
34. M. Pavlenko, K. Siuzdak, E. Coy, M. Jancelewicz, S. Jurga, I. Iatsunskyi. *International Journal of Hydrogen Energy*, **42**, 30076 (2017).
35. T.T. Chen, H.P. Liu, Y.J. Wei, I.C. Chang, M.H. Yang, Y.S. Lin, K.L. Chan, *Nanoscale* **6**, 5106 (2014).
36. Y. Mi, L. Wen, R. Xu, Z. Wang, D. Cao, Y. Fang, Y. Lei, *Adv. Energy Mater.*, **6**, 1501496 (2015)
37. M. Shaban, A.M. Ahmed, E. Abdel-Rahman, H. Hamdy, *Microporous and Mesoporous Materials*, **198**, 115 (2014).
38. S.H. Mohamed, O. Kappertz, J. M. Ngaruiya, T. Niemeier, R. Drese, R. Detemple, M. M. Wakkad, M. Wuttig, *Phys. Stat. Sol. A*, **201**, 90 (2004).
39. M. Shaban, M. Rabia, S. Ezzat, N. Mansour, E. Saeed, S.Sayyah, *J. Nanophoton.* **12**, 016009 (2018)
40. C. Chen, W. Yu, T. Liu, S. Cao, Y. Tsang, *Sol. Energy Mater. Sol. Cells*, **160**, 43 (2017).

Theoretical Model to Relate Morphology to Device Efficiency

Emine Meşe¹ and Nigel Clarke^{1,2}

¹University of Durham, Science Site, South Road, Durham DH1 3LE, UK

²University of Sheffield, Hicks Building, Hounsfield Road Sheffield S3 7RH UK
eminemese@yahoo.com, n.clarke@sheffield.ac.uk

Abstract. We have developed a computationally efficient method for modeling PV device, based on a mesoscopic drift-diffusion model, in 3D microstructures. It includes the photoactive layer modeling which is based on numerically generated morphologies. Polymer blend microstructures are generated using the Cahn-Hilliard model. The combined morphology/device performance is then explored in a systematic way.

Keywords: PV cells, morphology, device efficiency.

1 Introduction

Growing concerns over climate change and sustainability, renewable energy has come to play a central role on the long term future of energy supply. Solar cells have been one of the important energy conversion devices that can deliver electricity from sun light [1]. As the sun light shines to our planet, the electricity production via solar cells is expected endlessly without any payment for using the sun light. However, the electricity from solar cells is more expensive than conventional electricity from fossil fuel and/or nuclear power stations. The reason is related to the high manufacturing cost for conventional solar cells, which are mostly based on inorganic materials and need high temperature processes and expensive vacuum systems [1]. Thus, organic solar cells have attracted big attention due to being candidate for the low cost manufacturing of plastic solar modules featuring flexible, lightweight, ultrathin, roll able and bendable shapes. Power conversion efficiency of organic solar cells is low and required to be increased. However, such devices are critically dependent on the internal structure, or morphology, of the polymer constituents. The internal structure, or morphology, of the polymer constituents are explored in literature in detail [2], [3] and [4]. In addition power conversion efficiency of organic solar cells is explored in last decades e.g. [5-8]. Scott *et. al.* considered a simple mechanism of charge injection from metals to organic semiconductors [5], [6]. Amore exact treatment was developed by Buxton *et. al.* The model they developed enables to predict photovoltaic behavior for arbitrary morphologies [7], [8]. They illustrated the model by showing how diblock copolymer morphologies can be manipulated to optimize the photovoltaic effect in plastic solar cells. In this manner, they correlated photovoltaic properties with device structure and hence guide experiments to optimize polymer morphologies to meet photovoltaic needs [8].

However, their model was in 2D. In this study we extend their model to 3D microstructure which is a rather more realistic model. An increase obtained in efficiency which is agree with the exit results in literature e.g. [9-13].

Groves *et. al.* evaluated the accuracy of the first reaction method FRM as commonly used to reduce the computational complexity of mesoscale Monte Carlo simulations of geminate recombination and the performance of organic photovoltaic devices [12]. A wide range of carrier mobilities, degrees of energetic disorder, and applied electric field are considered. For the ranges of energetic disorder relevant for most polyfluorene, polythiophene, and alkoxy poly phenylene vinylene materials used in organic photovoltaic, the geminate separation efficiency predicted by the FRM agrees with the exact model to better than 2% [12].

Meng *et.al.* developed a model system for blend polymers. They obtained 2.2% power conversion efficiency using monte-carlo simulation method [13].

For emerging photovoltaic technologies to become commercially and technically viable, it is also important to understand how performance in the laboratory translates to the field [14].

The concept of three-dimensional 3D photovoltaic is explored computationally using a genetic algorithm to optimize the energy production in a day for arbitrarily shaped 3D solar cells confined to a given area footprint and total volume. Our simulations demonstrate that the performance of 3D photovoltaic structures scales linearly with height, leading to volumetric energy conversion, and provides power fairly evenly throughout the day [9]. Myers *et. al.* obtained about 6% efficiency in their macroscopic 3D photovoltaic tests [9].

A new study analyses the yearly changes in the energy yield of perovskite solar cells under simulated realistic temperature and irradiance conditions. These type of solar cells are one of the most promising next-generation photovoltaic (PV) technologies. The power conversion efficiency can reach 28% when used in a tandem configuration with silicon, which is greater than the current silicon record efficiency of 27.6% [14].

On the other hand the perovskite solar cells are unstable although there are various studies to gain stabilities [15-17].

The other interesting experimental technique used to increase the device performance is the Suzuki coupling procedure: Kettle *et. al.* report the optimization of OPV device performance from 2-ethylhexyl substituted PCPDTBT prepared by the Suzuki coupling procedure [18]. The current (J)–voltage (V) curves under AM1.5G conditions of the optimized PCPDTBT/C71-PCBM solar cells are studied in their work. Using this technique OPV cells with an average power conversion efficiency of 4.31% with J_{SC} 13.52 mA/cm², V_{OC} 0.648 V and FF 49.3, with the highest individual cell possessing a power conversion efficiency of 4.5% is obtained [18].

Numerically generated 3D morphologies and generation model the Cahn-Hilliard is given in Section 2. In this section drift diffusion which is used to explore the combined morphology/device performance. The results and discussion is given in Section 3 and the work is completed with a conclusion in Section 4.

2 Methods

2.1 Morphology

The known kinetic equation, which relates the time dependent composition with the thermodynamic driving force for phase separation, is given by equation (1) [3], [4].

$$\frac{\partial \phi(\mathbf{r})}{\partial t} = \nabla \cdot \left\{ M \left[\nabla \frac{\delta F}{\delta \phi} \right] \right\} \quad (20)$$

Where $\phi(\mathbf{r})$ is the local concentrations of the donor polymers and F is the free energy which has the form

$$F = \int \left[\frac{1}{N} \{ \phi(\mathbf{r}) \ln \phi(\mathbf{r}) + [1 - \phi(\mathbf{r})] \ln [1 - \phi(\mathbf{r})] \} \right] d\mathbf{r} \\ + \int \left[\chi \phi(\mathbf{r}) [1 - \phi(\mathbf{r})] + \frac{b^2 |\nabla \phi(\mathbf{r})|^2}{36 \phi(\mathbf{r}) [1 - \phi(\mathbf{r})]} \right] d\mathbf{r} \quad (21)$$

where $\phi(\mathbf{r})$ is the local concentrations of the donors, N is the degree of polymerization, the χ is the enthalpic parameter. The first two terms in the Equation (2) are the usual Flory-Huggins term and the third term energetically penalizes concentration gradients and drives coarsening [3], [4], [7], [8].

To predict morphology the discretization of the equation (1) is generalized to 3D and solved using the finite difference technique. In addition the surface effect is considered. The results for both cases are presented in the Section 3.

2.2 Drift Diffusion Equation

To simulate photovoltaic response of device drift diffusion method is used [7], [8]. The method involves solution of the following Equations (3):

$$\nabla \cdot (\epsilon \nabla \psi) = -q(p - n) \quad (22)$$

$$\frac{\partial n}{\partial t} = D(\mathbf{E}, x) - R(n, p) - \frac{1}{q} \nabla [qn\mu_n \nabla \psi - k_\beta T \mu_n \nabla n]$$

$$\frac{\partial p}{\partial t} = D(\mathbf{E}, x) - R(n, p) - \frac{1}{q} \nabla [qp\mu_p \nabla \psi - k_\beta T \mu_p \nabla p]$$

$$\frac{\partial x}{\partial t} = G(\mathbf{r}) + \frac{1}{4} R(n, p) - R(x) - D(\mathbf{E}, x) - \frac{1}{q} \nabla [-k_\beta T \mu_x \nabla x]$$

The first equation of Equations (3) is the Poisson equation which relates the electrostatic potential ψ to the concentration of the charged particles, ϵ is the permittivity and q is the elementary charge.

The other three equations are the continuity equation for electron, hole and exciton concentrations, respectively. In these set of equations μ_i is the mobility for the species i , k_β is the Boltzman constant and T is the temperature.

$D(\mathbf{E}, x)$, which is described by the Onsager theory, represents the dissociation of the exciton and responsible from the creation of the charge carriers while $R(n, p)$ is the Langevin form of the recombination term [8]. Finally $R(x)$ and $G(\mathbf{r})$ in the last

equations, respectively, are the term responsible from the decays of excitons and the term responsible from the photogeneration of excitons which depends on the incident photon flux [8].

In order to solve these equations the discretization of the equations [7], [8] is generalized to 3D and solved numerically.

To simulate photoelectric response of device we did not limit our investigation to any particular system. We rather chose typical material parameters to explore the physics of the device considering different morphologies. In this regard the parameters have been used in the simulation are given in Table 1. These parameters are taken from the Reference [7].

It is indeed worth to note that CUDA gpu programming is used for reducing computational time.

Table 8. The parameters used in the modeling.

Parameters	Symbol used	Value
Temperature	T	300 K
Mobility of electrons in the acceptor	μ_e^A	$1.0 \times 10^{-8} \text{m}^2 \text{V}^{-1} \text{s}^{-1}$
Mobility of electrons in the donor	μ_e^D	$1.0 \times 10^{-9} \text{m}^2 \text{V}^{-1} \text{s}^{-1}$
Mobility of holes in the acceptor	μ_h^A	$2.0 \times 10^{-9} \text{m}^2 \text{V}^{-1} \text{s}^{-1}$
Mobility of holes in the donor	μ_h^D	$2.0 \times 10^{-8} \text{m}^2 \text{V}^{-1} \text{s}^{-1}$
Exciton mobility	μ_x	$3.86 \times 10^{-9} \text{m}^2 \text{V}^{-1} \text{s}^{-1}$
Exciton Life time	τ_x	$1.0 \times 10^{-6} \text{s}$
Field dependant mobility parameter	γ	$5.0 \times 10^{-4} \text{m}^{1/2} \text{V}^{-1/2}$
Dielectric constant for the acceptor	ϵ_A	3.5
Dielectric constant for the donor	ϵ_D	3.5
Polaron binding energy	E_p	0.1 eV
Band offset between acceptor and donor	ΔE	0.7 eV
Exciton binding energy	E_x	0.5 eV
Shotky barrier height	ΔE_x	0.5 eV

3 Results and Discussion

We started by simulating device performance in 3D for the morphology including only Flory-Huggins terms in Equation (2). The simulated morphologies in 3D for the size 32^3 and also for 64^3 are produced by solving Equation (1). The results for the size 32^3 and for the size 64^3 are shown in Fig.1 and Fig.2, respectively. In both morphologies the parameter $N\chi$ is kept to be 2.1.

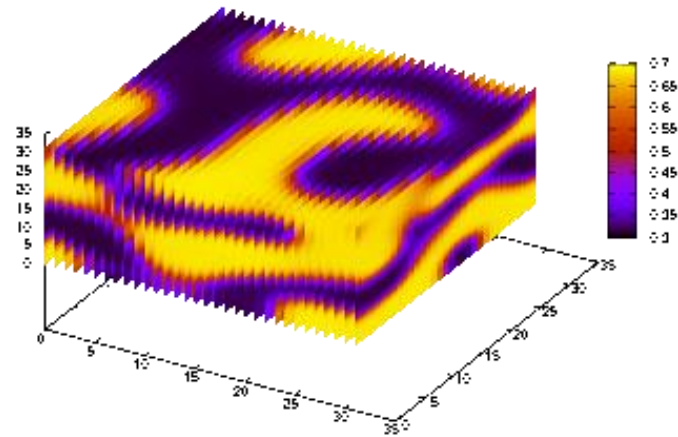


Fig. 9. Diblock copolymer thin film morphology in 3d for the size of 32^3 .

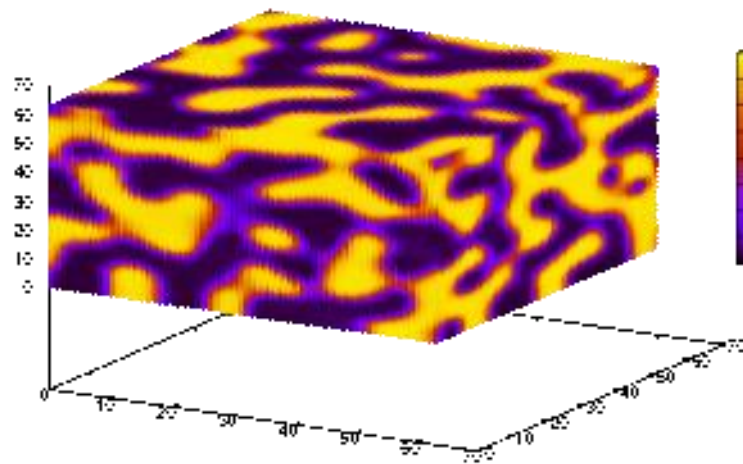


Fig. 2. Diblock copolymer thin film morphology in 3D for the size of 64^3 .

We simulate device performance for both morphologies. An example of the corresponding concentration profiles for excitons, electrons and holes are presented in Fig.3 for the 3D morphology with the size 64^3 . In this figure the concentration profiles for excitons, electrons and holes are given from top to bottom, respectively. Here in the applied field is taken to be zero.

The device performance is also calculated with an applied field in y direction for both sizes. The current voltage curves for both sizes are given in Fig. 4; the blue line with the filled square points for the size of 32^3 and the purple line with the filled circle points for the size of 64^3 . The following system size effects on the I–V characteristics obtained: The short-circuit current (I_{SC}) is higher for the larger volume since the larger system includes more charge carriers. However, the open-circuit voltage (V_{OC}) is smaller for the system with larger volume. That is considered to be due to lower diffusion. It has been obtained that the maximum efficiency also depends on the size of the system. It is 2.36% for the system size of 32^3 and 2.2% for the size of 64^3 . Moreover, there is a significant increase compared to 2d model (0.6% [7]). This highlights importance of 3d modeling for complex microstructures.

For a further investigation of maximum efficiency of the device with respect to morphology we used all terms in Equation (2). Including the term responsible from the concentration gradients and domain coarsening in the morphology has changed the maximum efficiency although the general trend given above has not changed. The obtained efficiency is 2.36 for the size of 32^3 and is 2.2 for the size of 64^3 .

To see effect of degree of polymerization, N and χ the following two investigations have been done: At first we kept $N\chi = 2.1$ for different value of N we changed χ . Then, we kept $N = 50$ and changed χ within $N\chi \geq 2.1$. Maximum efficiencies for both morphology investigations are exhibited in Table 2. From this table we can see that there is not much change in efficiency changing the number of N with keeping $N\chi$ fixed which proofs that the modeling morphology does not depend on N . However, there is a small change in efficiency with respect to $N\chi$ in the region concerned. First the efficiency increases slightly then decreases while $N\chi$ is increasing. This observed for both size but decreasing for each size start at different value of $N\chi$.

Table 2. Effects of degree of polymerization on efficiency.

Size	N	χ	$N\chi$	Efficiency in %	$I_{sc} \text{ m}^{-2}$
32^3	50	0.042	2.1	2.35891	-6.495
	50	0.044	2.2	2.38013	-6.568
	50	0.046	2.3	2.39735	-6.718
	50	0.048	2.4	2.38587	-6.627
	50	0.05	2.5	2.38005	-6.629
	500	0.0042	2.1	2.36071	-6.597
64^3	50	0.042	2.1	2.20464	-9.974
	50	0.044	2.2	2.34560	-10.12
	50	0.046	2.3	2.36441	-10.73
	50	0.048	2.4	2.37841	-10.82
	50	0.05	2.5	2.36374	-10.65

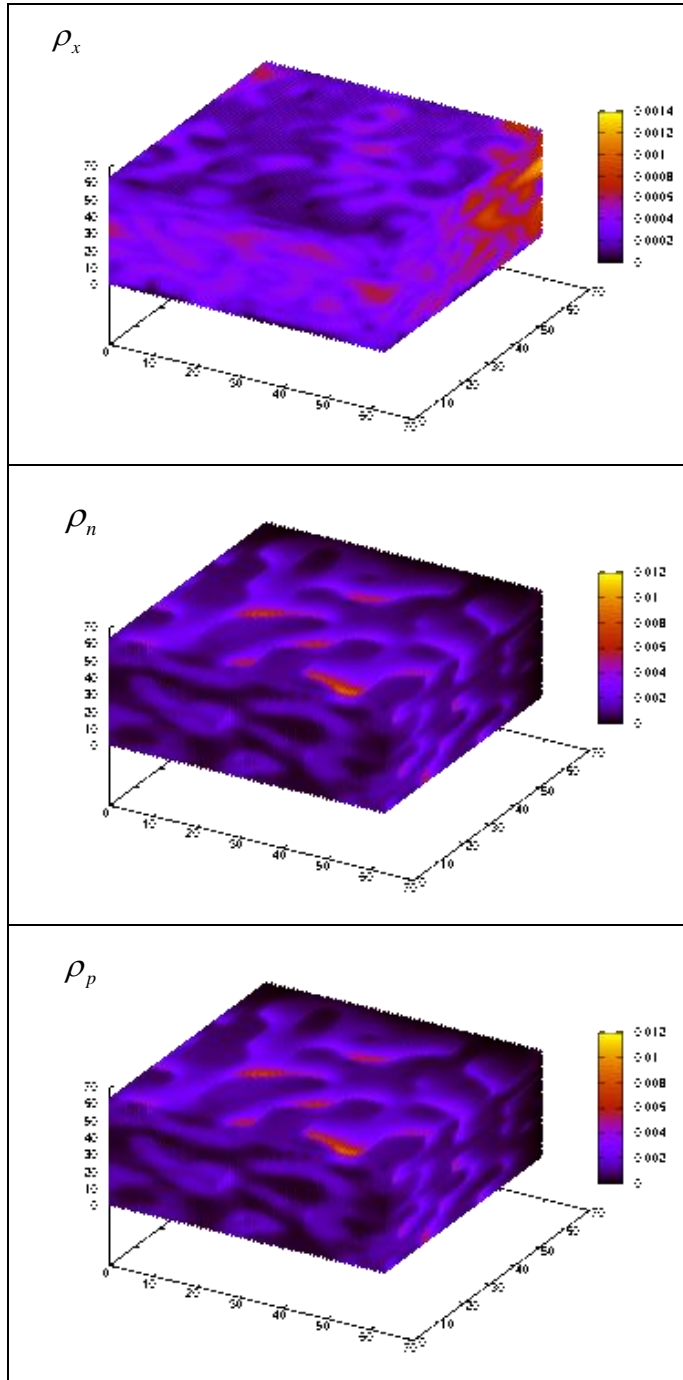


Fig. 3. Concentration profiles for excitons at the top and for electrons in the middle row and holes at the bottom row. These are for the 3d morphology with the size of 64^3 .

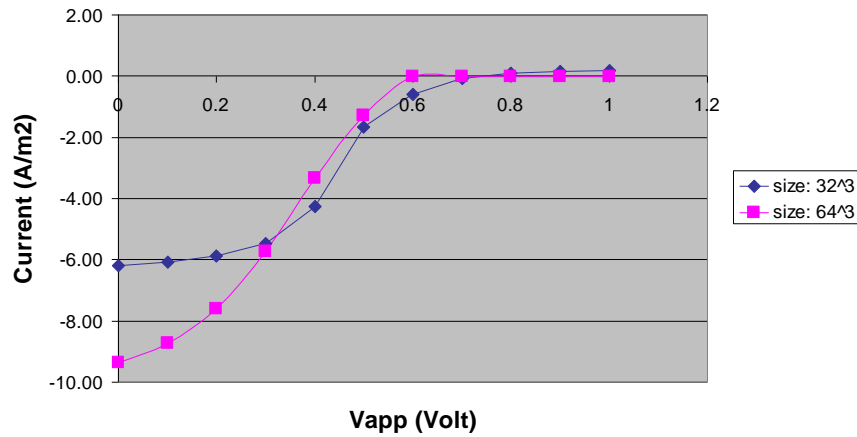


Fig. 4. Current-voltage ($I - V$) curves for diblock copolymer thin film morphologies in 3D: The blue line with the filled square points for the size of 32^3 and the purple line with the filled circle points for the size of 64^3 .

4 Conclusions

Our study highlights the importance of 3D modelling for complex microstructures. We presented that short-circuit current is higher for larger volume since the larger system includes more charge carriers and open-circuit voltage is smaller due to lower diffusion.

Acknowledgement

This work is supported by EPSRC under the project numbered EP/F056303/1.

References

1. Hwajeong K., Sungho N., Jaehoon J., Sooyong L., Jooyeok S., Hyemi H., Youngkyoo K.: Organic solar cells based on conjugated polymers. History and recent advances. *Korean Journal of Chemical Engineering* 31(7), 1095-1104 (2014).
2. Glotzer S. C. Computer simulations of spinodal decomposition in polymer blends. In: Editor, Stouffer D., *Annu. Rev. Comput. Phys. II*, World Scientific (1995).
3. Henderson I.C., Clarke N.: Two step phase separation in polymer blend. *Macromolecules* 37, 1952-1956 (2004).
4. Henderson I.C., Clarke N.: On modeling Surface Directed Spinodal decomposition. *Macromolecular Theory and Simulations* 14, 435-443 (2005).
5. Scott J. C., Malliaras G. G.: Charge injection and recombination at the metal organic interface. *Chemical Physics Letters* 299 (2), 115-119 (1999).
6. Ruhstaller B., Carter S.A., Barth S. Riel H. Riess W., Scott J. C.: Transient and steady-state behavior of space charges in multilayer organic light-emitting diodes. *Journal of Applied Physics* 89 (8) 4575-4586 (2001).

7. Buxton A.G., Clarke N.: Predicting structure and property relations in polymeric photovoltaic devices. *Physical Review B* 74(085207), 1-7 (2006).
8. Buxton A.G., Clarke N.: Computer simulation of polymer solar cells. *Modeling and Simulation in Material Science and Engineering* 15, 13-26 (2007).
9. Myers B., Bernardi M., Grossman J. C.: Three-dimensional photovoltaics. *Applied Physics Letters* 96(071902), 1- 3 (2010).
10. Coakley K. M., McGehee M. D.: Photovoltaic cells made from conjugated polymers infiltrated into mesoporous titania. *Applied Physics Letters* 83 (16), 3380-3382 (2003).
11. Coakley K. M., Liu Y., Goh C., McGehee M. D.: Photovoltaic cells made from conjugated polymers infiltrated into mesoporous titania. *MRS Bulletin* 30 (1), 37-40 (2005).
12. Groves C., Kimber R. G. E., Walker A. B.: Simulation of loss mechanisms in organic solar cells: A description of the mesoscopic Monte Carlo technique and an evaluation of the first reaction method. *The Journal of Chemical Physics* 133 (144110), 1-7 (2010).
13. Meng L., Shang Y., Li Q., Li Y., Zhan X., Shuai Z., Kimber R. G. E., Walker A. B.: Dynamic Monte Carlo Simulation for Highly Efficient Polymer Blend Photovoltaics. *Journal of Chemical Physics B* 114, 36-41 (2010).
14. Kettle J.: Ready cells for large scale systems. *Nature Energy* 4, 536-537 (2019).
15. Leijtens T., Prasanna R., Bush K.A., Eperon G.E., Raiford J.A., Gold-Parker A., Wolf E.J., Swifter S.A., Boyd C.C., Wang H.P., Toney M.F., Bent S.F., McGehee M.D.: Tin-lead halide perovskites with improved thermal and air stability for efficient all-perovskite tandem solar cells. *Sustainable Energy & Fuels* 2 (11), 2450-2459 (2018).
16. Leijtens T., Prasanna R., Bush K.A., Eperon G.E., Raiford J.A., Gold-Parker A., Wolf E.J., Swifter S.A., Boyd C.C., Wang H.P., Toney M.F., Bent S.F., McGehee M.D.: Tin-lead halide perovskites with improved thermal and air stability for efficient all-perovskite tandem solar cells. *Sustainable Energy & Fuels* 2 (11), 2450-2459 (2018).
17. Raiford J.A., Belisle R.A., Bush K.A., Prasanna R., Palmstrom A.F., McGehee M.D., Bent S.F.: Atomic Layer deposition of vanadium oxide to reduce parasitic absorption and improve stability in n-i-p perovskite solar cells for tandems. *Sustainable Energy & Fuels* 3 (6), 1517-1525 (2019).
18. Kettle J., Horie M., Majewski L.A., Saunders B.R., Tuladhar S., Nelson J. Turner M.: Optimisation of PCPDTBT solar cells using polymer synthesis with Suzuki coupling. *Solar Energy Materials & Solar Cells* 9, 2186-2193 (2011).

Potential Analysis of Manure Based Biogas to Electricity Generation: Case Study of Burdur

Doğancan Beşikci¹[0000-0003-1668-7831] and Egemen Sulukan²[0000-0003-1138-2465]

and Tanay Sıdkı Uyar³[0000-0002-0960-1203]

¹ Marmara University, Mechanical Engineering Department, Turkey

² National Defense University, Turkish Naval Academy, Mechanical Engineering Department, Turkey

dogancanbesikci@outlook.com

Abstract. This paper presents biogas based electricity generation in Burdur-Turkey to foresee economic and environmental effects between 2016-2031. To achieve this, detailed technology based reference energy system were established to see flows of commodities between technologies and relevant data installed to database. Burdur is a rural city that placed in south-western part of Turkey. Due to geographical location, solar irradiation rates and hours, agriculture and animal breeding are one of the important economic incomes. According to Turk-Stat data, total number of animals (sheep, cattle and chicken) are vary between 860,000 to 1,250,000 in 2020-2031 time interval. Results shows that, total electricity generation potential from manure reaches to 0.78 PJ in 2020 and 1.26 PJ in 2031 if this potential used efficiently.

Keywords: Biogas, Burdur, Renewable Energy, Answer-TIMES.

1 Introduction

Similar to the other developing countries, Turkey has an emerging economy dealing with energy issues. Developing industry or high population growth leads to increasing energy consumption rates, where high energy consumption rates may result in energy supply security problems. To ensure the supply safety, renewable sources can be implemented into the grid to lower the external dependence, energy road maps and strategic plans can be created, energy consumption can be decreased via efficient technologies and renewable energy based electricity production methods such as biogas can be implemented into grids.

In this context, this paper aims to oversee the economic and environmental effects of the manure-based biogas to electricity production technologies into a medium-profile city of Burdur, in Turkey. To find the consequences of the candidate biogas electricity generation; the first step is to build an energy reference system of the city. Next step is to establish a 15 year-long energy model by Answer-TIMES energy model generator. The final step is to create an alternative scenario and collect results that focused on biogas-based electricity generation.

Gusano et al conducted a study about the discount rates in energy modeling methods. They tried to find effects and optimal level of social discount rate in energy systems. In

this study, they compared the rates between two different model, ETSAP-TIAM and TIMES-Norway. The results showed that, 4-5% is the top level of social discount rate for the European countries.[1]

Another study made by Dal and Koksal in 2017 about effects of technological, political and environmental constrains in electricity generation of renewable energy sources. They developed the model between 2016-2035 and selected 2015 as a base year. Their results shows that, if the external costs are not considered, total discounted system cost increase by 4% CO₂ mitigation scenario. If the external cost considered, system cost increased by 30% for both CO₂ and BAU (Business as usual) scenario [2].

Celestino conducted a study about modeling and optimization of electricity systems in Portugal. The results shows that, if the renewables such as biogas, wind and solar implemented to energy system, Portugal can be one of the electricity exporter in medium-long term to Iberian electricity system [3].

This paper continues with material and methodology section that explains the basic mathematical model behind this study and energy system description of Burdur City in chapter 2. Chapter 3 gives the results of the alternative scenario with the concluding remarks.

2 Material and Methodology

2.1 Objective Function of TIMES

In this study, a MARKAL based Answer-TIMES platform has been used in the analysis. Basically, TIMES is an optimization method used for energy-economy-environment models. A developed model can work in a multi-regional and multi-period level, which means that one can simulate multiple different regions with multiple different time-slices. The model basically calculates and chooses the least-cost method by economic, environmental and technological parameters under given conditions.

TIMES energy model structure is designed by the modeler and then respective energy carriers, technologies, environmental emissions, and demands are specified with relevant qualitative and quantitative data input for each separate region. The specified items characterizes both currently exists in the energy system and the future candidates within the specified time horizon. Specified time-series and time-independent data contain the economic and technology-based policy assumptions over the identified region and time horizon. Reference year is set on a past year and the statistical values are fixed on this year by the modeler.

The objective function of a TIMES run is to minimize the net total cost of the system while meeting a number of defined constraints; as the summation of all regions of the reduced present value of annual costs, occurred over a predetermined time horizon.

Therefore:

$$NPV = \sum_{r=1}^R \sum_{YEARS} (1 + d_{r,y})^{REFYR-y} x ANNCOST(r, y) \quad (1)$$

In equation (1), NPV (Net Present Value) of the model shows the total value of the system. ANNCOST refers to the annual cost. The general discount rate is shown by "d". REFYR is the reference year for discounting, YEARS is the number of years in each period "t" and the letter "R" is the number of regions.

$$VAR_OBJ_{(z)} = \sum_{r \in REG} REG_OBJ(z, r) \quad (2)$$

The equation (2) represents the overall objective function including all regions.

$$REG_OBJ_{(z,r)} = \sum_{y \in (-\infty, +\infty)} DISC(y, z) x \{INVCOST(y) + INVTAXSUB(y) + INVDECOM(y) + FIXCOST(y) + FIXTAXSUB(y) + VARCOST(y) + ELASTCOST(y) - LATEREVENUES(y) - SALVAGE(z)\} \quad (3)$$

Where;

$O(z)$: Total system cost, discounted to the beginning of year z,
 $VAR_O(z)$: Total cost of all regions, discounted to year z,
 $REG_O(z, r)$: Total cost of the region r, discounted to year z.
 $INVCOST(y)$: It is the investment cost,
 $INVTAXSUB(y)$: The tax and subsidy costs,
 $INVDECOM(y)$: Decommissioning capital costs,
 $FIXCOST(y)$: It is the fixed annual cost,
 $FIXTAXSUB(y)$: Fixed annual tax and subsidy,
 $VARCOST(y)$: All variable costs (proportional to some activity),
 $ELASTCOST(y)$: Cost incurred when demand is reduced due to price elasticity,
 $LATEREVENUES(y)$: Revenue accounts for commodity recycling occurring after the end of horizon,
 $SALVAGE(z)$: Salvage value of all capital costs of technologies whole life extends beyond the end of horizon [4].

2.2 Reference Energy System and Database

RES (reference energy system) structure represents the connections of process/conversion technologies, demand devices and demands by commodities. It also represents how the commodities enter or leave to/from the region by mining, import and export. Commodities imported or mined can be processed in the process or conversion technologies or facilities. Processed commodities (coal, crude oil, natural gas etc.) or commodities already processed at outside of the region go to demand devices or end-use technologies as coal, natural gas, diesel fuel, gasoline, LPG, electricity, low-temp. heat or high-temperature heat. etc. In the final part of the RES, end-use technologies meeting the respective demands. Figure 2 represents the reference energy system of Burdur province.

Burdur province imports coal, gasoline, diesel fuel, LPG and two-thirds of its electricity imported from the national grid. The last one-third of its electricity is generated by two hydroelectric power plants, a natural gas power plant and fifteen solar photovoltaic facilities. At the demands side, Burdur can be divided into five major sectors. Residential and commercial demand group contains; space conditioning, cooking, illumination, cleaning and entertainment sub demands. Main industry sectors are sugar production, cement production, marble quarry, marble process and dairy products, this demand groups consisting of the industrial demand major group. Other sectoral groups are city service demands, passenger and freight transportation demands and agricultural demand. In Figure 1, all the demand devices or end-use technologies can be seen under “Demand Technologies” column.

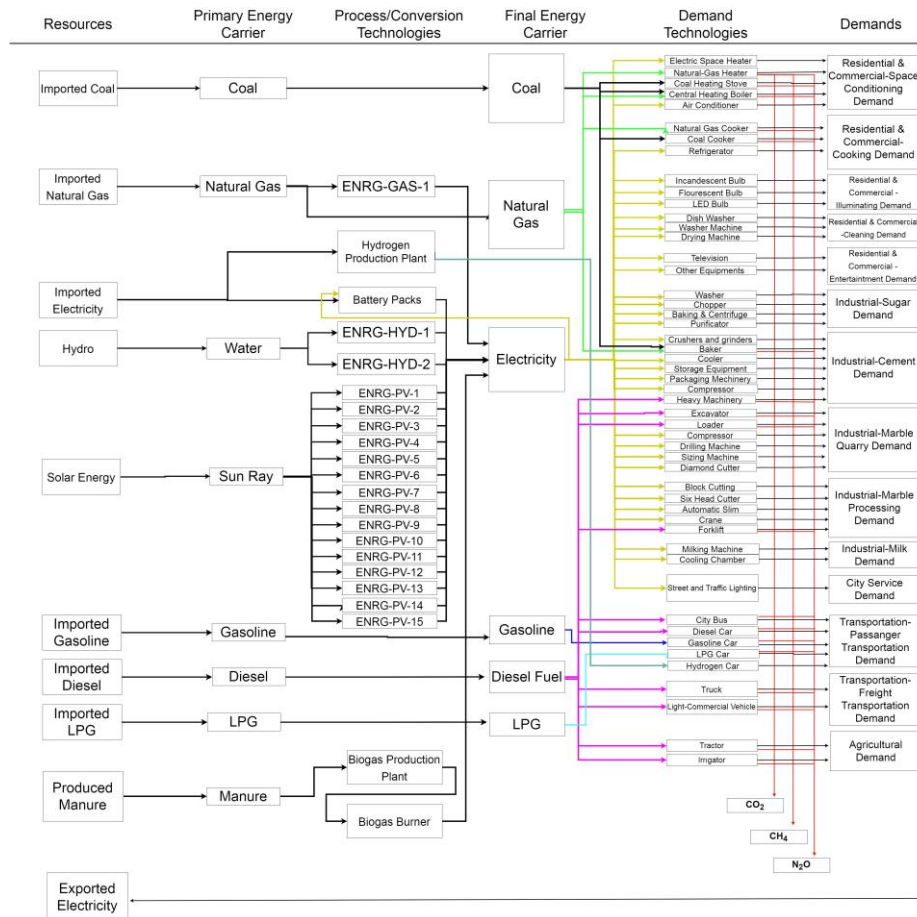


Fig. 1. Reference energy system of Burdur.

To fill up the reference energy system, sectoral parameters and all the data has been collected from face-to-face meetings with experts from sub directorates of ministry of-fices at Burdur, official reports of Electricity Market Regulatory and Turkish Statistical

Institute (TURKSTAT) database [5]. All emissions factors calculated using Intergovernmental Panel on Climate Change (IPCC) methodology and National Greenhouse Gas Inventory Reports [6]. Official reports on demand increases, population growth rate and gross domestic product (GDP) forecastings were used for demand projections. Table 1 shows demand groups and demand amounts in PJ unit.

Table 9. Demand groups and business as usual energy usage trends.

Comm. Group	Commodity	2016	2021	2026	2031
Residential and Commercial	Cleaning	0,130	0,162	0,202	0,252
	Cooking	0,401	0,499	0,622	0,775
	Entertainment	0,130	0,162	0,202	0,252
	Illumination	0,035	0,044	0,055	0,068
	Space conditioning	1,244	1,551	1,933	2,408
Industrial	Cement	0,668	0,832	1,037	1,292
	Marble processing	0,682	0,850	1,059	1,320
	Marble quarry	0,343	0,428	0,533	0,664
	Milk production	0,177	0,221	0,275	0,343
	Sugar	0,041	0,050	0,063	0,078
City Services	Service	0,016	0,020	0,025	0,032
Transportation	Freight transport	3,631	4,525	5,639	7,027
	Passenger transport	0,911	1,135	1,415	1,763
Agricultural	Irrigation and greenhouse heating	0,107	0,133	0,166	0,207

2.3 Description of the Alternative Scenario (BIOGAS)

The aim of this paper is to find economic and environmental effects of biogas based electricity generation. In the model time horizon, generation starts in 2020 with 0.78 PJ level and with the potential raises, generation also increases to 1.26 PJ in 2031. To find this, two different scenarios were examined in this analysis. First scenario is business as usual (BAU) scenario. BAU scenario represents the continuation of current conditions.

The second scenario is manure based biogas generation implementation. In this scenario, total manure potential calculated and projected with the animal breeding trends to the 2031. As a result, 0.78 to 1.26 PJ electricity generation occurred.

Total investment, fixed and variable O&M costs of biogas power plants are calculated from report that made by International Renewable Energy Agency. Figure 2 shows the levelised cost of electricity biogas projects across continents.

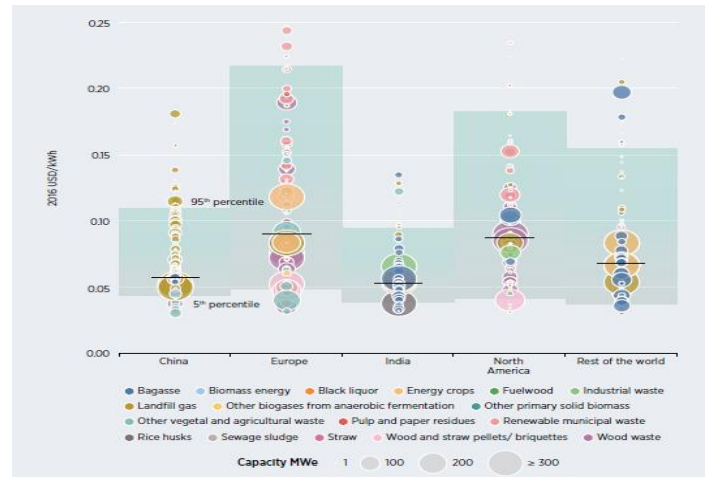


Fig. 2. Levelised costs of biomass production methods [7].

Figure 3 shows the capacity factors of different type of production methods via levelised costs of electricity. In this study, 0.09 USD/kWh average levelised cost and 0.8 capacity factor selected in calculations.

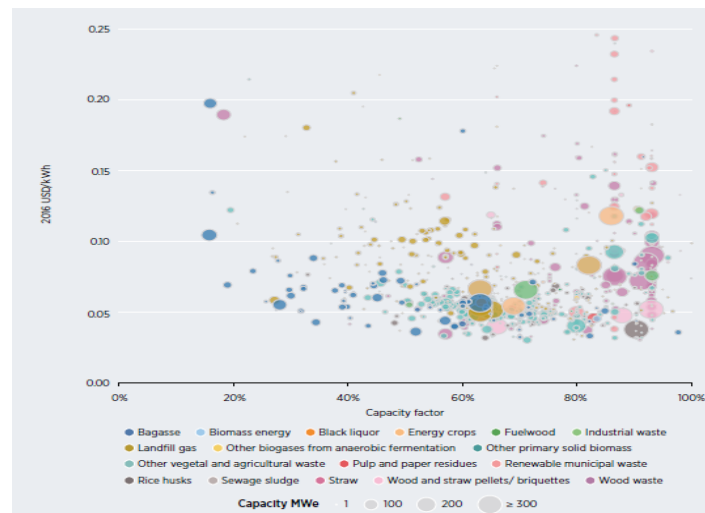


Fig. 3. Capacity factors of power plants by installed capacity.[7]

4 Results

Biogas power plant started the generation in 2020. After that total levelised cost of the plant occurred as 22.81 mil\$ in 2020 and 36.53 mil\$ in 2031, as given in Table 2. On the other hand, total electricity generation is 0.7866 PJ in 2020 and increases to 1.2599 PJ in 2031. It means that, this potential can feed the electricity needs of 73,000 house hold in 2020 and 116,000 in 2031.

Another result is emissions. Biogas technology is carbon neutral electricity generation method. During the emission calculations, it is assumed that biogas based generation substituted equal coal based electricity generation. Results shows that, this potential can mitigate 61 kT CO₂ in 2020 and 98 kT CO₂ in 2031.

Last results are total installed capacity. 80% capacity factor used in calculation. With this biogas potential level, in 2020, 31.2 MW of new capacity have to be built. With the increasing potential, total installed capacity increases to 49.9 MW in 2031.

Table 2. Results of alternative biogas to electricity generation scenario.

Parameter	Units	2016	2017	2018	2019	2020	2025	2030	2031
Total Levelised Cost	2000\$USm	0	0	0	0	22.8112	28.2468	35.0006	36.5359
Total Electricity Generation	PJ	0	0	0	0	0.7866	0.974	1.2069	1.2599
Emission Mitigation	KT-CO ₂	0	0	0	0	-61.1734	-75.75	-93.8619	-97.9791
Total Installed Capacity	GW	0	0	0	0	0.0312	0.0386	0.0478	0.0499

5 Conclusion

It is possible to build self-sufficient, environment friendly, cost-effective cities with today's renewable technology. All this problems can be solve by renewable potentials of our geography. Biomass related technologies and potentials are one of the most important one to develop cities.

In this paper, total manure based biogas potential evaluated to see the results in environmental, technological and economical level. In this context, Burdur selected as a case city and reference energy system developed between 2016-2031. Total levelised costs are vary between 22.81 to 36.53 mil\$. Total electricity generation occurred 0.78 PJ in 2020 and 1.26 PJ in 2031. This potential can mitigate 61.17 kT CO₂ in 2020 and 97.97 kT CO₂ in 2031 by itself.

References

1. Gusano D. G, Espegren K, Lind A, Kirkengen M. The role of the discount rates in energy systems optimization models. *Renewable and sustainable energy reviews*. Vol-59. Page 56-71
2. Dal E, Koksal M. A, Modeling the use of renewable energy sources for electricity generation based on technological, political and environmental constraints. *Energy procedia*. Vol-142. Page 3129-3134.
3. Celestino N. Modeling and optimization of Portuguese electricity system with regional disaggregation. University of Lisbon. 2014
4. Loulou R, Lehtila A, Kanudia A, Remme U, Goldstein G. Documentation for the TIMES Model Part 2. 2016.
5. <http://www.tuik.gov.tr>. Accessed 05.11.2018
6. https://www.ipcc-nggip.iges.or.jp/EFDB/find_ef.php?ipcc_code=2.A.2&ipcc_level=2. Accessed 06.11.2018
7. Renewable power generation costs 2017. Report. International Renewable Energy Agency. 2017

Transition to a Low Carbon Future in Maritime Fleet for Climate Change

Alperen SARI¹, Egemen SULUKAN², Dođuş ÖZKAN², Tanay Sıdkı UYAR³

¹ Barbaros Naval Science and Engineering Institute/ National Defense University

² Mechanical Engineering Department/ National Defense University
Tuzla-Istanbul, 34942, Turkey.

³ Mechanical Engineering Department/ Marmara University
Kadıköy-Istanbul, 34722, Turkey

alperensari@gmail.com, esulukan@dho.edu.tr, dozkan@dho.edu.tr,
tanayuyar@marmara.edu.tr

Abstract. Climate change is a recent important issue for transportation sub-sectors and the environmentalists have been working to combat climate change for decades. As 90% of the world-trade carried out by maritime transport; the ships play a crucial role among the transport and trade vehicles. Approximately, 2,5% of the global greenhouse gas emissions (GHG) are caused by the ships and it has been ever increasing, depending on the expanding maritime transport demand. Reducing the maritime-based GHG is a global challenge task, determined by the International Maritime Organization (IMO). Nowadays; a number of measures to reduce carbon footprint and respective course of actions are recently being discussed and developed globally. IMO encourages shipping industry to minimize the carbon footprint by fostering energy efficient onboard technologies, as the global top decision-maker. In this study, the current technology configuration on a chemical tanker ship has modelled by LEAP (Long-range Energy Alternatives Planning System), one of the widely-used energy decision support tool. Then we focused on reducing greenhouse gas emissions with an alternative scenario according to IMO regulations and future technology developments. The results show that reducing the ship-based GHG is possible and that is sure to give us a more secure future, in a cleaner atmosphere.

Keywords: Reference Energy System, Energy Modelling, Ship Energy System Analysis, Low Carbon, LEAP.

1 Introduction

The geographical characteristics of the world have changed greatly in certain periods due to the deterioration of the natural balance due to various reasons. These changes, which are mostly related to natural factors, have been caused by people since the mid-19th century. The accumulation of greenhouse gases released into the atmosphere due to the use of fossil fuels in transportation has been increasing rapidly since the industrial revolution.

As the growth in the world economy after the industrial revolution, the transportation demand has been continuously increasing. Thus, the transport sector plays a key role in

climate change and global warming as one of the main sectors that lead to the emission of carbon dioxide (CO₂), which is the main greenhouse gas. Carbon dioxide is emitted by the combustion of fuels such as petroleum, natural gas and coal, causes greenhouse gas effects by mixing into the atmosphere. Thus, the sun's rays reflected from the earth cannot escape from our atmosphere. This causes an increase in surface temperatures in the world which called global warming or climate change that is one of the leading environmental problems that threaten the world.

2 The Significance of Energy System Analysis of Ships

The rapid growth in the world population leads to an increase in the demand for international transport, which tends to increase CO₂ emissions in the transportation sector. In a study conducted by the International Clean Transport Council, it was estimated that if international transport was considered a country, it would be the sixth largest carbon dioxide emitter in the world [1].

Ships carry approximately 90% of international trade by volume and more than 70% by value, and they are the most fuel-efficient means of transport. CO₂ emissions from global maritime transport also account for about 2.6% of total emissions [2]. This ratio, calculated for 2015, was equivalent to 931 million tonnes a year which is on the same level as Germany's CO₂ emissions [3]. One basic method to evaluate the possible CO₂ emissions is to examine the quantity of fuel that is used up by ship on a weekly, monthly and yearly basis and calculate the CO₂ emissions that those volumes would bring out. These statistics can then be used to clear existing bunkers and see what can be done to protect existing engines.

Although its considerable part in contaminating the planet, shipping was not taken into consideration in the Paris agreement on climate change. According to the 1997 Kyoto Protocol, the responsibility to limit and reduce the emissions from maritime was given to The International Maritime Organization (IMO). IMO has improved its own procedure to set concrete aims for reducing the carbon footprint from ships. Energy Efficiency Design Index (EEDI) and the Ship Energy Efficiency Management Plan (SEEMP) are examples of the technical and operational measures adopted by IMO to increase energy efficiency and reduce GHG emissions from international shipping.

3 RES Concept and Decision Support Tools

The Reference Energy System (RES) is a diagram figuration of all of the technical processes from supply various forms of energy to end-use activities [4]. This diagram shows the resources, energy carriers, conversion and process technologies, demands and demand technologies used in an energy system and their relationship with each other. The RES contains useful information about energy demand and energy services, which enables energy conversion and process technologies to affect fuel-technology connections in an energy system [5].

Once the RES has been created, energy analysis is carried out by using one of the energy decision support tools. Decision support tools provide the analysis of the current

economic and ecological analysis of an energy system, as well as analysis of future improvements.

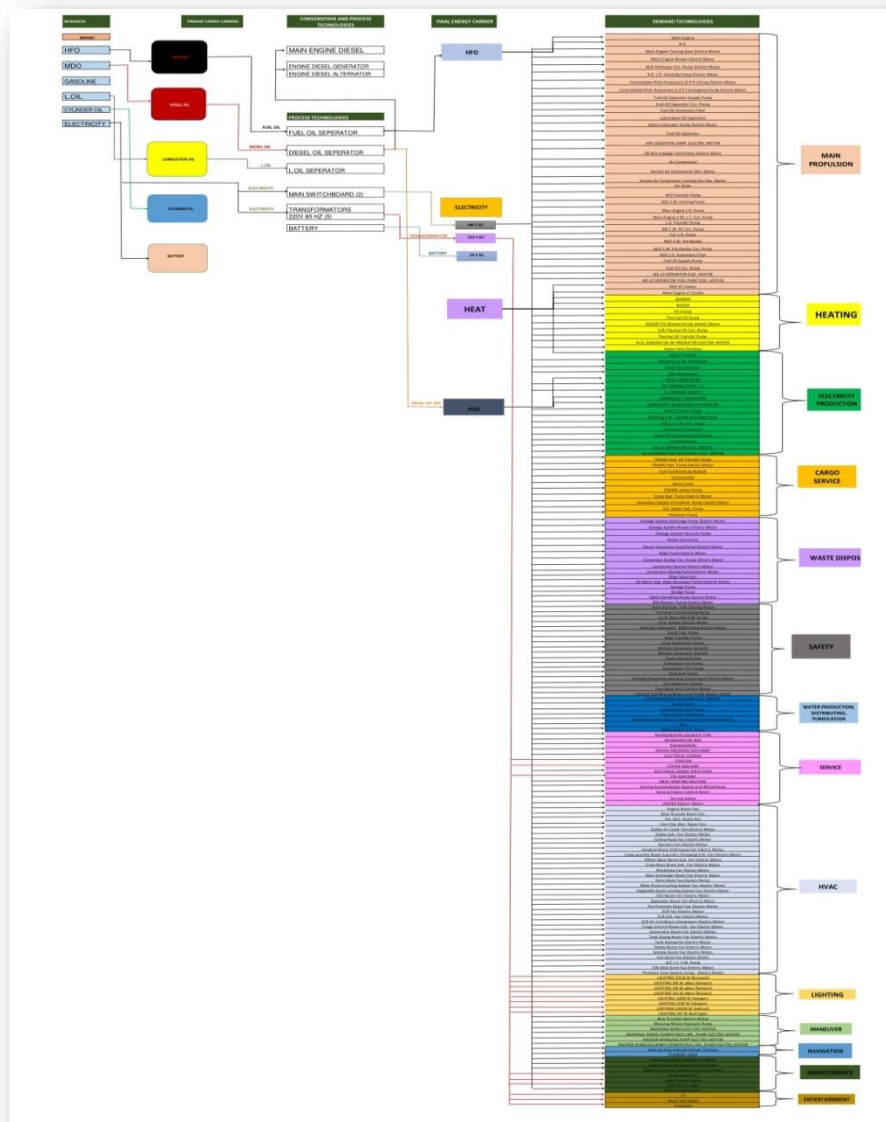


Fig. 1. RES of a Chemical Tanker.

3.1 Reference Energy System of a Chemical Tanker

As better identify the ship energy system and to create the contacts between its units, the Reference Energy System of a chemical tanker was established and defined the

energy sources, storage technologies, conversion and process technologies, energy carriers and demands getting in the system.

4 Methodology

There are a variety of decision support tools; e.g. Energy PLAN, HOMER, Energy and Power Evaluation Program (ENPEP), Global Emission Model for Integrated Systems (GEMIS), MARKAL, REAP, etc. In this research, we preferred utilizing the Long-Range Energy Alternatives Planning (LEAP) as an energy modelling tool.

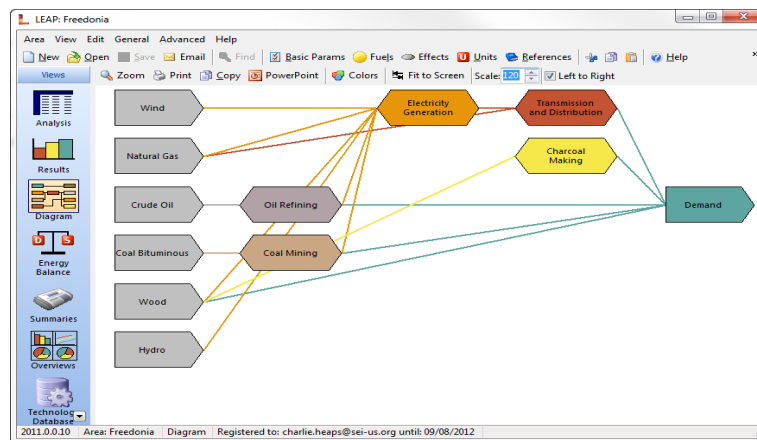


Fig. 2. RES Diagram of the LEAP.

4.1 About the LEAP Model

The Long-range Energy Alternatives Planning (LEAP) is a decision support tool advanced by the Stockholm Environment Institute, Boston (SEI-B) [6]. It is a widely used tool for energy and climate change mitigation planning chosen by thousands of organizations in 190 countries around the world, including government agencies, academics, non-profit organizations, consulting firms and energy organizations [7]. It is a bottom-up model. LEAP shows the present and future energy consumption and used to calculate the carbon emission by connecting the environmental emission factors based on the scenarios [8].

4.2 Emission Analysis of LEAP

While using LEAP, demand and resource values involving one year should be entered into the model. These values named as a base year value by LEAP while use calculations. Then according to the IMO regulations reference scenarios was created and calculated. The energy consumption for every device was calculated in the LEAP model using the following equation:

$$Ec = Ea \times Ei \quad (1)$$

As given in Equation (1); “ E_c ” is energy consumption for the device, “ E_a ” is the activity level and “ E_i ” is the energy intensity. The carbon emission for every device was estimated by the equation as follows:

$$C_e = E_c \times EF \quad (2)$$

As given in Equation (2); “ C_e ” stands for the carbon emission for the device, and “ EF ” stands for the localized carbon emission factors. Whether LEAP’s environmental results are affected by edits to the chemical composition of fuels.

$$EF = NCV \times CEC_u \times COF \times \frac{44}{12} \quad (3)$$

As given in (3); EF is localized carbon emission factors, NCV is qnet, CEC_u is the carbon oxidation rate of energy, $44/12$ is the molecular weight ratio of CO_2 and C .

5 Energy Modelling of a Chemical Tanker via LEAP

This paper focuses on the current and future energy consumption and CO_2 emissions via LEAP model. First of all, the basic parameters were entered into the LEAP model. 2017 was chosen as the base year. Scenarios are calculated every year from 2018 (First Scenario Year) to 2040 (end Year).

5.1 Demands and End-use Technologies

After defining the basic parameters, a chemical tanker ship main demand sectors are determined as follows: Main propulsion, electricity generation, cargo service, heating, waste disposal, safety, water production distributing purification, service, HVAC, lighting, navigation, maneuver, entertainment and maintenance. 14 demands are satisfied by 186 end-use technologies which using various types of final energy carriers and shown in Figure 1 [5].

5.2 Conversion and Process Technologies

Energy exists many forms all around us. The first rule of thermodynamics represents as Energy can be neither created nor destroyed, but converted from one form to another. Process and conversion technologies change form, quantity or amount of primary energy in an energy system and became useful energy for that energy system [9].

Main engine diesel, engine diesel generator and engine diesel alternator define as conversion technologies of a chemical tanker. Fuel oil separator, diesel oil separator, lubricate oil separator, main switchboard, transformer and battery have been defined as the process technologies of a chemical tanker.

5.3 Primary and Final Energy Carriers

Different natural sources supply energy requirement as primary energy and final energy in an energy system. Primary energy is an original form of energy which found in nature. Mostly non-renewable energy sources use in a ship like fuel oil and diesel oil. When primary energy has undergone a conversion process, it is named secondary energy and shown in Fig.3 [9].

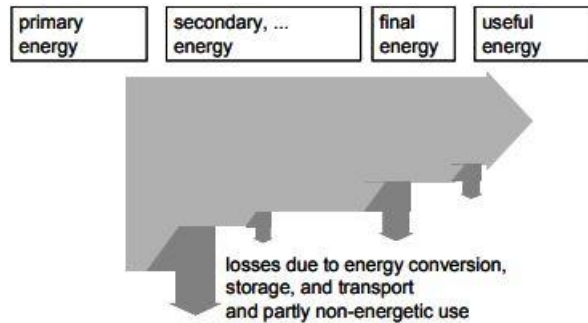


Fig. 3. The Flow of Energy Described by a Sankey Diagram [9].

Energy which meets the demands via demand technologies named as final energy in an energy system and primary and final energy carriers of a chemical tanker ship is shown in Fig. 1.

5.4 Energy Balance Analysis

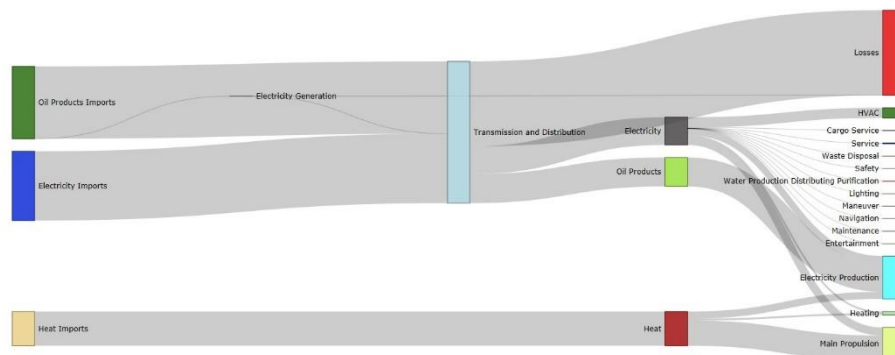


Fig. 4. Sankey Diagram of a Chemical Tanker Energy Balance.

Total primary supply of a chemical tanker is 796,5 gigajoules and shown in Table 1 and supplied by primary energy carrier imports. It is seen in Table 1 that 353,6 gigajoules of energy has been lost during the energy conversion, process, storage and transport steps. Total demand value is calculated 442,9 gigajoules in a chemical tanker ship.

Table 1. Table of a Chemical Tanker Energy Balance.

Energy Balance for Area "SEA OF CHEMICAL TANKER"				
Scenario: REF, Year: 2017, Units: Million Gigajoule				
	Electricity	Oil Products	Heat	Total

Production	-	-	-	-
Imports	273,1	316,3	207,2	796,5
Exports	-	-	-	-
Total Primary Supply	273,1	316,3	207,2	796,5
Electricity Generation	0,0	-0,1	-	-0,0
Transmission and Distribution	-163,9	-189,7	-	-353,6
Total Transformation	-163,9	-189,8	-	-353,6
Main Propulsion	59,3	52,7	184,4	296,3
Electricity Production	17,2	73,8	18,1	109,1
Cargo Service	0,5	-	-	0,5
Heating	4,4	-	4,6	9,0
Waste Disposal	0,0	-	-	0,0
Safety	0,1	-	-	0,1
Water Production Distributing Purification	0,0	-	-	0,0
Service	1,7	-	-	1,7
HVAC	25,9	-	-	25,9
Lighting	0,1	-	-	0,1
Maneuver	0,0	-	-	0,0
Navigation	0,1	-	-	0,1
Maintenance	0,0	-	-	0,0
Entertainment	0,0	-	-	0,0
Total Demand	109,3	126,5	207,2	442,9
Unmet Requirements	-	-	-	-

As we see in Figure 4 and Table 1, main propulsion is the most important demand by the value of 296,3 gigajoules for a chemical tanker ship. Electricity production, HVAC and heating demands are followed the main propulsion demand. Business As Usual (BAU) Scenario for a chemical tanker ship is analyzed and shown in Table 2.

Table 2. Table of a Chemical Tanker Energy Balance in Reference Scenario.

Scenario: REF, All Fuels				
Branch: Demand				
Units: Million Gigajoules				
Branches	2017	2020	2025	2030
Main Propulsion	296,3	306,9	321,3	335,6
Electricity Production	109,1	113,9	122,6	132,1
Cargo Service	0,5	0,5	0,5	0,5
Heating	9,0	9,0	9,0	9,0
Waste Disposal	0,0	0,0	0,0	0,0
Safety	0,1	0,1	0,1	0,1
Water Production Distributing Purification	0,0	0,0	0,0	0,0
Service	1,7	1,7	1,7	1,7
HVAC	25,9	25,9	25,9	25,9
Lighting	0,1	0,1	0,1	0,1
Maneuver	0,0	0,0	0,0	0,0
Navigation	0,1	0,1	0,1	0,1
Maintenance	0,0	0,0	0,0	0,0
Entertainment	0,0	0,0	0,0	0,0
Total	442,9	458,3	481,3	505,2

5.5 CO₂ Emissions Analysis

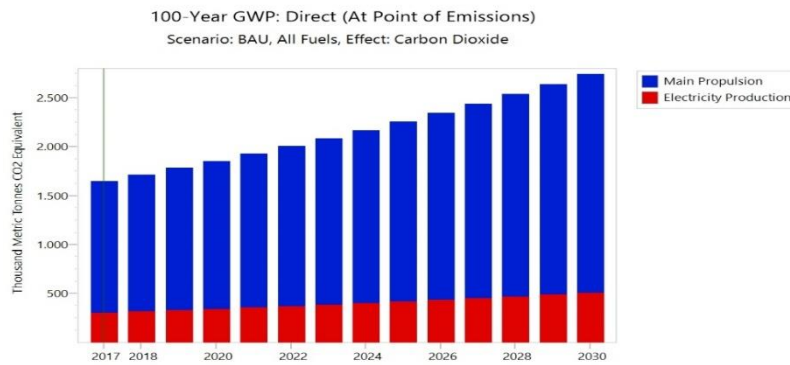


Fig. 5. BAU Scenario CO₂ Analysis.

The Base Scenario can be used as a reference scenario to be analyzed and compared with other scenarios [10]. For the reference scenario, the information for a chemical tanker have been obtained by Transal Shipping Co. and used to identify the energy network of the ship for the year 2017. We analyzed and compared the energy analysis of a chemical tanker ship from 2017 to 2030. The world maritime trade volume is expected to increase by 4% in 2018 [11]. Therefore, if no measures are taken, the amount of CO₂ from a chemical tanker ship by 2030 is estimated to reach 2746 thousand metric tonnes CO₂ equivalents. Total CO₂ emissions amount increases from 1649,2 to 2746 thousands metric tonnes in a chemical tanker energy system, so the total CO₂ emissions would increase at a rate of 60% in a period of 2017-2030 as illustrated in Figure 5 above.

IMO aims to reduce CO₂ emissions per transport work, as an average across international shipping, by at least 40% by 2030, pursuing efforts towards 70% by 2050, compared to 2008 according to the MEPC 72nd session [12]. Therefore, we aim to reduce the CO₂ emissions per chemical tanker at least %40 by 2030 compared to the base scenario year as a reference. According to the reference scenario, total CO₂ emissions will reduce from 1649,2 to the level of 989,5 thousand metric tonnes in a chemical tanker energy system. As shown in Figure 6 below, 40% of CO₂ emissions reduction is fulfilled by 2030 compared to the base scenario year 2017.

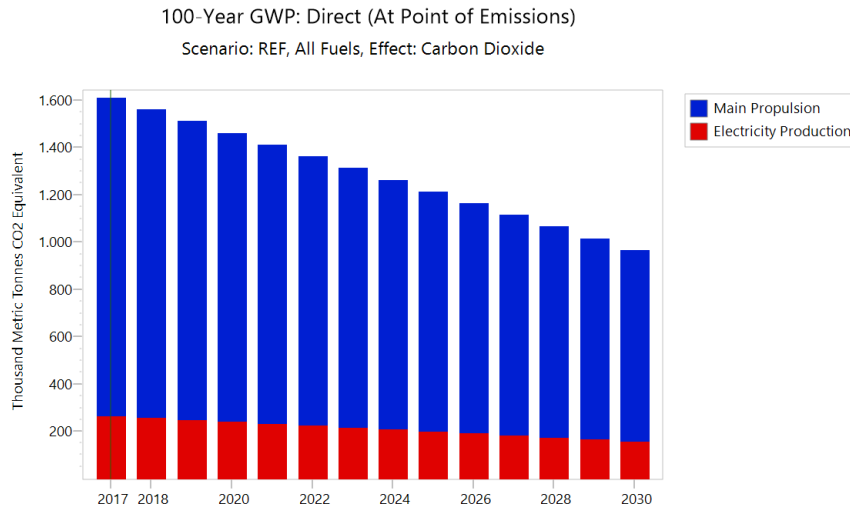


Fig. 6. Reference Scenario CO₂ Analysis.

6 Results and Conclusion

In this study, the interaction and the relationship between each element were examined for the reference energy system and the energy system of a chemical tanker was analyzed in detail first and then the energy network from the energy input to final energy carrier was examined. Based on the data received from Transal Shipping Co., the base scenario for 2017 was created and energy balance analyzes were fulfilled. Environmental constraints were carried out the envisage the life cycle of the analyzed chemical tanker energy system within the environmental aspects and was evaluated against the base scenario by the legislation of the International Maritime Organization. As the future work; technical, economic and environmental constraints will be applied to evaluate chemical tanker energy system within the financial and environmental aspects and alternative scenarios based on the prospective course of actions on IMO regulations will be conducted against the base scenario.

Acknowledgments

The Authors would like to express gratitude to Captain Umut BOZKURT for his guidance, technical and professional support and Transal Shipping Co. for sharing their expert knowledge and information.

References

1. The International Council on Clean Transportation- Marine homepage, <https://www.theicct.org/marine.>, last accessed 2019/03/16.
2. IMO, Third IMO GHG Study 2014, 4 Albert Embankment, London (2015).
3. N. FREESE, CO2 Emissions from International Maritime Shipping, 2017. http://orbit.dtu.dk/ws/files/158911010/Working_Paper_4_Emissions_from_Shipping.pdf. last accessed 2019/03/14.
4. M.BELLER, Reference Energy System Methodology, <http://adsabs.harvard.edu/abs/1976STIN...7717574B>. last accessed 2019/03/16.
5. Mustafa SAĞLAM, Tanay Sıdkı UYAR, Egemen SULUKAN, A Native Energy Decision Model for Turkey, Towards 100% Renewable Energy Techniques, Costs and Regional Case-Studies, pp. 167-177, Springer, Switzerland (2017).
6. LEAP homepage, <https://www.energycommunity.org/default.asp?action=introduction>. last accessed 2019/03/16.
7. LEAP homepage, <https://www.sei.org/projects-and-tools/tools/leap-long-range-energy-alternatives-planning-system/>. last accessed 2019/03/16.
8. J. F. G. L. D. J. K. L. 5. a. Y. W. Zeng Li, Multi-Scenario Analysis of Energy Consumption and Carbon Emissions: The Case of Hebei Province in China, *Energies*, pp. 1-17, Volume 12, Issue 4 (2019).
9. H. MEHLING, Technologies of Energy Conversion, Storage and Transport in the Energy System., Hamburg: Verlag (2016).
10. E. SULUKAN, M. SAĞLAM, T. S. UYAR ve M. KIRLIDOĞ, Determining Optimum Energy Strategies for Turkey by MARKAL Model, *Journal of Naval Science and Engineering*, cilt 1, no. 6, pp. 27-38, Istanbul (2010).
11. United Nations Conference on Trade and Development, Review of Maritime Transport 2018, United Nations, New York (2018).
12. IMO Marine Environment Protection Committee (MEPC), 72nd session, 9-13 April 2018. <http://www.imo.org/en/MediaCentre/MeetingSummaries/MEPC/Pages/MEPC-72nd-session.aspx>. last accessed 2019/03/16.

A Residential Energy Simulation Tool Design

Salih Korhan Zorlu¹, Egemen Sulukan², Dođuş Özkan², Tanay Sıdkı Uyar³

¹ Barbaros Naval Science and Engineering Institute, National Defense University, İstanbul 34942, Turkey

² Mechanical Engineering Department, Turkish Naval Academy, National Defense University, İstanbul 34942, Turkey

³ Mechanical Engineering Department, Marmara University, İstanbul 34722, Turkey
szorlu@tsk.tr, esulukan@dho.edu.tr-dożkan@dho.edu.tr,
tanayuyar@marmara.edu.tr

Abstract. Synchronized with the recent improvements in computer and internet based data collection and processing technologies; the governments and private energy suppliers have been looking for alternative pathways to encompass more precise calculation based projections and decisions while considering the investments on low or zero carbon and renewable energy solutions. Therefore, decision-making support tools, e.g. data mining and machine learning software stand out among various options. Since these actors have the ability and infrastructure to gather the required data to process, residents-the demand side players in the sector- have almost no chance of benefiting their energy consumption data while making their decisions on energy efficiency in their residences.

This paper aims to design a user-friendly simulation software to let a resident or a building manager to build own reference energy system by defining the energy input-output processes within easy steps. The software has been designed to apply alternative scenarios on the reference energy system created by the user, such as replacing the obsolete electrical water heater with a more efficient solar water heating system; regarding to the factors including statistical weather and sun light data in the region and installation/decommissioning costs of respective technologies. In addition to the scenario mode, the software is considered to have the ability to make assumptions for the future energy consumption and develop fundamental recommendations for the resident to improve the energy efficiency.

Keywords: Reference energy system, residential energy demand, energy modelling.

1 Introduction

While we have already been exhausting our natural resources and causing mass pollution in our environment the balance between supply and demand becomes more prominent and stays out as the most critical issue for the energy sector. Energy suppliers and

local or centralized governments are already struggling to prevent supply-demand imbalance while they are trying to adapt their technologies to the emission legislation. At this point, internet and computer-based technologies come to help. Thanks to the never-ending developments on internet and data processing technologies, now administrators have chance to make more accurate decisions by using tools which are powered by machine learning and artificial intelligence algorithms. These tools let the decision makers to create a virtual model of their systems and guide them through tough break-points.

Although we already have these promising developments for the energy management in hand there is almost no chance of benefiting the technology for the residents or energy managers who are placed on the demand side. Considering the importance of more aware customers for a better globe utilizing renewable energies and reducing emissions, it is highly crucial to help residents to make more accurate decisions on their own energy management.

This study aims to develop an easy to use software tool for the residents regarding to the fact that almost none of the decision making tools are designed to help to the individuals who are located on the demand side.

2 Energy Management Decision Tool for Residences

A Visual Basic based energy modelling tool has been developed in order to; first establish a framework identifying the general structure of the residential energy system, then characterize the input-output interaction of energy carriers and demands. The main objective of this tool is to give residents the opportunity to manage their own energy efficiency in their residences and encourage them to switch to renewable energy systems unlike most of the tools which are designed to assist the companies or governments.

The use of this software tool will be explained in the following headings under four main sections which are; data entry, modeling the reference energy system (RES) of the residence, future work and applying a scenario on the RES model sections.

2.1 Data Entry

Data entry section is considered as “must be the easiest part of the software” to encourage the residents to use this tool. The first goal is to create an easy user interface so the consumers could have create their own RES within couple of easy steps. Although there are some improvements to be done on the interface design, users can now add their demand devices in the database in a minute by defining the respective parameters of the utilized energy technologies. Future improvement aims to make the software download the information automatically for the latest products on the market and let the user to pick their product’s brand and model. So the only information to be given by the user will be defining their habitual usage. E.g. user will pick their TV brand and model from the list supplied from an online database and then define their habitual usage such as

“How many hours is my TV “on” in a week or weekend day”. User can reach both “Demand Technologies” and “Energy Carriers” database by clicking the “Items Database” menu on the main window.

Demand Technologies Database

As mentioned earlier, the next objective is to create an online database of current products on the market. But with this tiny and easy to use interface (Fig.1.) the user can easily add their devices to the offline database within minutes as well.

The screenshot displays the 'DEMAND TECHNOLOGIES' application window. The interface is organized into several sections:

- Base Parameters:** Includes fields for Device Name (Refrigerator A++), Installation Cost (4000), Category, Sub Category, Maintenance Cost per Year (0), Decommissioning Cost (100), and Warranty Ends in (3) months.
- Energy Specs:** Includes Source Energy (1) (Electricity), Source Energy (2), Consumption Per Hour (1) (0.9), and Consumption Per Hour (2).
- Emissions (PPM):** Includes input fields for CO2, CH4, N2O, and H2O, all currently set to 0.
- Consumptions:**
 - Hours per Day:** A row of input fields for each day of the week (Monday to Sunday), all containing the value 6.
 - Weeks per Month:** A row of input fields for each month (January to December), all containing the value 4.
- Navigation and Search:** A row of buttons: Delete Device, New Device, Edit Device, Save Device, + Import to Project, and a Search field with a Search button.
- Footer:** A 'Browse Items' button with navigation arrows.

Fig. 1. Demand Technologies Database

Device Name

Device names can be typed and input manually as a user defined string value. It must be unique to get more accurate search results when the database reaches higher volumes.

Installation Cost

The installation cost is the total value spent starting from buying the product until the first start of the product. The software will count that “0” if not specified. This could result in inaccurate calculations in the scenario mode.

Maintenance Costs

The maintenance cost is the net expenditure for periodical or unscheduled maintenance, and this value must be defined as “per year”. If the product does not need any periodical maintenance or user does not specify any value the software will count that as “0”.

Decommissioning Costs

Decommissioning cost is the expenditure that includes all spending to decommission a current device or system such as labour service, waste disposal etc. It is necessary to define that value for further scenario calculations. The software will count that value as “0” if not specified.

Warranty

Warranty option has been considered as another important feature for the energy efficiency management of the residence. Although it is not capable of doing so yet it is a future objective to make the software create recommendations for the user such as “*This device is not protected under warranty options anymore. It is recommended to replace it with a new one to prevent unexpected maintenance or over-consumption costs*”.

Source Energy (1) and Source Energy (2)

Source energy type(s) of the device that can be picked by clicking the drop-down box. Energy carriers must be defined on the “Energy Carriers” database-which will be explained under the next heading. User must define the second source of energy if necessary. e.g. an oven could use both electricity and natural gas at the same time.

Consumption per Hour(1) and Consumption per Hour(2)

Consumption per hour values are the factory consumption data for the device which can be found on the label of the device or on the website of the manufacturer. With the future improvements the user will not have to find this value and define that to the database. The software will automatically download that from an online database after the user pick the device’s brand and model.

Emissions

While supply-demand balance is prominent for the energy management, emission legislation puts formidable boundaries for the sector as well. For example, current legislation in Turkey (Nu. 27075 “Energy Efficiency Management for Buildings” regulation under the Energy Efficiency Law Nu.5627) obliges the constructors to obtain a certificate named “Energy Class ID” for their buildings which has construction area larger than 1.000 square meters. This document includes data about building’s energy efficiency, emissions and isolation values. So one can say that emission values are important as supply-demand balance for energy management and emission control is a “must” for an energy management decision tool.

This section is designed to define the emission values of the device in “Parts per Million (PPM)”. These values can be gathered from the manufacturer’s manual or device’s factory label. In the future the software will be capable of calculating the total emission created by the residence and create recommendations to adapt the residence’s emission value to the legislation.

Consumption Section

In this section users are expected to define their usage habits for the specified device regarding to days and months. First row should include daily usage of the device in hours. Second row should include average week count out of four for the month specified.

Average “On” time for the automatic devices such as refrigerators must be entered. Adding the stand-by time could cause miscalculations. Average “On” time for a refrigerator in a day is close to 6-8 hours and 6 is chosen for the demonstration model as shown in Fig.1.

In the future the software is considered to have the capability to get local outdoor weather data for the residence and process that data to create assumptions for future usage habits by using machine learning and artificial intelligence algorithms.

In conclusion after defining these features on this section in couple of minutes users can easily import the newly created/edited device to their RES Model.

Energy Carriers Database

This database is considered as another important section of the software. The user is expected to define the “unit price per month” value for the current and twelve previous months which can be gathered from receipts. User can choose whether to include tax ratio to this value or use the gross value. This data will be processed in scenario mode when calculating total spending. Additionally, the software will be capable to create assumptions for the unit price regarding to the earlier pricing trends.

Energy Carrier Description: Electricity Supplier: Unit: kWh/h

Unit Price

Month -12	Month -11	Month -10	Month -9	Month -8	Month -7	Month -6	Month -5	Month -4	Month -3	Month -2	Month -1	Current
0,3117	0,3117	0,3117	0,3117	0,3117	0,3117	0,3117	0,3347	0,3347	0,3347	0,3347	0,3347	0,3347

Future Price Assumptions

Month +1	Month +2	Month +3	Month +3	Month +4	Month +5	Month +6	Month +7	Month +8	Month +9	Month +10	Month +11	Month +12
0	0	0	0	0	0	0	0	0	0	0	0	0

Create Assumptions

New Item Edit Item Save Item Delete Item + Import to Project Search

Browse Items

Fig. 2. Energy Carriers Database

Conversion Technologies Database

Conversion Technologies Database section will include devices or systems such as indoor diesel generators, thermal, solar and wind turbine systems which are both consuming and producing energy.

As soon as this section is developed, the software will be able to recommend user to add the most suitable system to their residence after calculating the effects on costs and emissions. That can be named as the “main objective” of this project.

2.2. Modeling the Reference Energy System (RES) of the Residence

Modeling the RES of the Residence is the next step after defining all items to the database.

By using the “Project” menu on the main window as shown in Fig.3. users can create, edit or delete a RES Model for a residence or a building. Predefined Energy Carriers, Conversion and Demand Technologies in the database can be imported to the RES model by clicking “Add” button.

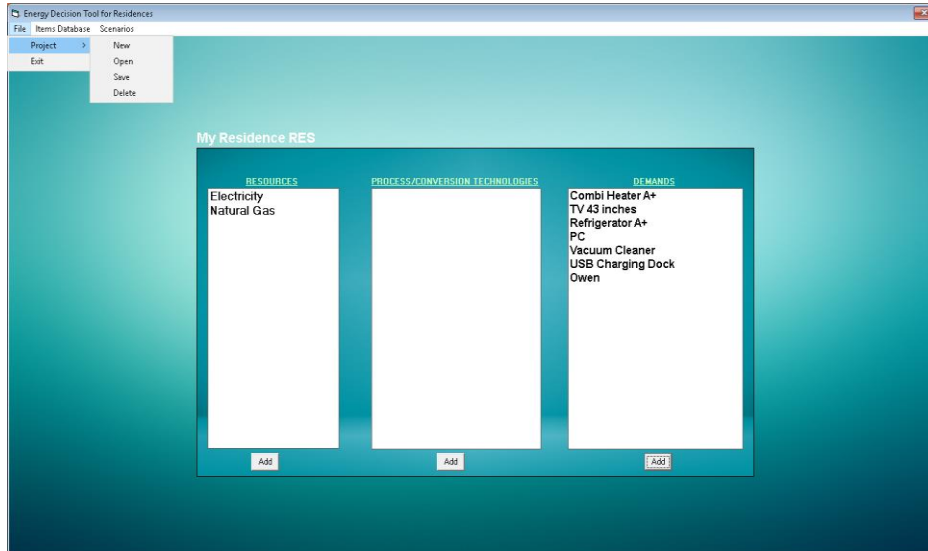


Fig. 3. Creating a Reference Energy System (RES) Model.

2.3. Applying a Scenario on the RES Model

On this section users will be able to create a scenario such as replacing an obsolete device with another one which are in the same class but have different energy features. After defining the scenario, the software gives visual results to the user comparing the consumption and spending values for both current and scenario models. It is intended to help the user to decide whether it is profitable for their energy management or not, to replace a device with another one while considering the installation/decommissioning costs and emissions as well.

For demonstration;

- Two main types of energy carriers (electricity and natural gas) defined in Energy Carriers Database
- Combi Heater A+, Combi Heater A++, 40 inches TV, 43 inches TV, Refrigerator A+, Refrigerator A++, PC, Vacuum Cleaner, USB Charging Dock and an Oven are also defined in the database with real consumption data,
- While defining usage habits, an average four persons family's habits had been taken into account,
- After defining energy carriers and demand side devices a new model named "My Residence RES" had been created as shown in Fig.3.

- For the final step; a scenario had been defined to replace 40 inches TV with 32 inches TV, Refrigerator A+ with Refrigerator A++ and Combi Heater A+ with Combi Heater A++.

After clicking the “Apply Scenario” button on the Scenario Menu, the software gives a comparing result for both Current and Scenario models as shown in Fig.4.



Fig. 4. Scenario Mode Result Screen of the Energy Management Decision Tool

The software first calculates the daily consumption and costs depending on the day and month for both energy carriers (electricity and natural gas) considering the last 12 months and then displays weekly consumption and total amount of spending per year as seen on Fig.4.

Now the residents can see they could reduce their electricity consumption per week from 50 to 40 kWh, Natural Gas consumption per week from 20 to 10 m³/h and Total Spending from 6740 to 4876 by replacing their TV with a smaller screen size and replacing both refrigerator and the combi heater with more energy efficient ones.

3 Future Work

Although this software is still under development as mentioned in previous sections of this paper, latest results reveal that the computer and internet technologies pledge many more new opportunities and brings convenience for energy and emission management on both macro and micro scale.

Regarding to the latest developments in computer and internet technologies studying on this subject will likely dominate the future individual energy management area.

Emphasizing this idea many new features are under development about this software including;

- Developing the conversion technologies interface to import renewable energy types to the models created,
- Adding future price assumption capability regarding to the previous pricing trends to the software by using machine learning and artificial intelligence algorithms.
- Creating an online database of products on the market to let the user easily pick their product and proceed with the next step without having to define it's factory energy data,
- Adding a new ability to gather previous weather data and forecast data from reliable internet resources depending on the region where the residence located will create a new opportunity for the software to recalculate future consumption values regarding to the usage habit trends in specific weather conditions,
- Developing a mobile version of the software so the users could manage their residential energy efficiency anywhere, anytime.

Subsequent to achieving these objectives, this software is considered to be integrated with a smart home system so the software could create more intelligent recommendations for the user by processing the actual data collected from the installed devices.

Calculating the Levelized Cost of Electricity by an Urban Scaled Simulation Approach

Utku Köker¹[0000-0001-7165-777X], Halil İbrahim KORUCA¹[0000-0002-2448-1772], Egemen Sulukan²[0000-0003-1138-2465], Tanay Sıdkı Uyar³[0000-0002-0960-1203]

¹ Industrial Engineering Department, Süleyman Demirel University, Isparta, Turkey

² Mechanical Engineering Department, National Defense University, Turkish Naval Academy, Istanbul, Turkey

³ Mechanical Engineering Department, Marmara University, Istanbul, Turkey

utku.koker@afad.gov.tr, halilkoruca@sdu.edu.tr,
esulukan@dho.edu.tr, tanayuyar@marmara.edu.tr

Abstract. Countries are working to define and track pathways decreasing CO₂ emissions since the Kyoto Protocol has been signed on 1992. Paris Agreement in 2015 fortified the renewable energy strongly; and as a result US and Europe had to step ahead in renewable energy roadmaps. In the renewable energy transition process, cost of annually generated energy has a great importance. On the other hand, as a small representative of a country, cities have more than one energy generation plant. Various fuel-based plants and energy generation technologies (from renewables to fossil fuelled plants) make the calculation of unit cost of energy generation more complex.

Manisa is an important city in Aegean Region of Turkey, rich in energy generation technologies from renewable to lignite plants presents with a wide opportunity for assessment of energy production costs. However, alternative energy cost calculation methods exist in the literature such as ESA and LCOE, with different limitations and assumptions. In this study, a code on MATLAB environment is prepared to simulate the Manisa electricity generation grid to determine the amount of electricity production for each power plant. The outputs of the simulation are used in cost calculation process on the MS Excel sheets using a modified version of LCOE methodology for the base year 2016.

The same simulation has been applied on EnergyPLAN environment as an additional study to verify the results of the MATLAB code and provide a basis for discussion on the amount of energy and respective equivalent CO₂ emissions by these two platforms.

Keywords: Renewable Energy, Emissions, Energy Costs, LCOE, Manisa.

1 Introduction

1.1 Overview

Energy is the main propulsion of the modern world since it drives all the sectors from health to entertainment today. Due to its critical role, it has become an important part of various disciplines such as economics, international relations and military. The main issue of the *International Relations* discipline was the oil for its critical role beginning from the early twentieth century. As the oil transformed firms to international mega companies and became the most important issue in the international commodity market, the term “energy security” gained importance [1]. The oil crises of the 20th century deepened the academic works on oil and energy. Somehow as the stabilization period followed the oil crises, a flourish in energy works occurred after the 2000s for various reasons mainly because of environmental facts. On the other hand, the works through the sixties to now show different characteristics. Initial academic works on energy security were about a stable supply of oil at the cheap price in the conditions of embargoes [2]. Today energy security covers new issues like agendas against climate change.

There is not a unique meaning of “energy security” today. The term was defined multiple times by authorities. Baldwin defined environmental, identity or social security as “different forms of security”. Energy security can be thought of as a type of securitization matter from this point of view which is not a fundamentally different concept [3]. Some key elements are added onto the definition over time like 4As which are availability, affordability, accessibility and acceptability). IEA defined energy security as “the uninterrupted availability of energy sources at an affordable price” [4] with two of the 4As. APERC report included 4As in 2007 [5]. Hughes [6] and Winzer [7] also developed different frameworks for energy security.

Hence the international relations framework focused on energy security from a state-centric point of view. Somehow the focus of energy security has also shifted from securitization of oil trade to electricity grid security and minimization of blackouts over time. As Yergin emphasizes, oil is so powerful that it is already the main commodity in the world. But providing the uninterrupted energy to the consumers gained significance importance in the 2000s. Another problem of the governments is obeying the emission constraints after the Kyoto Process. Many countries launched projects to pass to renewable energy partially or fully. Denmark and Sweden put 100% renewable energy transition plans by 2050 [8]. Large scale wind energy integration of Croatia [9], renewable energy progress of China [10] and Portugal [11], Irish target of 100% renewable energy [12] can be counted in this group. These projects are all at a nationwide level.

Not only national but international solutions are also on the table to handle the uninterrupted energy problem today. *Energy integration* is the precise term to be used when two or more countries make an agreement to lead the legislation issues to promote local energy industry via a permanent installation [13]. Regardless from the name of the unions, every union carries institutional and regulatory asymmetries in it. Relatively richer countries and others have different targets on their agendas and all these differences make the implementation of the policies costly.

At the opposite end of the energy integration, local/regional solutions exist. Since nationwide and international solutions tell so few in local/provincial level, this approach had to emerge over time. As a complementary trend to nationwide solutions, a local/provincial level sensitivity has evolved in the 2000s and some worldwide groups of municipalities are formed like Covenant of Mayors [14] to emphasize the local critical issues. As a classical example, municipalities developed local plans for the reduction of CO₂ emissions from local transport to energy generation processes.

In the provincial level, studies focus on minimizing the fossil-fueled electricity generation technologies and converting fossil fuel to a feasible renewable alternative. Lund shows the methodology that connects the national and provincial energy systems [8]. Paper presents the transition of the two cities to 100% renewable energy.

Turkey has invested heavily in the energy sector since the beginning of the 2000s to redesign the whole energy sector [15]. The privatization process of distribution branch of the sector is finalized and transmission, trade and contracting firms are left in the public sector. During this evolution period, renewable energy is supported by different mechanisms in Turkey (from tax supports to bonus payments per kWh of renewable energy produced) and was opened to the private sector [16]. As a result, renewable energy is fully supported by the private sector over time. Numerous guidelines and amendments were published during the 20 years.

As Figure 1 presents below, the electricity demand of Turkey had incredible growth between 2000-2012. Installed power capacity of the Turkish electricity sector doubled in this period and almost tripled until 2017 to accompany this demand.

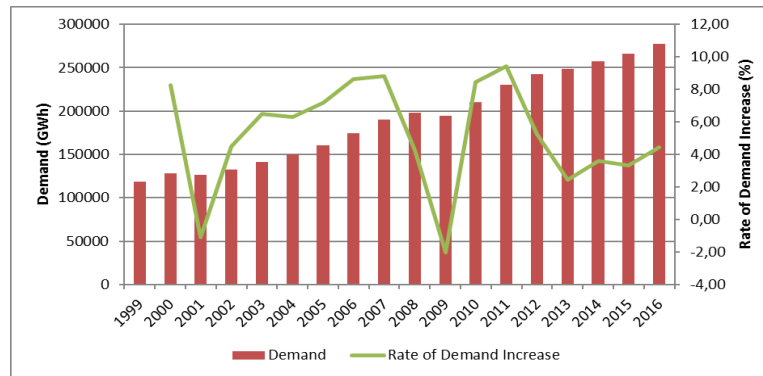


Fig. 1. Demand Growth in Turkey since 1999 [17]

Manisa is an important city in the Aegean Region of Turkey known with industrial and agricultural activities. High technology firms exist in the region and as a result of the annual growth figures, Manisa needs to feed the industrial zone with increasing amounts of electrical energy every year. Electrical energy consumption in Manisa increased 137,83% from 2004 to 2016 which is the highest increase among all TR33 provinces including Kütahya, Afyonkarahisar and Uşak. Next to the high energy need of 4,293 TWh of energy for household, industry etc, Manisa exports its energy to the main grid which makes it a net energy exporter in the region, unlike Uşak that has

limited energy generation assets. Table 1 shows the installed power plants in Manisa to answer such a powerful energy demand:

Table 1. Installed Power Capacities of Manisa

Installed Power Capacities of Manisa in 2016 (MW)	
Technologies	Manisa
Solar Power Plants (PP)	12,95
Wind PP	575
Geothermal PP	118
Hydro PP	69,00
Nat Gas PP	255,594
Coal PP	990
Total	2020,544

This paper includes a simulation of electrical energy generation in Manisa based on 2016 data. A MATLAB code is developed for the simulation and an EnergyPLAN simulation is also prepared by using the same input data to examine if both of the simulation results are in accordance. As a further study, the simulation results are used as an input for cost analysis and the unit costs of electricity produced in the region are shown on the tables.

2 Methodology

2.1 Simulation with the MATLAB Code

Manisa is a big province having different types of electrical energy generation plants. These energy technologies are as follows:

- Solar power plants
- Wind power plants
- Geothermal power plants
- Hydropower plants
- Natural Gas power plants (cogeneration)
- Coal (thermal) power plants.

These generation technologies are represented with at least one power plant in the province. The planning of energy production is a complex work under these conditions. Because these technologies dictate to produce unstable amounts of energy every hour since renewable energy technologies are affected from the natural sources at every hour of the day. PV production reduces as the sunlight diminishes and wind production may increase as the wind speed rises at the region. For this reason, rather than an annual study, an hourly analysis is more realistic and chosen for Manisa.

There are simulation tools free/on sale in the market that are capable of handling the hourly simulation of a region. Instead of using commercial software, a MATLAB code is prepared to make the hourly calculations of the electricity generation and equivalent CO₂ emissions of Manisa. Figure 2 shows the interface of the software below:

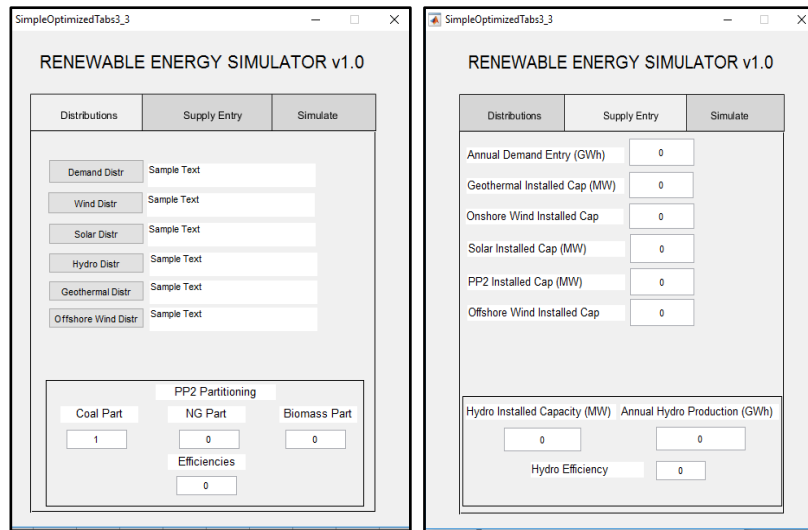


Fig. 2.

MATLAB interface.

The MATLAB code gives priority to renewable energy power plants and utilizes the electricity of them (PV, wind, hydro, biomass power plants) in the first hand. The remaining part of the demand is met with the fossil-fueled power plants like coal and natural gas plants.

At the preparation phase of the study, a reasonable period of time is spent on gathering the required data of the 2016 power plants and demand of Manisa. Since there is not a complete database that shows hourly/annual energy production of the power plants in the region in the given year, lots of different resources are used to obtain information. Current list of power plants (in 2019) are found in some websites [19-20] but to obtain the list of active power plants in 2016, more detailed searches are executed. After the data gathering process, installed power capacities of each power plant and annual demand, are used in the simulation phase. The distribution files (input files) of the technologies are taken from EnergyPLAN distribution files. There are 2 reasons for this usage. First one is, there is not an alternative data file available to use. The second one is to prepare a basis of comparison with the EnergyPLAN simulation which will be implemented during the verification phase.

The interface includes two user entry pages. The first page is used to enter the distribution files of renewable power plants like solar and wind plants. Fossil fuels and biomass power plants are covered under PP2 title and the ratio of each of the three installed capacities are entered to the *PP2 Partitioning* part on the first page. A

weighted average of the efficiencies of the PP2 plants is entered to the edit box of the MATLAB interface either.

The second page is the data entry platform of the installed power plants. The amount of the installed capacities of wind, solar, geothermal, PP2 as well as the annual overall demand are written to the relevant boxes. Similar to the *PP2 Partitioning* part on page one, page two has a special part for hydro data entry.

After the initialization of the regional data according to the above procedure, the simulation is run by activating a *SIMULATE* button on page 3 and outputs are written on an excel sheet. The output data is hourly and includes the amount of energy produced by each different energy generation technology in the province.

2.2 Verification by EnergyPLAN Software

After the MATLAB code simulation, a verification phase is planned with EnergyPLAN software.

EnergyPLAN is a “deterministic simulation model” [21]. The program gives the opportunity to model various scenarios of a given region/state. The software prioritizes renewable energy and adds the remaining amount of energy from fossil power plants if the renewables are insufficient to answer the required demand. The illustration of the components of the program is given in Figure 3 below:

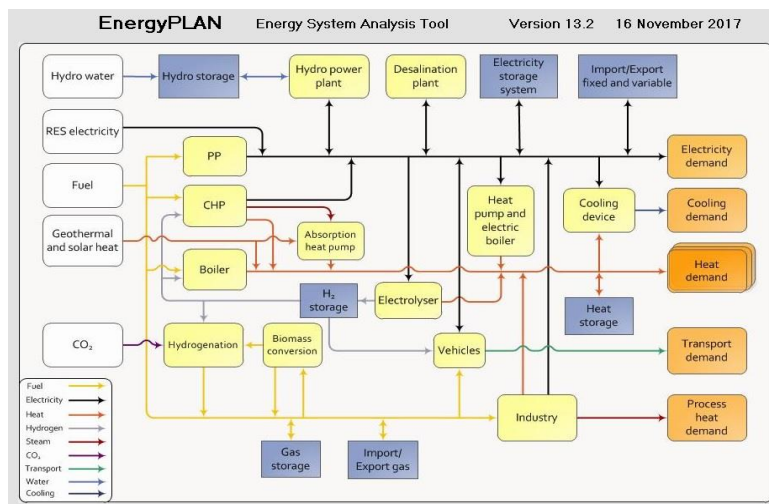


Fig. 3. Components of EnergyPLAN

The input data of the MATLAB code is used in the EnergyPLAN simulation and it is seen that the output of the two simulation methods verified each other perfectly.

2.3 LCOE

Simulation results are used as inputs for a modified LCOE calculation process through MS Excel sheets. LCOE can be formulated as it is given in Eq 1:

$$\sum_{t=0}^T \frac{C_t + M_t}{(1+r)^t} = \sum_{t=0}^T \frac{LCOE * Q_t}{(1+r)^t} = LCOE * \sum_{t=0}^T \frac{Q_t}{(1+r)^t} \quad (1)$$

Where C_t represents the capital costs, M_t is the operational costs, Q_t is the annual energy output and r is the discount rate of capital in time t . When Eq 1 is solved according to LCOE, it becomes:

$$LCOE = \frac{\sum_{t=0}^T \frac{C_t + M_t}{(1+r)^t}}{\sum_{t=0}^T \frac{Q_t}{(1+r)^t}} \quad (2)$$

If the annual output is Q , and the production cost is M , then the formula can be simplified as it is given in Eq 3:

$$LCOE = LFC + LVC \quad (3)$$

LCOE can be formed again as follows:

$$LCOE = \frac{(I+F) + (C_F + V)}{E} \quad (4)$$

Where I is the investment cost, F is fixed O&M, V is variable O&M, C_f is the unit generation cost and E represents the total energy produced in the project duration (18).

With a slight modification LCOE becomes:

$$LCOE_{2016} = \frac{\text{Fuel}_{2016} + (\text{FixedO\&M}_{2016} + \text{VariableO\&M}_{2016}) + \text{InvCost}_{2016}}{E} \quad (5)$$

Equation five is used in the excel sheets for every energy production process in Manisa in the base year 2016.

3 Results

3.1 Environmental Outputs

Environmental outputs are the equivalent CO₂ emissions calculated by the MATLAB and EnergyPLAN simulations. The root cause of CO₂ emissions of electricity production in Manisa in the given base year is the fossil fuel power plants which use the natural gas or coal.

Both simulation tools proved that 990 MW coal power plant and 250 MW natural gas power plants in Manisa produced approximately 4 mt of CO₂ in 2016. Table 2 shows the decomposition of the CO₂ emission among the energy production processes (renewable energy emissions are neglected during the calculations):

Table 1. Decomposition of CO₂ emissions in Manisa in the base year 2016

CO ₂ EMISSIONS (kt)	
Province	Manisa
Coal	3633,384168
N.Gas	266,9822
TOTAL	3900,37

3.2 Output Shares of Electricity Generation Technologies

The amount of energy produced by the relevant technologies in Manisa in the base year 2016 are obtained by the simulation programs both MATLAB code and the EnergyPLAN as shown in Table 3 below:

Table 2. Amount of Electrical Energy Produced by Various Technologies

Technologies	Proportions of Electricity Generation in Manisa in 2016						
	Hydro PP	Geo. PP	Wind PP	Solar PP	Coal PP	NG PP	Export
Electricity Generation (MWh)	116.304	775.344	1.522.397	19.606	5.000.684	615.660	2.420
% in Total	1%	10%	19%	0%	62%	8%	0%

3.3 Unit Costs of Electrical Energy in Manisa

Data of energy produced by various technologies in Manisa are transferred to Excel environment for LCOE calculations. Lazard unit costs [22] are provided for a comparison of the regional outputs. A slight difference occurs at onshore wind and geothermal power plant unit costs which are caused by the high investment and operation and

maintenance cost figures of LAZARD. Calculations are based on EIA cost data [23]. Unit costs of electrical energy produced by each technology are given in Table 4 below:

Table 3. Technology-based electrical energy production costs in 2016.

Technology Unit Costs (\$c/kWh)			
TECHNOLOGY	Unit Cost	LAZARD Lower Bound	LAZARD Upper Bound
Nat Gas Plant	0,11663	0,061	0,23
Onshore Wind Plant	0,09806	0,037	0,081
PV Plant	0,25328	0,18	0,265
Hydro Plant	0,03245	0	0
Coal Plant	0,06807	0,066	0,151
Geothermal Plant	0,07798	0,087	0,116

Various approaches can be developed by using the data above. For example the unit cost of energy produced from renewables and conventional processes can be calculated by Excel. This point of view is presented in Table 5:

Table 4. Unit costs of renewables and conventional technologies.

MANİSA			
	Unit Cost of energy produced from renewables (\$c/kWh)	Unit Cost of energy produced from conventional technologies (\$c/kWh)	Unit Cost \$/kWh
MANİSA	0,09	0,073392458	0,07832

4 Conclusions

Regional energy models are important for both academic and energy sectors of Turkey. Academic works are scarce and provincial analyses are so few in this genre. This paper includes a regional simulation and the cost analysis of Manisa. After a close look at the results, some important remarks are apparent. Some of these key points will be discussed later on.

The equivalent amount of CO₂ is found to be high in Manisa with app 4 mt. This amount should be reduced over time if the climate change measures are to be applied. Kütahya and Manisa are the two cities in TR33 region having significantly high installed power of coal (and natural gas) power plants because of the advantage of coal mines in those provinces. Seyitömer, Tunçbilek, Polat coal plants in Kütahya, Manisa OSB Cogeneration Power Plant and Soma Coal Power Plant in Manisa are the plants using fossil inputs and releasing the emission. The Kyoto process is putting new bounds on the governments to make action plans on mitigation of the emissions in a given time span. It is almost certain that new measures which will be activated due to the international agreements will have effects on fossil-fueled power plants in the near future.

The analysis is based on the reference year 2016 and currently, some of the natural gas plants in Manisa are inactive due to economic problems. This change will be considered in the further optimization and simulation analysis of the region.

Renewable energy unit costs are relatively higher than conventional technologies. The incentives given to the suppliers of renewable energy are important financially. The investment cost figures dropped over time drastically and this trend is expected to go on in the near future. It is concluded that the difference in the unit costs of the fossil-fueled and renewable energy is closing over the years.

5 Future Work

Base year calculations of the simulation phase of TR33 Region is completed with Manisa study. EnergyPLAN results verify the MATLAB code outputs, as it was desired. The next step of the work is planned to be the simulation of the target year (2031). Simulation phase of the work will be completed with the analysis of 2031 outputs.

The core of the PhD thesis is the optimization process of the TR33 provinces electricity generation data. Optimization phase will be modeled with Answer-TIMES and Gams-CPLEX combo. So similar to the simulation stage a business as usual aggregate model of the TR33 region of 2016-2031 time span will be built including various scenarios. Financial and environmental aspects of the scenarios will be analyzed and compared to the simulation results. The best feasible solution to the problem will be obtained by the optimization method under various assumptions mainly favoring renewable energy.

6 Acknowledgments

The findings in this paper result from a research project with project number FDK-2019-6839 and is supported by the Scientific Research Projects Coordination Unit of Süleyman Demirel University, Turkey.

References

1. Yergin, D.: *The Prize: The Epic Quest for Oil, Money and Power*. Simon & Schuster, New York pp13-15 (1991).
2. Colglazier Jr, E. W., & Deese, D. A.: Energy and security in the 1980s. *Annual review of energy*, 8(1), 415-449 (1983).
3. Baldwin, D. A.: The concept of security. *Review of international studies*, 23(1), 5-26 (1997).
4. IEA (International Energy Agency). "Energy Security" IEA Energy Technology Systems Analysis Programme. Paris 2014. (<http://www.iea.org/topics/energysecurity/>) last accessed 2019/03/14.
5. APERC, A.: *Quest for Energy Security in the 21st Century: Resources and Constraints*. Asia Pacific Energy Research Centre, Tokyo, Japan (2007).
6. Hughes, L.: A generic framework for the description and analysis of energy security in an energy system. *Energy Policy*, 42, 221-231 (2012).
7. Winzer, C.: Conceptualizing energy security. *Energy policy*, 46, 36-48 (2012).
8. Thellufsen, J. Z., & Lund, H.: Roles of local and national energy systems in the integration of renewable energy. *Applied energy*, 183, 419-429 (2016).
9. Cerovac, T., Čosić, B., Pukšec, T., & Duić, N.: Wind energy integration into future energy systems based on conventional plants—the case study of Croatia. *Applied energy*, 135, 643-655 (2014).
10. Liu, W., Lund, H., Mathiesen, B. V., & Zhang, X.: Potential of renewable energy systems in China. *Applied Energy*, 88(2), 518-525 (2011).
11. Fernandes, L., & Ferreira, P.: Renewable energy scenarios in the Portuguese electricity system. *Energy*, 69, 51-57 (2014).
12. Connolly, D., & Mathiesen, B. V.: A technical and economic analysis of one potential pathway to a 100% renewable energy system. *International Journal of Sustainable Energy Planning and Management*, 1, 7-28 (2014).
13. Santos, T.: Furthering Regional Energy Security Instead of National Approaches. *Economía del Caribe*, (22) (2018).
14. The Global Covenant of Mayors Homepage, <http://www.globalcovenantofmayors.org>, last accessed 2019/03/14.
15. Erdogdu, E.: Regulatory reform in Turkish energy industry: An analysis. *Energy Policy*, 35(2), 984-993 (2007).
16. Serim, N., & Oran F. C.: The Renewable Energy Policy Convergence in the EU: A Comparison on Germany and Turkey's Incentives for the Wind and Solar Energy Resources. *International Journal of Energy Economics and Policy*, 7(3), 308-320 (2017)
17. Electricity Market Development Report 2016, Republic of Turkey Energy Market Regulatory Authority Strategy Development Department, Ankara, 2017 (<https://www.epdk.org.tr/Detay/DownloadDocument?id=NX82lcTl3w8=>) last accessed 2019/03/14.
18. Lotfi, H., Majzoobi, A., Khodaei, A., Bahramirad, S., & Paaso, A. (2016). Levelized Cost of Energy Calculation for Energy Storage Systems. arXiv preprint arXiv:1610.07289.
19. Official Site of Energy Exchange Istanbul (EXIST) Transparency Platform, Hourly Utilized Capacity of Power Plants in Turkey. Available At: <https://seffaflik.epias.com.tr/transparency/uretim/yekdem/uretim-tahmini.xhtml> [accessed 12.12.2018].
20. Official Website of ENERJİATLASI. Data of Installed Power in Manisa. Available At: <https://www.enerjiatlasi.com/sehir/manisa/> [accessed 12.12.2018].
21. Lund, H.: *Renewable energy systems: a smart energy systems approach to the choice and modeling of 100% renewable solutions*. Academic Press; 2010.

22. Lazard's Levelized Cost Of Energy Analysis, Version 8.0, September 2014. Available At:<https://www.lazard.com/media/1777/levelized_cost_of_energy_-_version_80.pdf>. [accessed 12.12.2018].
23. Official Website of U.S. Energy Information Administration, Updated Capital Cost Estimates for Utility Scale Electricity Generating Plants April 2013. Available At:<<https://www.nrc.gov/docs/ML1801/ML18019A915.pdf>>. [accessed 01.01.2019].

Designing Onshore Wind Farm for Marmara University Following The Global Experience

Gizem Ersoy ¹, Tanay Sıdkı Uyar ²

¹ Department of Electrical and Electronics Engineering, Marmara University, Eğitim Mahallesi,
Fahrettin Kerim Gökay Cd., Istanbul, 34722, Turkey

gizemersoy@marmara.edu.tr

² Department of Mechanical Engineering, Marmara University, Eğitim Mahallesi, Fahrettin
Kerim Gökay Cd., Istanbul, 34722, Turkey

tanayuyar@marmara.edu.tr

Abstract. According to increase of population, energy demand around the world, and environmental damage of fossil fuels, clean and sustainable sources such as wind, solar, thermal, hydro..etc. aroused interest in the World. Especially last decades, discovering a reliable source is a big concern for the community due to the previous reasons.

Renewable energy is a hopeful choice for electricity generation particularly wind energy systems which is called clean energy sources. Fossil fuel reserves such as oil, natural gas, and coal are depleting and have lots of disadvantages for environment. In this point of view, cheap electricity from renewable energy is a great solution.

Wind turbines may be installed on Başbüyük Campus of Marmara University to produce clean energy. In consideration of commonly used wind power programs, wind turbines energy production for the Campus need can calculate. One of the software is Windsim. Windsim needs climate data for the selected area. Wind data collected from Merra Dataset to reach the results. According to the Windsim software results the Campus is suitable for producing wind energy to ensure Campus need. Desired wind farm includes 3 wind turbines whose total rated power is 6 MW. As a result, 17,4 GWh/year can be generated from the wind farm for university need. The total consumption in GWh is 17,2 for a year for the campus according to electricity bills.

Keywords: Renewable energy, wind energy, windsim, wind farm design

1 Introduction

Wind energy is a clean energy resource to produce electricity. Due to increase of awareness of renewable energy sources, wind energy interest rise. Also, wind power capacity increase due to falling costs, fierce competition, lower perceived risks and enabling technologies. According to these developments, bid prices were down. Wind power capacity became 539 GW by adding 52 GW in 2017 around the World. In Europe and India had rise year in 2017, whereas China decrease. Regulatory changes effect increment of producing energy from wind. Almost 13 countries about %10 energy need to deplete from wind energy. Wind energy has a significant potential. Its' production increases %17 over last year. %4.4 of Worlds' power usage is provided by wind energy in 2017 according to its production rise. [1] Turkey's wind power capacity is expanding especially at Aegean and Marmara regions. Turkey has 6.54 GW established wind power capacity in the end of the 2018. 7.33 GW is ultimate value, by adding 0.79 GW power capacity in 2019. [2]

Considering the potential of the wind energy of the Marmara Region, Marmara University's energy need can be covered by wind energy. In this project, Wind farm design will be realized by calculation of energy losses, areal evaluation, environmental factors caused by wind farm by using related software. Maximum energy production will be provided by this Project. Windsim software was used to reach energy calculations.

Güzel is used to Windsim to show the energy production in different height and turbine. The results are compared by using 3 anemometers data and 10 different turbines data. Also, wind blow potential in all sectors are found and the maximum wind blow potential is determined by Windsim.[3]

Özdede obtained wind roses and Weibull parameters at 100 m from Windsim software. In different cases, AEP (Annual Energy Production) for offshore and onshore results are calculated. [4]

Windsim accuracy is high in complex terrain. Also, A.Z. Dhunny and his friends are compared the measured and simulated wind speed data at multiple heights. [5]

Wind is simulated in the Chanthaburi and Trat provinces of Thailand at different heights using Windsim software. MERRA dataset and local wind stations' wind data is used. These data are compared each other. Thanks to results, the potential area for generating electricity is found in the Chanthaburi and Trat provinces of Thailand. [6]

Simisiroglou used both Windsim and WindPRO for wind resource assessment in Greece. The thesis indicates that these software calculate different AEP. Percentage differences between two models are nearly %0,2 - %2. [7]

Wind energy systems installation on campus can provide university shift to %100 clean, renewable energy to satisfy energy need. Thanks to wind energy, people can shift away from carbon-based energy systems in campus. Additionally, on-shore wind energy prices has dropped, and government supports these investmens by providing tax incentives. Engineering faculty students can benefit from wind energy plants in campus. It would be great training for them.

Marmara University have an excellent location for producing wind energy rather than another Universities in İstanbul. From the point of view, in this paper, wind energy assessment is calculated by using Windsim software. Also, Windsim calculation model, method, results, and discussions will be explained in the paper.

2 Methodology

First of all, Marmara Universitys' energy need for a year, need to be determined. This data was collected from the electrical bills. Thus, wind energy production can be evaluated whether it is enough or not.

2.1 Implementation of Windsim Software

In this work, Windsim software is used to calculate the prediction of wind energy generation. This software is based on Computational Fluid Dynamics (CFD). CFD is a calculation model for transmitting the wind in measurement point to turbine hub. Wind data can be collected from on-side measurement method or mesoscale meteorological modelling such as Vortex. Wind data set can be obtained from Vortex an extended historical period. The roughness data effects the result because the local wind field is affected by the terrain. This data which includes terrain height and roughness data, is also given to software.

Windsim Express is used for solving and entering the data. In this section, turbine heights and models are indicated. Also, turbine locations are stated in geographic format. (Lan/Lot) Thanks to these locations, terrain data is obtained for the results.

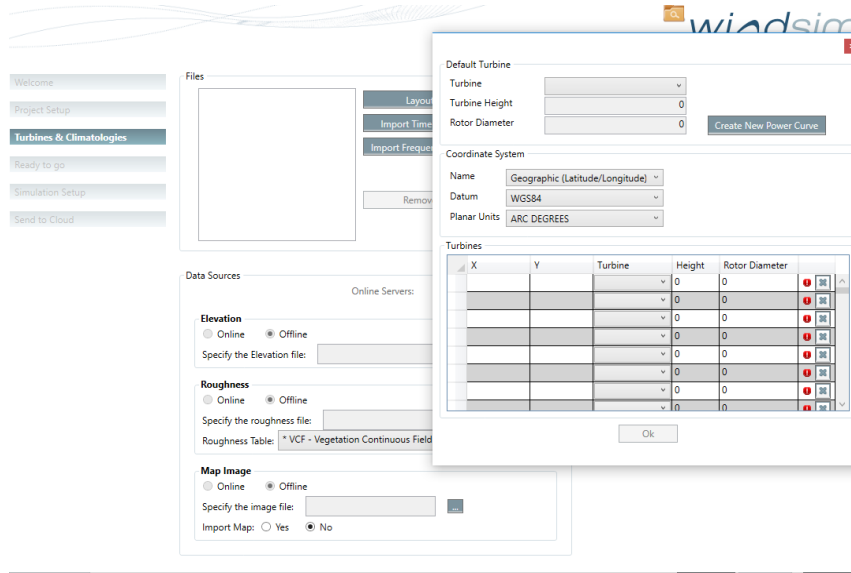


Fig. 1. Display of Windsim Express

Besides, climatology data is entered to the software. In this work, Marmara University's Başbüyük Campus wind data was obtained from MERRA dataset in Vortex for six month. To convert the data Windsim format, Windographer software was used.

After all the simulations finished, results can be seen in Windsim. All modules have the results according to data which is entered to Windsim Express.



Fig. 2. Modules of Windsim

Terrain module is showed terrain and roughness data according to inserted location. Some numerical calculations are solved in this software. To reach the results, initial and boundary conditions, calculation parameters, and physical models are inserted in Wind Fields module. In Objects module, climatology data and turbine specifications can be found. Results module includes 2D results for all sectors. Wind Source module has maps for the wind data. In Energy module, AEP is showed with/without wake losses.

2.2 Reynolds Averaged Navier Stokes Equations

This software uses Computational Fluid Dynamics (CFD) for its calculations. It consists of differential equations according to fluid flow. Also, head and mass transfer is taken into account by their chemical reactions. [8] This program needs wind speed, roughness data, hub height and turbine specifications. To have a 3D wind field, RANS (Reynolds Averaged Navier – Stokes) equations are solved in the software. RANS equations' aim solve the flow in a statistical way. Thanks to this equation, turbulence

effect, density, topography can be taken into account to predict annual energy production. For modelling wind flows especially in complex rural terrains, these equations are essential.[5] The Navier-Stokes formulations have energy conservation, mass conservation, and momentum conservation.

The volume into the fluid must be same leaving volume. This equation can be represented by 3.1. [8]

$$\frac{\partial \rho}{\partial t} + \nabla \cdot \rho \mathbf{u} = 0 \quad (1)$$

where ρ is the fluid's molecular density, and the vector \mathbf{u} is the flow velocity in the x, y, and z directions. The wind speed is very lower than sound speed so, we can assume that the 2.1 equation will be [8]

$$\nabla \cdot \mathbf{u} = 0 \quad (2)$$

Then, the momentum conservation is represented by 2.3.

$$\sum \mathbf{F} = m\mathbf{a} = \rho V \frac{d\mathbf{u}}{dt} \quad (3)$$

So, the general equation will be

$$\frac{\partial u_i}{\partial t} + u_j \frac{\partial u_i}{\partial x_j} = -\frac{1}{\rho} \frac{\partial p}{\partial x_i} + \nu \frac{\partial^2 u_i}{\partial x_j \partial x_j} + f_i \quad (4)$$

where p represents pressure, ν kinematic viscosity, and f_i external forces. Vector size are i and j like $u_i = \mathbf{u} = \{u_x, u_y, u_z\}$. [8]

RANS equations are derived from the Navier-Stokes formulations.[8] For incompressible flows RANS equations will be

$$\frac{\partial u_i}{\partial x_i} = 0 \quad (5)$$

$$\rho \frac{\partial u_i}{\partial t} + \rho u_j \frac{\partial u_i}{\partial x_j} = -\frac{\partial p}{\partial x_i} + \frac{\partial}{\partial x_j} (2\mu S_{ij} - \overline{\rho u'_i u'_j}) \quad (6)$$

where μ represents the eddy viscosity and S_{ij} is the strain rate tensor is represented in 2.7. [8]

$$S_{ij} = \frac{1}{2} \left(\frac{\partial u_i}{\partial x_j} + \frac{\partial u_j}{\partial x_i} \right) \quad (7)$$

the specific Reynolds stress tensor is $-\overline{\rho u'_i u'_j}$. It occurs because of the non-linearity of convective term. [8]

Reynolds stress tensor is derived from approximation like in Windsim calculation. Turbulence models can be explained like in equation 2.8. Boussines hypothesis is used to approach the results. [8]

$$-\overline{p u'_i u'_j} = 2\mu_T S_{ij} - \frac{2}{3} \delta_{ij} \frac{\partial u_k}{\partial k} + pk \quad (8)$$

where μ_T is the eddy viscosity, δ_{ij} is the Kronecker delta function, and k is the TKE (turbulence kinetic energy). [8]

Turbulent dissipation rate is represented ϵ and k is the TKE (turbulence kinetic energy). C_μ is a calibrated constant. Eddy viscosity can be represented in a relationship between ϵ and k . [8]

$$\mu_T = \frac{C_\mu \rho k^2}{\epsilon} \quad (9)$$

Standart constant values need to be used in the calculations to limit the scope of investigations. [8]

3 Results and Discussions

The results are obtained from the Windsim software. Firstly, to reach the results, climatology objects are needed to add to the Windsim software. Wind data can be obtained on-site measurements or from reanalysis datasets. Wind data is collected from MERRA data set which is provided by Vortex. After entering the data to the program, it is shown in table 1.

Table 1. Climatology object characteristics

Climatology Name	Height(m)	Averaged Wind Speed (m/s)	Representative Period
Climatology	80	6.72	31/12/2017 03:00 – 02/07/2018 02:00

To obtain estimation of the gross AEP, the full load hours and capacity factor climatology objects have been used. Wind farm averaged wind speed is about all turbine positions at hub height. It is calculated that averaged wind speed without any kind of losses except from wake losses. Wake losses are included the results.

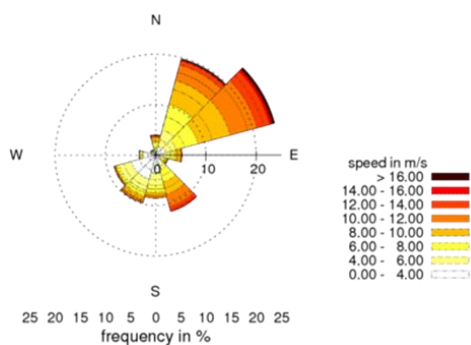
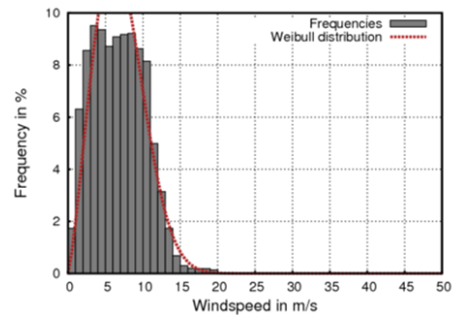


Fig. 3. Wind rose (left) and frequency distribution with Weibull fitting (right) for all sectors

Simulated wind farm includes 3 turbines. Turbines layout is represented in the Figure 2. Turbine technical characteristics are used in wind farm design. Triangles in the Figure 2 represent the turbines, and climatology results are obtained from the location that dots are seen.

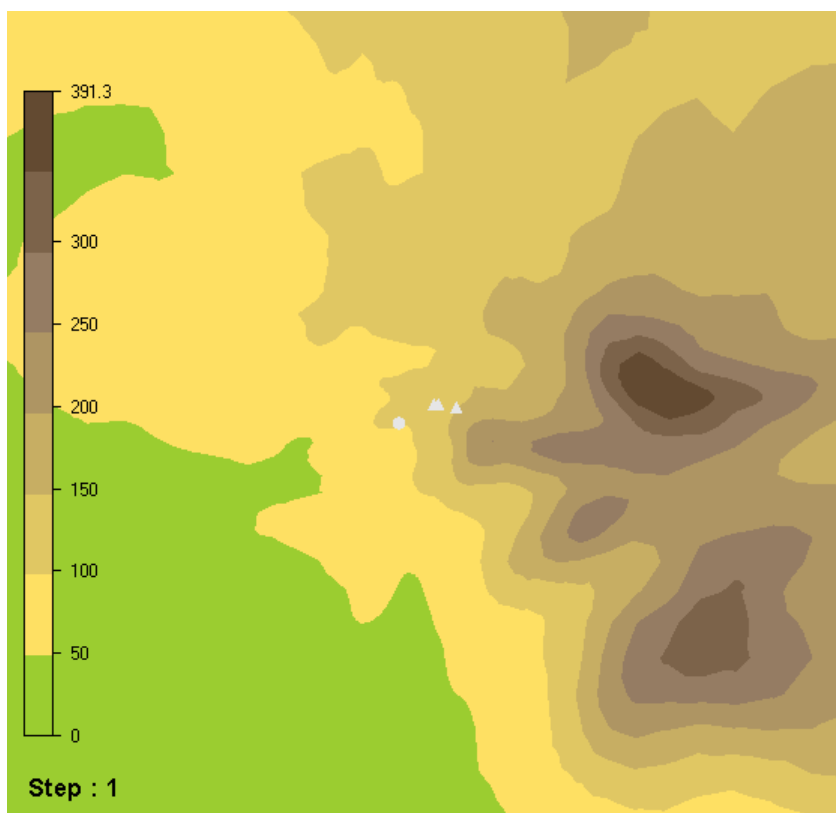


Fig. 4. Wind farm layout; triangles represent turbines, dots represent climatologies

Also, turbines' coordinates are represented in Table 2. These locations are set according to university new campus.

Table 2. Turbine names, types and positions

Turbine name	Hub height	Easting	Northing	Z
Turbine1	80	680003	4537418	144,6
Turbine2	80	679802	4537457	131,7
Turbine3	80	679754	4537411	125,4

Wind turbine characteristics have also great importance explained in Table 3.3 and Figure 3.3.

Table 3. Turbine characteristics

Turbine type	V80mode0
Rated wind speed (m/s)	16
Cut-in wind speed (m/s)	4
Cut-off wind speed (m/s)	25
Diameter (m)	80.00
air density (kg/m ³)	1.225

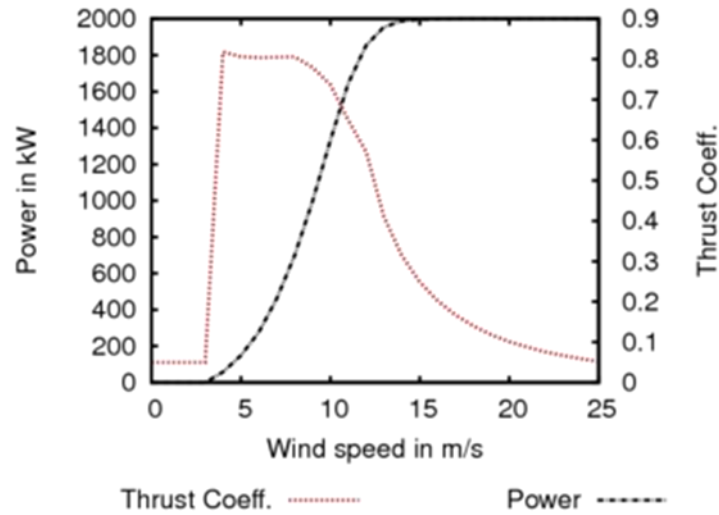


Fig. 5. Turbine characteristics with power and thrust coefficient

The numerical wind database is used to transfer the wind conditions from the measurement point to the wind turbine hub positions. A digital terrain model containing elevation and roughness data has been established for the area given in table 4 and figure 4.

Table 4. Coordinates, extensions and resolution of the digital terrain model

	Min (m)	Max (m)	Extension (m)	Resolution Terrain Data (m)
Easting (m)	674554	684803.1	10249.4	59,1
North-ing (m)	4532436.0	4542257.0	9821.0	59,1

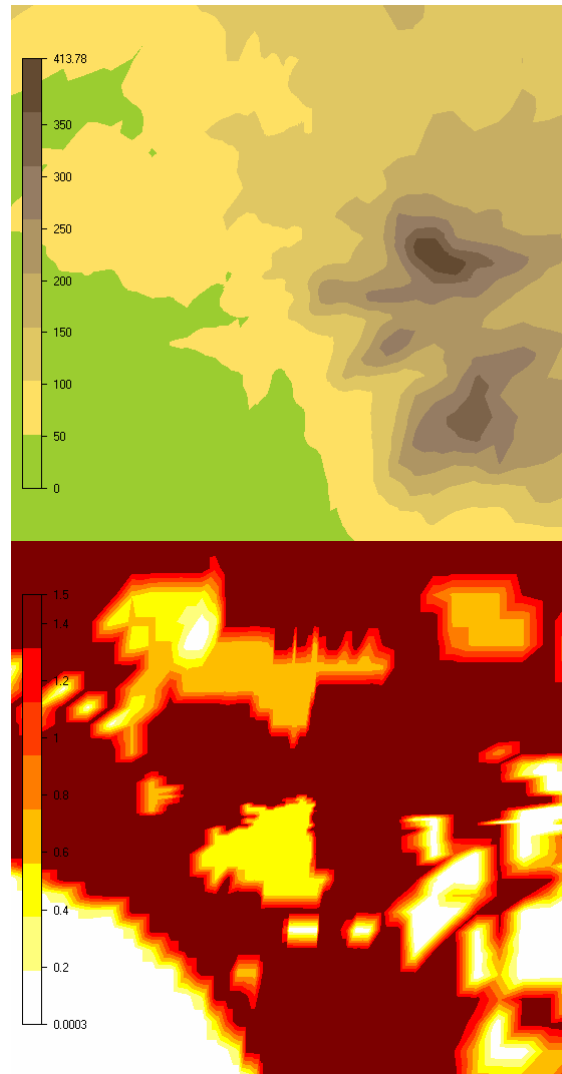


Fig. 5 Terrain elevation (m) (left) and roughness (m) (right)

The complexity at the site depends on the changes in elevation and roughness. Terrain inclination and logarithmic roughness are also generated.

Additionally, A three-dimension domain is obtained from the above roughness and elevation data by the Windsim software. The cells are created with a variable horizontal and vertical resolution. The grid is generated and optimized from the digital terrain model, as seen in figure 6.

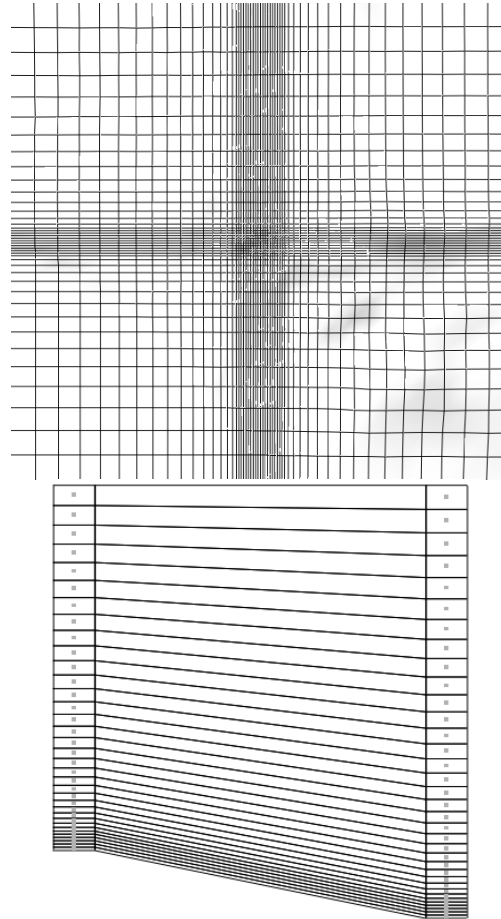


Fig. 6 Horizontal grid resolution (left) and schematic view of the vertical grid resolution (right)

Table 5. Grid spacing and number of cells

	Easting	Northing	Z	Total
Grid spacing (m)	49.4-501.2	51.2-533.8	Variable	-
Number of cells	52	41	35	74620

The grid extends 2236 (m) above the point in the terrain with the highest elevation. The grid is refined towards the ground. The left and right columns display a schematic view with maximum and minimum elevation. The nodes, where results from the simulations are available, are situated in the cell centers indicated by dots.

Table 6. Distribution of the first 10 nodes in z-direction, relative to the ground, at the position with maximum and minimum elevation

	1	2	3	4	5	6	7	8	9	10
z-dist. max (m)	10	30	50	70	90	109	130	154	182	213
z-dist. min (m)	10	30	50	70	90	111	136	164	197	235

Reynolds averaged Navier – Stokes equations represent the digital model. For every 30 degree sector 12 simulations have been numerically solved to obtain a 3D wind field. In the table 7, simulation time and number of iteration can be seen. C indicates that the solution is found and the numerical procedure has converged.

Table 7. Simulation time, number of iterations and convergence status

Sectors	Simulation time	Iterations	Status	Sectors	Simulation time	Iterations	Status
0	00:01:05	76	C	180	00:01:16	78	C
30	00:01:09	78	C	210	00:01:56	82	C
60	00:01:11	86	C	240	00:01:27	84	C
90	00:01:08	80	C	270	00:01:47	81	C
120	00:01:14	86	C	300	00:01:23	87	C
150	00:01:15	85	C	330	00:01:43	90	C

Spot and residual values are evaluated for the the velocity components (U1,V1,W1), the turbulent kinetic energy (k) and its dissipation rate (ϵ). The simulation results are obtained for all sectors.

The average wind speed is seen in the wind resource map. It is obtained from CFD results and long term on-site wind conditions.

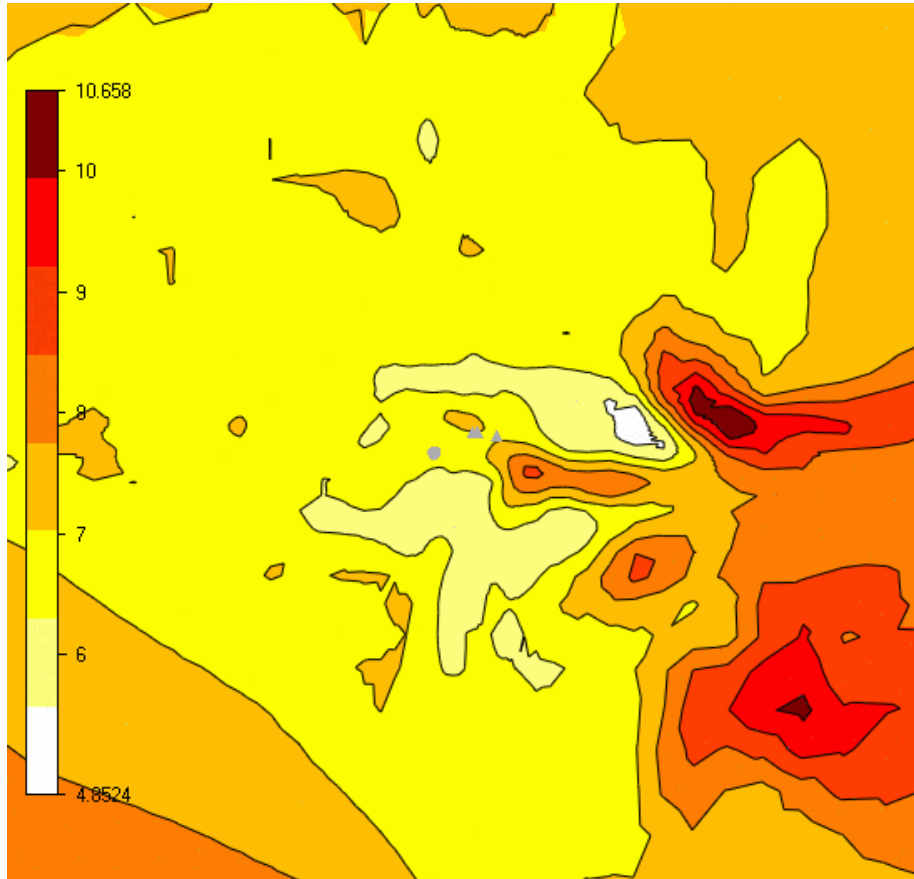


Fig. 7 The wind resource map with average wind speed (m/s) at a hub height of 80 meters

To reach gross energy production of the wind farm, predicted wind speed distribution at the hub height of each turbine, and turbine's specifications are taken into account.

Also, the wake losses are considered and calculated by WindSim wake model. Then, the potential energy production is obtained.

Table 8. Key wind farm and production characteristics

Turbine Type	Hub Height (m)	No. of turbines	Capacity (MW)	Gross AEP (GWh/y)	Average wind speed (m/s)	Wake losses (%)	AEP with wake losses (GWh/y)	Full load hours (hours)	Capacity factor(%)
V80mode0	80,0	3,0	6,0	17,6	7,0	1,0	17,4	2896,9	33,1

Table 9. Energy production in GWh/y based on climatology represented by the frequency distribution

Climatology name	Gross AEP (GWh/y)	AEP with wake losses (GWh/y)	Wake losses (GWh/y)	Wake losses (%)
Climatology	17,558	17,382	0,177	1,007

Table 10. Annual energy production per turbine

Turbine name	Air density (kg/m ³)	Average wind speed (m/s)	Gross AEP (GWh/y)	Wake Losses (%)	AEP with wake losses (GWh/y)	Full load hours (hours)
Turbine1	1,225	6,950	5,746	0,322	5,727	2863
Turbine2	1,225	7,020	5,916	1,440	5,831	2915
Turbine3	1,225	7,000	5,897	1,238	5,824	2911

3.1 Conclusions

Marmara University's one-year consumption is calculated from utility bills. For all campuses total bills price is 7.825.717 TL and the total consumption in GWh is 17,2 for a year. In dollar currency, the price is nearly 1.205.286 \$

Total possible production of the wind energy is 17,4 GWh/year.

Excess energy is 0,2 GWh/year.

This excess energy can be sold to electric distributor firm from the price of 7,3 \$ cent/kWh.

The amount of money that the University can get every year is $200000 \cdot \frac{7,3}{100} = 14.600$ \$

In this project, 3 turbines is used and every turbine is 2 MW. Total capacity is 6 MW. Their investment cost is nearly 6 million dollars. Its lifetime is nearly 20 years. We can say that in 10 years total investment cost can be met from electricity bills price. Then, 10 years wind generation can be used for selling the electricity and university energy need.

4 References

1. Wind power, https://en.wikipedia.org/wiki/Wind_power, 20/03/19
2. http://www.ren21.net/wpcontent/uploads/2018/06/178652_GSR2018_FullReport_web_1.pdf, 20/03/2019
3. Güzel, S., May 2014, Rüzgar Enerjisi Potansiyel Hesaplamalarında Kullanılan Bilgisayar Programlarının Karşılaştırılması, İstanbul Technical University, İstanbul
4. Özdede, S., September 2013, Wind Resource Assessment And Wind Farm Modeling in Complex Terrain: Bodrum Peninsula Case Study Using Computational Fluid Dynamics, Middle East Technical University, Ankara
5. Dhunny, A.Z., Lollchund*, M.R., 2016, Wind energy evaluation for a highly complex terrain using Computational Fluid Dynamics (CFD), S.D.D.V. Rughooputh Department of Physics, Faculty of Science, University of Mauritius, Mauritius
6. Thongyai, N., Assawamartbunlue, K., 2017, Wind atlas of Chanthaburi and Trat provinces, Thailand, Energy Procedia (2017) 389-393, 4th International Conference on Power and Energy Systems Engineering, CPESE 2017, 25-29 September 2017, Berlin, Germany
7. Simisiroglou, N., June 2012, Wind Resource Assessment Comparison On A Complex Terrain Employing Windpro And Windsim, Gotland University, School of Culture, Energy and Environment, Gotland, Sweden
8. Ivanell, S., Sørensen, J.N., 2017, Improvement of RANS Forest Model via Closure Coefficient Modification, Uppsala University Campus Gotland, Department of Earth Sciences, Sweden

User-Focused Designing and Pricing of an Off-Grid Photovoltaic Solar Energy System

Emre LEBLEBİCİOĞLU^[1]

¹ Mechanical Engineering / Department of Energy / Institute of Science and Technology
Marmara University
Göztepe, 34722 / Kadıköy – İstanbul
emreleblebicioglu@marun.edu.tr

ABSTRACT

Solar energy is an immense renewable energy source to obtain electricity and heat. Producing electricity by solar energy is the one of the best solutions for area in which, there is no electrical grid. Photovoltaic (PV) solar power systems are the most known method to convert sunlight to electricity. Although there are different types of PV solar power systems, this article underlines off-grid solar PV system (battery-based). Moreover, an importance of user-focused designing off-grid solar PV system is highlighted and compared with traditional calculation methods. Even though, the subject of this article looks like simple, it puts forward many mistakes, while determining capacity of PV system's component by companies that are specialized over PV systems. Designing user-focused system provides minimum initial system cost and maximum efficiency. Therefore, this design method can play vital role to deployment of usage of solar energy for all over the world.

Keywords: off-grid photovoltaic system, solar energy, user-focused, battery

1 Introduction

Solar PV system is the direct transformation solar energy into electricity. Today, more than 1.4 billion individuals everywhere throughout the world need access to power. To enhance access to power to the next level in the rural areas on the planet, a decentralized off-grid installations are considered in type of solar PV. An Off-grid PV Systems are systems which utilize photovoltaic innovation. The systems utilize the DC yield of the PV modules to power DC loads, while a battery bank is utilized to store energy when there is demand [1]

1.1 Off-Grid Solar PV System

One might encounter such solar system when there is no grid in such a rural area or even when the utility power pricing is quite high. Here, the solar panels become the utility company and generate the needed energy by one's home or any energy dependent system. There may be no option other than to go with an off-grid solar system. [1] Off-grid systems require more care and maintenance but can give a strong sense of independence, so one is no longer being subjected to the risk of a loss of power from

the utility grid. Off-grid solar systems where the solar energy is generated and consumed in the same place meaning it does not interact with the main grid at all. [1]

1.1.1. Solar Panel

The heart of a photovoltaic system is the solar module. Many photovoltaic cells are wired together by the manufacturer to produce a solar module. When installed at a site, solar modules are wired together in series to form strings. Strings of modules are connected in parallel to form an array. [2]

1.1.2. Batteries

Batteries store direct current electrical energy for later use. This energy storage comes at a cost, however, since batteries reduce the efficiency and output of the PV system, typically by about 10 percent for lead-acid batteries. Batteries also increase the complexity and cost of the system. [2]

Types of batteries commonly used in PV systems are:

Lead-acid batteries;

- Flooded (a.k.a. Liquid vented)
- Sealed (a.k.a. Valve-Regulated Lead Acid)
 - ✓ Absorbent glass mat
 - ✓ Gel cell
- Alkaline batteries;
 - ✓ Nickel-cadmium
 - ✓ Nickel-iron

1.1.3. Charge Controller

A charge controller, sometimes referred to as a photovoltaic controller or battery charger, is only necessary in systems with battery back-up. The primary function of a charge controller is to prevent overcharging of the batteries. Most also include a low voltage disconnect that prevents over-discharging batteries. In addition, charge controllers prevent charge from draining back to solar modules at night. Some modern charge controllers incorporate maximum power point tracking, which optimizes the PV array's output, increasing the energy it produces. [2]

1.1.4. DC-AC Inverter

Inverters take care of four basic tasks of power conditioning:

- Converting the DC power coming from the PV modules or battery bank to AC-power
 - Ensuring that the frequency of the AC cycles is 60 cycles per second
 - Reducing voltage fluctuations
 - Ensuring that the shape of the AC wave is appropriate for the application, i.e. a pure sine wave for grid-connected systems. [2]

2 Designing Parameters of User-Focused Off-Grid Solar PV System and A Sample System For Istanbul

In spite of the fact that user-focused off-grid solar PV system is considered as an ordinary way to design PV system, it provides an economical PV system with maximum efficiency. Customer requirement is the one of the main rule of user-focused system. This rule means that determining electrical device usage by customer is so important to design the system properly. Thus, every solar energy company should meet with customer before designing and pricing the system. Unfortunately, some companies submit the PV system to their customers without considering their demand. This kind of companies usually install the system which has unnecessarily big capacity.

Another main rule of user-focused system is designing and sizing components in harmony each other. This is crucial to create a system with long lifetime and high efficiency. Especially, the capacity of solar panels and batteries should be calculated by matching each other. In other words, if solar panels do not charge batteries by 100% during a sunny day, then, the battery lifetime might be short and accordingly the system's efficiency can be low. This article is organized to show an importance of these rules and supported by calculation, equations, graphs and tables.

2.1 Load Assessment

Knowing daily electricity usage of a house which needs solar PV system is vital factor for designing of the system components. It is obvious that off-grid solar PV system is generally installed to regions in which there is no electrical grid. Hence, the daily power consumption cannot be calculated by electricity bills.

Daily energy demand can be calculated by the following criteria;

- List the all of the electrical machines, devices and appliances to be supplied power with by the solar PV system being introduced.
- Determine the specific operating time of electrical machines and devices by meeting with user.
- Considering the load type (3-phase or 1-phase) of devices by their label data.
- The daily power consumption (kWh/day) should be determined by calculation and analyzing the load of electrical machines, devices and appliances.
- If there is no any devices in the resident. User should be convinced to buy electrical devices which are in A+ energy efficient class.
- The minimum solar radiation and peak sun hour in winter season of the building should be determined.

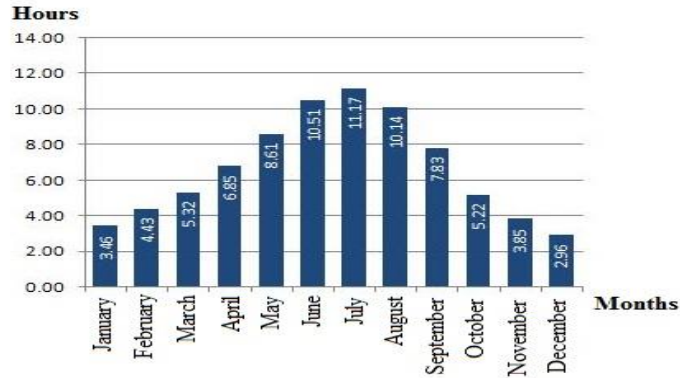


Fig 1. Peak Sun-hours of Istanbul by months [3]

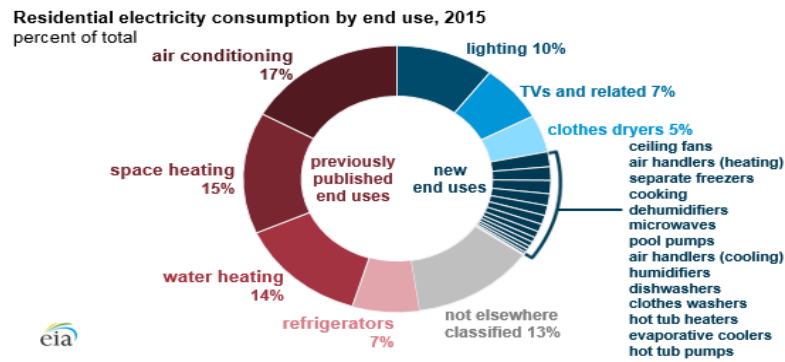


Fig 2. Residential electricity consumption by end use 2015 [4]

While designing off-grid solar PV system, the lowest peak sun-hours is always considered in the calculations, which is 2,96 on December in Istanbul. In this article, this value is used as 3 hours for sizing PV array.

Table 1. Load Profile of the Appliances

Electrical Devices	Quantity	Rated Power (W)	Hours Used Per A Day (hours/day)	Daily Energy Consumption (Wh/day)
Refrigerator	2	50	24	2400
TV-Receiver	1	100	12	1200
Lighting	10	12	6	720
A+ Washing Machine	1	1200	2	2400
A+ Dishwasher	1	1000	1	1000
Air Conditioning	2	1200	8	19200
Other Devices	5	1000	2	2000

Total: 28.920 Wh/day

Solar energy companies usually design a system by average daily electricity consumption. They just design the system by electrical devices without considering their operating hours during a day. Even though this kind of designed system has a big power capacity, it is also quite expensive. In our sample, daily energy demand is **35 kWh/day**, if it is calculated by average usage. In this article, user-focused and standard calculation methods and systems are compared with each other.

2.2 Designing of Components

Off-grid solar PV system is consisted of four fundamentals components: solar PV panel, battery, charge controller and inverter. Though, mounting system equipment is included to this system, this article mostly underlines designing of four main components.

By using criteria of the power assessment, the capacity of PV array and batteries can be calculated. On the other hand, the charge controller is chosen by the total current and voltage of PV array and batteries. As for that the type of inverter is depended on the rated power of electrical devices. Furthermore, the capacity of the new type inverters within charge controller can be determined by PV array, batteries and of course appliances.

2.2.1 PV Array Sizing

The capacity of PV array is determined by the following criteria;

- Daily energy demand (kWh)
- The total output voltage and ampere-hour of batteries (V, Ah)
- The area of rooftop (m²)
- The sunshine duration (hours)
- Maximum operating voltage of inverter (V)

$$PV \text{ Array Capacity} = \frac{\text{Daily Energy Demand} \left(\frac{kWh}{\text{day}} \right)}{\text{Peak Sun Hour} \left(\frac{\text{hour}}{\text{day}} \right)}$$

$$S_p = \text{The Number of PV Panel} = \frac{PV \text{ Array Capacity} (W)}{\text{Selected PV Panel Power} (W)}$$

Daily Energy Demand (kWh/day) = 30 kWh/day

$$PV \text{ Array Capacity} = \frac{30 \text{ kWh/day}}{3 \text{ hours}} = 10 \text{ kW}$$

$S_p = \text{The Number of PV Panel} = \frac{10000}{290} = 34,48 \rightarrow \mathbf{36 \text{ PV Panels (User-focused)}}$

$$PV \text{ Array Capacity} = \frac{35 \frac{kWh}{day}}{3 \text{ hours}} = 11,66 \text{ kW}$$

$S_p = \text{The Number of PV Panel} = \frac{11666}{290} = 40,22 \rightarrow \mathbf{42 \text{ PV Panels (Standard)}}$

Table 2. The selected solar PV panel specifications

Maximum Power-Pm [W]	290
Open Circuit Voltage-Voc [V]	39.5
Short Circuit Current-Isc [A]	9.52
Maximum Power Voltage-Vm [V]	31.9
Maximum Power Current-Im [A]	9.09
Module Efficiency- η [%]	17.7

2.2.2 Charge Controller Selection

The charge controller is the one of the most important components to keep the system safe. Especially, it is the vital device to obtain maximum efficiency from battery and to provide long lifetime. The charge controller is sometimes mounted and selected separate from inverters which are the old model. However, the new generation inverters contain charge control device. In this article, the selection of charge controller is underlined by assuming separate from inverters.

Charge controller selection by the following criteria;

- The total voltage and current output of PV array module,
- The total output voltage of batteries.

The current range of charge controller should not be less than total short circuit current of PV panel string. Moreover, increasing current in high operating temperature of PV panel should be considered as well. For this reason, the total short circuit current of PV panels multiplies with a constant. This can be seen following equation;

$$\frac{I_{SCC} \cdot S_p \cdot 1,25}{2} \leq I_{CCC}$$

I_{SCC} : Short circuit current per PV panel (A)

S_p : the number of PV panel

I_{ccc} : Selected minimum operation current of charge controller

The denominator is 2 on the equation due to connection of PV panels. Because, the PV modules in Off-grid solar energy system are generally consisted of two parallel strings, which means the half of number of PV panels.

$$\frac{9,52 \cdot 36 \cdot 1,25}{2} \leq I_{ccc}$$

$$214,2 \text{ A} \leq I_{ccc} \text{ (User-focused)}$$

In this article, each inverter which is chosen contains 48V/80A charge controller. Inverters provide totally 160 A charging capacity. By adding a 48V/60 A controller, we obtain 220 A capacity of charge controller and this is enough for our system.

$$\frac{9,52 \cdot 42 \cdot 1,25}{2} \leq I_{ccc}$$

$$249,7 \text{ A} \leq I_{ccc} \text{ (Standard)}$$

By standard calculation, our system needs 2 pieces of 48V/60A charge controllers. On account of the fact that, the minimum charging capacity should be more or less 249,7 A by the equation.

2.2.3 Battery Bank Sizing and Selection

Battery is the heart of off-grid system. Thereby, the quality and capacity of batteries play key role for lifetime and efficiency of the system. Although, there are diverse type of batteries on the market, only a few kind of batteries (Gel, OPzS, lead-acid etc.) can be efficient for solar PV system.

Battery bank sizing is determined the following criteria;

- The capacity of battery should be at least two times more than the daily energy consumption owing to cloudy days.
- The number of average cloudy days and decreasing efficiency by the high temperature is considered.
- The chosen inverter's capacity is also important to calculate battery bank sizing. Since, inverters operate by different voltage ranges (12V,24V,48V) of battery.
- Selecting the deep-cycle and high temperature battery type is significant for the system's efficiency.

$$\text{The number of batteries} = \frac{E_T \cdot t_0 \cdot C_C}{\eta_B \cdot P_B \cdot HF}$$

E_T : The daily energy demand (W/day)

t_0 : The duration when PV panel does not produce enough electrical current. (day)

η_B : The efficiency of battery

HF : Heat factor (the efficiency loss of battery under high temperature)

P_B : The power of selected battery (W)

C_C : The correction constant (User-focused: 0,61,Standard: 0,8)

The correction constant is used for user-focused system designing. This constant is determined to keep battery lifetime long. Moreover, batteries can be charged so fast by solar panels because of this constant and this is significant not to force batteries by operating electrical devices. When batteries are full charged, devices is operated by PV panels during a day.

$$\text{The number of batteries} = \frac{30000 \frac{Wh}{day} \cdot 3 \cdot 0,61}{0,8 \cdot 0,8 \cdot 12 \cdot 200} = 35,74$$

= 36 pieces of battery (User-focused)

$$\text{The number of batteries} = \frac{35000 \frac{Wh}{day} \cdot 3.0,8}{0,8 \cdot 0,8 \cdot 12 \cdot 200} = 54,68$$

= 56 pieces of battery (Standard)

2.2.4 Inverter Sizing

An inverter that can handle the maximum rated electric power that must be drawn by all of the electric appliances when they are all turned on at the same time should be chosen. However, a safety factor is needed to design such a proper off-grid PV system. Thus, the safety factor is 1.3.

Table 3. The rated power and quantity list of electrical appliances

Electrical Devices	Quantity	Rated Power (W)	Hourly Rated Power
Refrigerator	2	50	100
TV-Receiver	1	100	100
Lighting	10	12	120
A+ Washing Machine	1	1200	1200
A+ Dishwasher	1	1000	1000
Air Conditioning	2	1200	2400
Other Devices	5	1000	1000

Total Rated Power: **5920 W**

The capacity of inverter = 5.920 W x 1,3 = 7.696 W → **8 kW**

There is no 8 kW off-grid inverter on the solar market. Thereby, the two pieces of 4 kW inverter are used by paralleling each other.

3 Pricing of User-Focused Off-Grid Solar PV System

From Table 5 and Table 6, there are two results of the system designing. It is undeniable the fact that user-focused system is the cheaper than standard system. Since, user-focused system is based on user demand, system lifetime and efficiency (especially batteries). Even though, the standard system gives the bigger capacity of battery and PV panels than user-focused system, it is unnecessarily huge and accordingly expensive.

As can be seen on the tables, battery is the most expensive system component of off-grid solar PV system. Hence, the calculation of determining battery bank's capacity should be carefully done. A harmony between PV panels and batteries is significant. Due to the fact that, solar panels should charge batteries by % 100 during a day. If batteries are not charged enough, then their lifetime will be short and their efficiency is getting lower day by day. Therefore, user-focused system gives a suitable solution to both solar companies and customers.

Table 5. The components and price list of the user-focused system that is designed

Components	Quantity	Power Capacity	Unit Price	Total Price
290 W Polycrystalline Solar Panel	36	10,44 kW	0,3 W/\$	3132 \$
12/200 Ah Deep-Cycle Gel Battery	36	86,4 kW	240 \$	8640 \$
48V 60A MPPT Charge Controller	1	48V/60A	170 \$	170 \$
4K Inverter with 48V/80A MPPT Controller	2	8 kW	550 \$	1100\$
Mounting Equipment	Set	-	-	500 \$

Total: 13.542 \$

Table 6. The components and price list of the standard system that is designed

Components	Quantity	Power Capacity	Unit Price	Total Price
290 W Polycrystalline Solar Panel	42	12,18 kW	0,3 W/\$	3654 \$
12/200 Ah Deep-Cycle Gel Battery	56	134,4 kW	240 \$	13.440 \$
48V 60A MPPT Charge Controller	2	48V/120A	170 \$	340 \$
4K Inverter with 48V/80A MPPT Controller	2	10 kW	600 \$	1200\$
Mounting Equipment	Set	-	-	600 \$

Total: 19.234 \$

4 CONCLUSION

As a result, user-focused system should be a fundamental method to design solar PV systems by solar companies. While this designing method provides a profit for companies, users get affordable off grid solar PV system. Table 5 and 6 depicts that standard system is roughly 5500 \$ more expensive than user-focused system due to the cost of extra solar panel, charge controller and batteries.

Using of solar PV systems can only increase by decreasing the initial cost of the system. Necessity of off-grid solar PV system is an incontrovertible fact for rural regions where there is no electrical grid. Off grid system is the best solution to provide electricity to 1.4 billion people in the world, who do not have electricity access.

5 REFERENCES

[1] Ammar A. T. Alkhalidi, “Design of an Off-Grid Solar PV System for a Rural Shelter”, Research gate, pp. 17-27, 2018.

[2] Solar Electric System Design, Operation and Installation, Washington State University, pp. 8-18, October 2009.

[3] T.C. Enerji İşleri Genel Müdürlüğü
<http://www.yegm.gov.tr/MyCalculator/pages/34.aspx> , 2018

[4] U.S. Energy Information and Administration
<https://www.eia.gov/consumption/residential/>, 2015

Investigation of Engine Performance and Emission Parameters of Ethanol-Acetylene Mixture in an SI Engine at Partial Load

Reyhane Doğan^{1*}, Mehmet İlhan İlhak¹,
Selahaddin Orhan Akansu¹, Sebahattin Ünalın¹

¹Erciyes University Engineering Faculty Department of Mechanical Engineering,
Kayseri, Turkey

reyhanedgn@gmail.com, s-unalan@erciyes.edu.tr

ilhanilhak@gmail.com, akansu@erciyes.edu.tr

Abstract. Population growth in recent years has led to tremendous growth in fossil energy demand, and limited oil reserves forced researchers to search for alternative fuels. In this context, ethanol and acetylene which can be obtained from renewable and non-petroleum energy sources, have great potential. In this study, the effects of ethanol and acetylene mixtures on the general performance, emission values of a spark ignition engine have been investigated. In these experiments, acetylene flow rates were fixed at 250 g/h, 500 g/h, 750 g/h and 1000 g/h. The experiments have been carried out on a four-cylinder, four-stroke and water-cooled SI engine designed to develop the rated power output of 75 kW at 5500 rpm under 25% constant load at 1500 rpm and in different air-fuel ratios. As a result of the experiments, it was observed that with the increased amount of acetylene added to ethanol, the excess air ratio range increased and the specific fuel consumption decreased. Exhaust emissions were observed to be decreased in high excess air ratios compared to pure ethanol.

Keywords: Ethanol, Acetylene, Emissions, Internal combustion engine

1 Introduction

Petroleum reserves are gradually decreasing by looking at production and consumption [1]. Because of the decrease in fossil fuel reserves, alternative fuel research is one of today's research topics for researchers. It is possible to see ethanol and acetylene in the fuel. Ethanol production is not dependent on petroleum and ethanol is added to fuels in some countries and is used in internal combustion engines. Acetylene is obtained from the reaction of the calcium carbide with water.

Çolak studied engine performance and emission tests using 100% ethanol and 100% gasoline at different compression rates. As a result of the tests, the specific fuel

consumption of ethanol in all compression ratios was higher than gasoline. In the study of ethanol, there were significant decreases in CO, NO_x and CO₂ emissions except for HC emissions [2].

The engine performance or emission values were investigated by adding various amounts of ethanol to gasoline by the studies in the spark ignition engines. Eyidoğan et al. Used ethanol gasoline and methanol gasoline mixtures and observed that HC, NO, CO, CO₂ emissions decreased with the use of alcohol mixtures [3]. Örs et al. Conducted studies on fuels containing 10-20-30% ethanol by volume and examined vehicle performance and exhaust emission effects [4].

Lakshmanan and Nagarajan have chosen a four-stroke, 4.4 kW diesel engine with a slight modification of the intake manifold to hold the gas injector controlled by an electronic control unit (ECU), and experiments have been conducted for various gas flow rates. As a result, they observed that performance was nearer to diesel at the full load and a safe operation of acetylene replacement up to 24% was possible to reduction in emission parameters [5,6,7].

Ilhak et al. examined engine performance and emission values by stabilizing the flow rates of acetylene and changing the engine load from 25% to full load. At lower loads, NO emissions were lower compared to gasoline, whereas HC emission values for all loads decreased with acetylene addition. In another study, have been experimentally investigated the engine speed was 1500 rpm, different loads (25% and 50%) and different excess air ratios [8,9].

2 Experimental Setup and Test Procedure

The experiments were carried out at the Erciyes University Engineering Faculty of Mechanical Engineering Engines Laboratory. In studies, engine performance and emission values were analyzed for 100% ethanol and ethanol-acetylene mixtures. The characteristics of the fuels are given in Table 1. The experiments were carried out in different excess air ratio at 1500 rpm and 25% partial load. A summary of the test procedures is given in Table 2.

Experimental studies were performed in a four-stroke, four-cylinder, water-cooled Ford MVH418 1.8L internal combustion engine. Engine specifications are given in Table 3. Ethanol fuel quantity was measured by Krohne liquid mass flow meter and acetylene ratio was measured by Alicat M100 gas flow meter. Motor speed and torque values were measured by PCS dynamometer. Cylinder pressure values were measured with PCB 113B22 piezoelectric pressure sensor and the emission values were measured with the Bosch BEA 060 gas analyzer.

Table 1. The properties of fuels

Properties	Acetylene	Ethanol
Formula	C ₂ H ₂	C ₂ H ₅ OH
Density (kg/m ³)	1.092	785
Ignition energy (MJ)	0.019	0.7
Auto ignition temperature (°C)	305	558
Adiabatic flame temperature (K)	2500	1920
Lower calorific value (MJ/kg)	48.23	26.9
Flammability limits (vol.%)	2.5-81	3.3-19
Flame speed (m/s)	1.5	0.61
Stoichiometric air fuel ratio	13.2	8.93

Table 2. The summary of the experimental procedures

Item	value
Engine speed	1500 rpm
Load	25% partial load
Air fuel ratio	Different excess air ratios
Ethanol + Acetylene	100% Ethanol Ethanol + 250 g/h Acetylene Ethanol + 500 g/h Acetylene Ethanol + 750 g/h Acetylene Ethanol + 1000 g/h Acetylene

Table 3. Engine specifications

Item	Specifications
Engine	Ford MVH418
Cylinders	4 in line
Weight	123 kg
Bore/Stroke (mm)	80.6/88
Max. power/BMEP	75 kW/10.7 bar
Max Torque	150 Nm/4000 rpm
Compression ratio	10:1
Idle /max speed	800/6000 rpm
Engine stroke volume (L)	1.796

2.1 Brettschneider Equations

The BEA 060 calculates the excess air ratios from the measured HC, CO, CO₂ and oxygen concentrations. The Bosch BEA 060 gas analyzer measures the excess air ratio according to gasoline. We use the Brettschneider formula to find the correct values of the lambda for ethanol and acetylene.

Brettschneider formula:

$$\lambda = \frac{[CO_2] + \left[\frac{CO}{2}\right] + [O_2] + \left[\frac{NO}{2}\right] + \left(\left(\frac{H_{CV}}{4} * \frac{3.5}{3.5 + \frac{[CO]}{[CO_2]}} \right) - \frac{O_{CV}}{2} \right) * ([CO_2] + [CO])}{\left(1 + \frac{H_{CV}}{4} - \frac{O_{CV}}{2} \right) * ([CO_2] + [CO] + (n * [HC]))}$$

[XX] = Gas concentration in % volume

H_{CV} = Atomic ratio of Hydrogen to Carbon in the fuel

O_{CV} = Atomic ratio of Oxygen to Carbon in the fuel

n = Number of the Carbon atoms in the molecule of the selected HC

3 Results and Discussions

3.1 Brake Specific Fuel Consumption

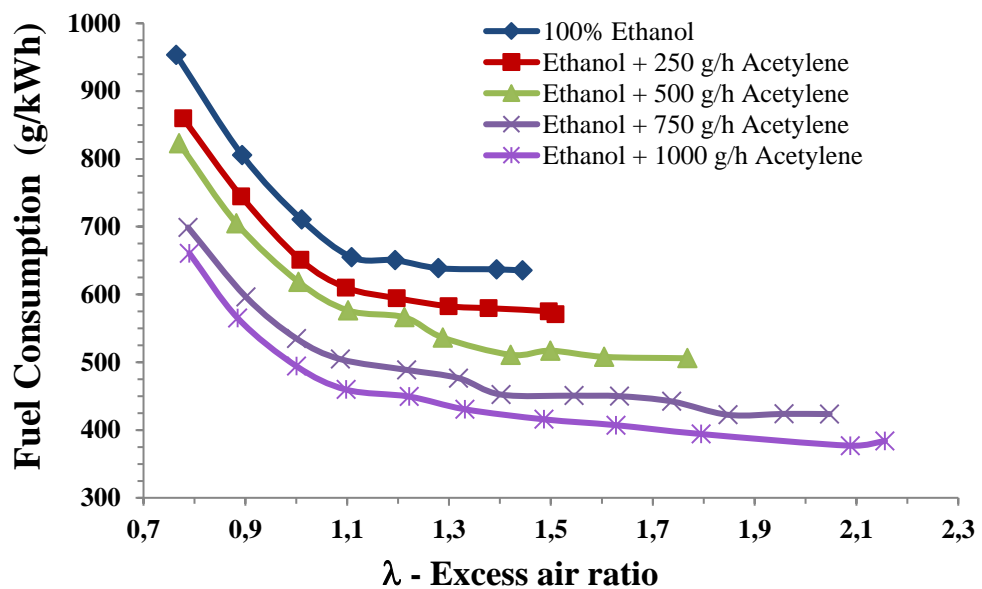


Fig. 10. Fuel consumption according to excess air ratio

In Figure 1, fuel consumption values are given according to excess air ratio. Lambda values for 100% ethanol were found to vary between 0.8-1.5. With the addition of 250, 500, 750 and 1000 g / h of acetylene to the ethanol, it is observed that the maximum values of the lambda increase and the fuel consumption decreases. The largest values of lambda appear to be ethanol + 1000 g / h of acetylene, which range is about 0.8-2.2 in the Figure 1.

3.2 Brake Thermal Efficiency

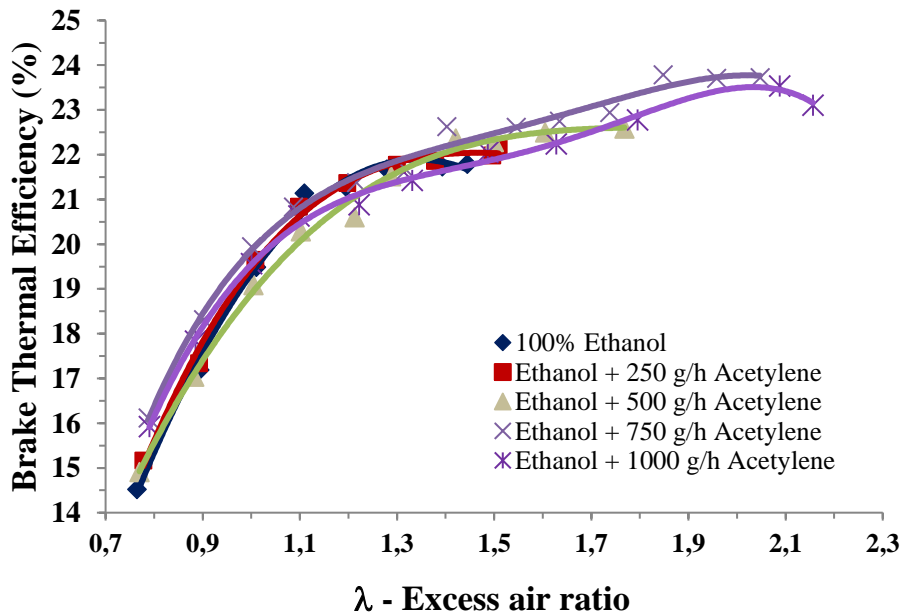


Fig.2. Variation of brake thermal efficiency by excess air ratio

The variation of the brake thermal efficiency for the various ethanol and ethanol-acetylene mixtures with the excess air ratio is shown in Figure 2. Lambda values with maximum thermal efficiency relative to fuel mixtures are approximately 100% ethanol, ethanol + 250, 500, 750, 1000 g/h respectively $\lambda=1.4$, $\lambda=1.5$, $\lambda=1.77$, $\lambda=1.85$, $\lambda=2.1$. The highest thermal efficiency of the mixtures is ethanol+750 g/h acetylene value.

3.3 Emissions (CO, HC)

Figure 3. shows the change in carbon monoxide values with lambda. As seen in the figure, the carbon monoxide emission value decreases rapidly with the increase of the lambda. When the carbon monoxide emissions in the same lambda values are

considered, it is seen that the highest values are obtained in 100% ethanol. As the amount of acetylene added increased (from 250 g/h to 1000 g/h), it was observed that the carbon monoxide emission at the same lambda values decreased and continued horizontally after a certain lambda value.

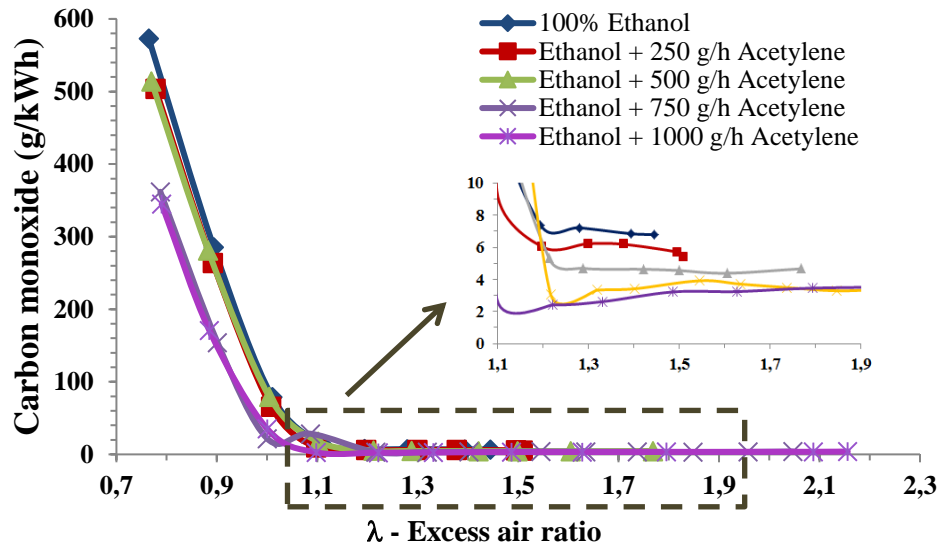


Fig. 3. CO emissions according to changing excess air ratio

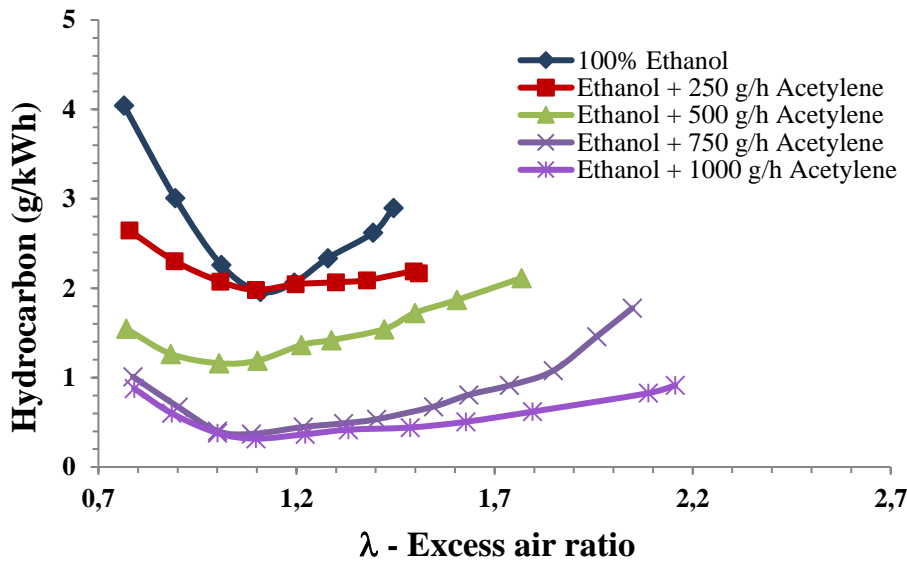


Fig. 4. HC emissions according to changing excess air ratio

As a result of our experiments, the change in the hydrocarbon emission values according to the lambda is given in Figure 4. When UHC values were compared according to the increasing lambda for each fuel, it was observed that increasing amounts of acetylene (for 250, 500, 750, 1000 g / h respectively) decreased UHC values. The lowest UHC values were obtained in $\lambda=1$ or $\lambda=1.1$.

3.4 Cylinder Pressure

In our experiment, the ignition advance was tried to be adjusted to 15 degrees after the upper dead point. In the figure given below, the values of the inside cylinder values in the lambda values with respect to the crank angle are given. It is seen in the figure that the peak pressures is 15 degrees after the upper dead point.

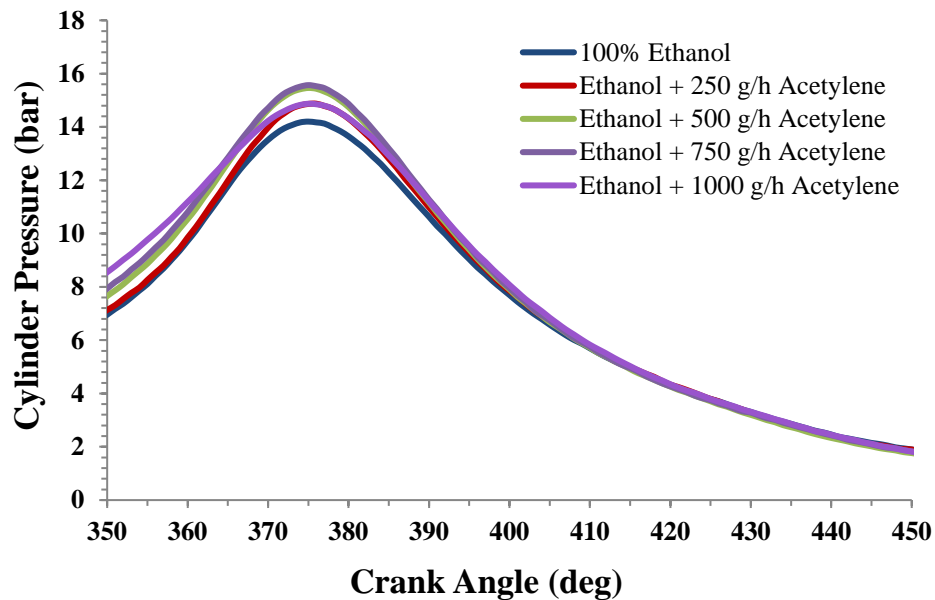


Fig. 4. Variation of cylinder pressure with CA at 25% load

4 Conclusions

This study was carried out to perform engine performance and emission values using a water-cooled, four-stroke four-cylinder internal combustion engine with a 1500 rpm cycle and a 25% constant load of ethanol and ethanol acetylene mixture. The research results are briefly as follows,

- The addition of acetylene to ethanol reduced specific fuel consumption and increased the range of excess air ratio that the engine was running.

- When the maximum yields are observed, it is seen that the values are in high parts of the lambda.
- UHC emissions of ethanol-acetylene mixture were lower than 100% ethanol. Furthermore, as the amount of acetylene in the mixture increases, the UHC emission decreases.
- It has been observed that CO emission values have decreased by increasing the addition of acetylene to ethanol and by the increase of the lambda.

Acknowledgements

The authors would like to acknowledge the Scientific Research Projects Unit of Erciyes University, Turkey.

References

1. <http://www.tpao.gov.tr/tp5/docs/rapor/sektorrapor3105.pdf>, last accessed 2019/04/09
2. Çolak, A.: Buji Ateşlemeli Bir Motorda Farklı Sıkıştırma Oranlarında Etanol Kullanımının Performans ve Emisyonlara Etkisinin İncelenmesi, Yüksek Lisans Tezi, Zonguldak Karaelmas Üniversitesi Fen Bilimleri Enstitüsü, Karabük, (2006).
3. Eyidoğan M., Çanakcı M., Özsezen A.N., Alptekin E., Türkcan A., Kılıçaslan İ.: Etanol-benzin ve metanol-benzin karışımlarının buji ile ateşlemeli bir motorun yanma parametrelerine ve egzoz emisyonlarına etkisinin incelenmesi , Vol 26, No 3, 499-507 (2011)
4. Örs İ., Tarakçıoğlu N., Ciniviz M.: Yakıt olarak benzin-etanol karışımlarının taşıt performansı ve egzoz emisyonlarına etkisinin incelenmesi , Vol: 12 No: 1 pp.13-19 (2009)
5. T. Lakshmanan, G. Nagarajan.: Experimental investigation on dual fuel operation of acetylene in a DI diesel engine. Fuel Processing Technology 91, 496–503 (2010)
6. T. Lakshmanan, G. Nagarajan.: Experimental investigation of timed manifold injection of acetylene in direct injection diesel engine in dual fuel mode. Energy 35 ,3172-3178 (2010)
7. T. Lakshmanan, G. Nagarajan.: Experimental investigation of port injection of acetylene in DI diesel engine in dual fuel mode. Fuel 90 , 2571–2577 (2011)
8. İlhak M.İ., Akansu S.O., Kahraman N., Ünalın S.: Experimental study on an SI engine fuelled by gasoline/acetylene mixtures , Energy, 151, 707-714 (2018)
9. İlhak M.İ., Tangöz S., Akansu S.O., Kahraman N.: An experimental investigation of the use of gasoline-acetylene mixtures at different excess air ratios in an SI engine , Energy, 175, 434-444 (2019)

Decentralization of The Power Sector In The City-Province Of Kinshasa For Achieving The Vision 100% Renewable Electricity By 2050

Arcell Lelo Konde ¹[009-533-870-0353] and Prof.Dr. Tanay Sidki UYAR ²[009-532-774-4525]

¹ Cyprus International University, Institute of Graduate Studies and Research, Energy Systems Engineering Department, North Cyprus via Mersin 10, Turkey

² Marmara University, Department of Mechanical Engineering, Götzepe campus 34772 Istanbul, Turkey
lncs@springer.com

Abstract.

Shifting worldwide municipalities and cities to 100% renewable electricity could be among alternatives to consider and support for achieving the millennium objectives of green cities and reducing threats from global warming. This paper provides an understandable review on different steps to be taken by Kinshasa municipalities and analyzes possibilities existing from today's technologies to allow the city to minimize its heavy reliance on hydropower in order to maximize it on solar and wind. Additionally, constraints and obstacles to decentralization, benefits, policies to be implemented locally, and recommendations, are all discussed and examined by the research findings. As policies continue driving investments globally, the study attempts to involve all actors at every level of society to participate in the adoption of other new forms of renewable energies, in particular, solar and wind power in order to increase efficiently and smartly the electrification rate which is currently assessed at 44.1% representing almost 490MW of the installed capacity of the latter. The energy demand is assessed at 1390MW and is, however, projected to highly rise by 2050 due to the increase of the population and their growing energy demand. Based on the city's power potential, the research results suggest a decentralization of the power sector with 4% electricity generation from hydropower, 10% from onshore wind and 86% from solar that could include solar technologies and any other related to this type. In this study, we assume that this vision would be achieved once the sector is completely decentralized in solar, wind, and hydropower.

Keywords: Decentralization, renewable electricity, city-province of Kinshasa

1 Introduction

The city-province of Kinshasa, the capital city and one the twenty-six provinces (states) of the Democratic Republic of the Congo, is located alongside the Congo River, one the largest and longest rivers on the African continent, and lies between 4°17'30" and 4°30'00" latitude south and 15°12' and 15°30' longitude east. Geographically, the city

is located in north and west by the Congo River, which is also the border with Brazzaville, the capital city of the Republic of the Congo, east and northeast by the province of Mai-Ndombe, Kwilu, and the Kwango, and south by the Kongo central province [1]. Actually, it is comprised of twenty-four municipalities, in particular, Barumbu, Gombe, Kinshasa, Kintambo, Lingwala, Mont-Ngafula, Ngaliema, Bandalungwa, Bumbu, Kalamu, Kasa-Vubu, Makala, Ngiri-Ngiri, Selembao, Kisenso, Lemba, Matete, Ngaba, Kimbanseke, Maluku, Masina, N'djili, and Nsele.

Point of view population, the total number of people living currently the Kinshasa agglomeration is estimated at around 13 million [2] and has a total surface area of around 9,965 square kilometers which makes it be the largest city in the country and one of the largest on the African continent [3]. Presently, about 44.1% of the population has access to electricity against 55.9% with no access as a result of the non-connection to the local grid often caused by power outages [4]. However, to face this issue, most of the people keep relying on petroleum products, currently considered as the only way to face power interruptions occurring in the city and keep supplying the electricity in residencies and/or industries. Although, recently, there have been significant advancements in the integration of solar photovoltaic systems in homes, commercial buildings and others, there is still much to do for these technologies to compete petroleum products on the power market due to their high costs. These petroleum products are mainly gasoline and diesel fuel, their use in the city as a back-up alternative to power interruptions, would dramatically have negative impacts and consequences on the environment. Due to the increase of the population, high rate of poverty, overcrowding as well as other related issues, as in most of the African cities, it is important to shift from dirty to clean energies to come up with these issues; for example, renewable energy sources, solar, wind and hydropower to name a few, can increase the lifestyle satisfaction of local communities, create a safe and clean environment with less air and water pollution, reduce any risks susceptible to raise global warming effects in the future and even to prevent them, and reduce energy supply insecurity as well, bring stability and more revenues for a long term period based on their unlimited capacity to renew easily and quickly in a very short period of time compared to fossil fuels subject of political uncertainties and instabilities in some corners of the globe and take about millions of years to be formed [5] [6] [7].

Moreover, they can create wealth for the local communities and provide safety to both local and foreign investors. And these renewable energy sources can be, however, found in the city. They are comprised of solar and hydropower both with an enormous energy potential as well as wind energy which speeds may differ from one to another municipality. In some municipalities, wind speeds can reach 5m/s, while in others they can be greater than this value. Nevertheless, for a height of 10m, the average wind speed is assessed at 1.3m/s per year [4]. Apart from the wind potential, there also exist high levels of solar irradiance and their values are between 3.22 and 4.89 KWh/m²/day. These high solar radiation levels make the city be in a favorable position to implement more projects on solar photovoltaic systems, concentrated solar power, and other related technologies to significantly improve the current electrification rate, by combining them together with other forms of renewable energies (wind and hydro) consisting to bring up the access to electricity and meet energy needs of the population. Out of the two types of energy discussed above, there also exist possibilities to exploit the

hydroelectric potential of the Congo River which is the world's largest river in terms of flow and its energy potential is estimated at over 100,000MW [8] [9] [10]. In fact, the electricity sector is highly dominated by hydropower which accounts for almost 96% of the electricity consumption in the whole city [11] [12]. Given some circumstances, in particular the repetitive series of power outages sometimes blackouts caused by electric overcharges and the high dependency of hydroelectricity from the neighboring province, the city now seeks for sustainable solutions to exploit on n place the three renewable energy sources that it possesses in particular solar, wind, and hydropower in order to reduce the transmission line costs and any risks from the collapse of an electricity transmission line during the power transportation as they are transported in long distances and could also be considered as one of the main causes of blackouts that occurred in Kinshasa municipalities there are a couple of years ago. These possible solutions seeking the latter can be evidently found through the roadmap 2050 initiated in this study aiming to power all municipalities with 100% renewable electricity. Yet, for the latter to achieve the millennium objectives of a green city by 2050 or earlier if possible, it is necessary that the government fosters the rapid development of renewable energies by promoting; for example, more public transport and increasing their availability in each municipality, foresees safe biking, walking infrastructures and other related in each construction project of roads or highways; timed walk signals, and so on [5]. Despite these ambitious steps, there is still much to be done in order to achieve the vision of 100% renewable electricity.

The roadmap 2050 would require a certain number of factors to be met, such as a consistent and strong policy that can easily implement laws to discourage imports of fossil fuels as well as their use and to provide more safety to investments in the power sector including exonerations for companies operating already or intending to operate in the sector. The involvement of all actors in the society, local communities, stakeholders, government and others; all should be committed and massively participate in the adoption of clean and renewable energies in order to increase access to electricity within the city and bring up the current electrification rate from its low rate to high rate, 100%. Energy efficiency measures are very common in the city due to some of the factors among them can be quoted the lack of training and awareness from customers (energy users). However, organizing workshops, seminars, mass campaigns or other related activities would much help to incentivize the local communities and other actors about their energy overuse and the importance of using energy efficiently and smartly.

2. Current Status of the Power Sector

The city-province of Kinshasa is endowed of tremendous energy potential in renewable resources principally solar energy with high rates of insulation in the day time representing one side an alternative to threats from global warming and the other side a potential solution to the decentralization. The current power sector is massively dependent on hydropower which represents over the two-thirds of the electricity consumed in the whole city [13]. This electricity is generated from Inga and Zongo dams both located at around 150 kilometers far away from the Congo River Basin in the province of

Kongo central. The city is actually supplied by a power line coming from both power plants Inga and Zongo [14]. The installed capacity is currently assessed at 490MW (44.1% of the electrification rate) whereas the energy demand is 1390MW and it is expected to significantly increase in the next five years (SNEL). This means that 900MW is needed in the whole city, in particular, solar and wind energy in order to reduce the dependency from hydropower as the city seeks the decentralization through clean energies. The transport of the electric energy consumed in the city-province from both production sites Inga and Zongo to distribution centers has been made possible thanks to three different power lines. The first electricity transmission line carries power to a capacity of 220KV between the regions of Inga located in the province of Kongo Central where power is generated and the city-province of Kinshasa. The second electric transmission line of 132KV between Zongo site located in the Kongo central province and Badiadingi site in the city-province of Kinshasa; both are extended at 59Kilometers. The third power line consisting of 70KV between Zongo site and the municipality of Gombe, Kinshasa. Actually, electric networks are comprised of 8 posts; 23 substations, 886 distribution transformers, and around 230,000 subscribers, as well as other new infrastructures, added recently by the National utility company, SNEL [7]. In addition, Kinshasa city possesses nearly 363 medium voltage power connection lines for a total length of 2,080 kilometers in which 76 of them are currently overcharged. These overcharges are often caused by the heavy increase of the energy demand due to a certain number of factors among which can be quoted: the creation of new quarters and small and medium enterprises in some residential areas as well as the lack of regular maintenance of infrastructures starting from the electricity generation in power plants to the delivery, and as a result, electric cables are deteriorated and a series of repetitive power outages occur in some corners of the city. Yet, the current urbanization of the city dating since the colonial period is no longer adapted to the current increase of the population which has also raised the energy demand in the whole agglomeration. But with the increase of the population including anarchic constructions caused by the lack of strong regulations in the sector, it is necessary to redesign a new urbanization plan that takes into account the present electric network including the distribution lines and their recent additions in the city.

3. Present and Future Energy Situation

3.1 Present Energy Situation

The electric energy is provided by the National utility company, SNEL. As discussed previously, the current energy demand is assessed at around 1390MW but due to heavy electric overcharges of energy consumers and very often huge energy losses in electric transmission lines alongside the power transportation; only 490MW is provided to consumers. The most important consuming energy sector either in the country or the city is the residential sector. For example, in the country, it accounts for almost 77% of the average electricity consumed followed by industries with 25% and other sectors, such as agriculture, transport, public services and other related represent just 2.5% [15]. These data collected are for the period ranging between 1980 and 2010 due to some

difficulties to access easily to data on the ground from public institutions or other private firms operating in the country. Further research should be conducted on the ground to determine the electricity consumption by sector for the last five years based on each of the sector stated above in order to make better projections in the future.

Point of view electricity consumption in the city-province of Kinshasa by energy source, The analysis has been made possible by collecting data from various organizations based on their reports and reviews on electricity either in the country or the capital city and have, however, allowed to minimize the gap from other sources in order to provide approximations that approach the true reality of the current status of the power sector in the city-province. To this end, it must be noted that 96% of the electricity consumed comes from hydropower followed by petroleum products and solar PV systems, both respectively 3.5% and 0.5%. The electricity consumption of the city for the period ranging between 2016 and 2018 is shown in the below figure.

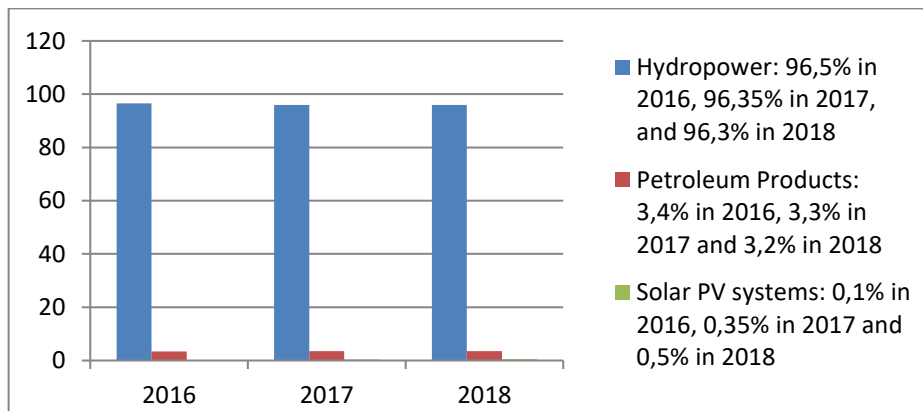


Figure 1 Electric Power Consumption in the city province of Kinshasa for the period 2016 – 2018

Source: Various (investigations, reports, and websites reviewed for the city-province)

Since the seventies, the industry trends for the electricity either in the whole country or the city have always been dominated by hydropower which keeps occupying a prominent place in the power sector and also the energy mix (electricity) as shown on the above figure. In the past two decades, the electricity consumed was over 95% from hydropower [10]. But again due to a series of repetitive power outages occurred during the year 2016 mainly caused by the lack of maintenance of turbines and other infrastructures in power plants, a great number of people in the city decided to move to other forms of energy and thus, began using petroleum products principally gasoline and diesel fuel to keep supplying electricity to their homes. In 2016, as it can be observed that from the above data, an increase in the consumption from petroleum products was much observed and thereafter, it started decreasing at the beginning of the year 2017 as shown on the above figure. On the contrary, during the years 2017 and 2018, there were significant advancements in the integration of solar photovoltaic systems on the power market and their deployment within the city allowed creating hundreds of jobs for local communities. The new renewable energy industry has, however, won the confidence of

many of the consumers but again there is still much to be done at the local level in order to boost their deployment for achieving the vision of the roadmap by 2050 or earlier if possible.

3.2 Future Energy Situation

The analysis has also been used research findings of a series of studies conducted recently on the ground to predict the energy mix (electricity) for the decentralization of the power sector of the city-province of Kinshasa through the roadmap 2050 which targets to power its municipalities with 100% renewable electricity. These long term projections obtained from research findings of recent studies aim principally to increase the electricity consumption from solar technologies from 0.5% up to 86% by 2050 given the fact that the latter is located in an area with high rates of insolation in the day time and also, it is a free energy generated directly from the sun. this means that solar technologies would occupy a prominent place in the energy mix with 86% in which 6.8% shall be generated from rooftop solar, 52.5% from solar power plants and 25% from concentrated solar power plants. Onshore wind and hydropower would provide 10% and 4% respectively [16]. The projected energy consumption in the city-province of Kinshasa by 2050 is shown in the figure below.

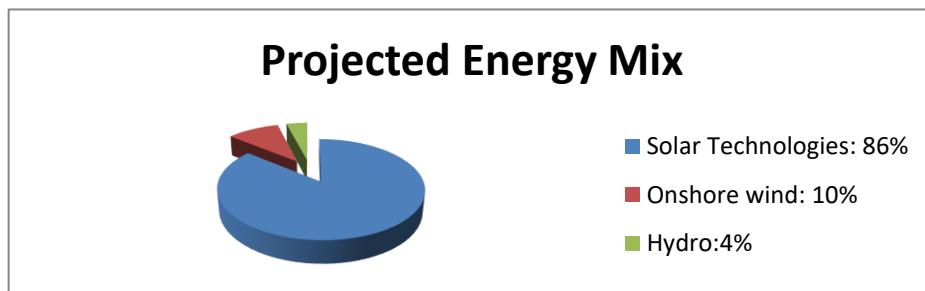


Figure 2 Projected Energy Mix by 2050 (Electricity)

Source: Data from Stanford University (The solutions Project)

Based on projections of these research findings, solar, wind, and hydropower technologies are expected to be more competitive on the power market and could even cost lower than those of fossil fuels upon the full completion of the decentralization. Based on the findings of the same studies, the study has projected the average of all combined solar, wind and hydropower technologies to be 4.5 USD c/KWh against those from fossil fuels 6.9 USD c/KWh [5] [16]. The research findings of data collected have also demonstrated that it is possible for the city-province to move and go towards 100% renewable electricity. The below figure shows the cost of electricity projected between fossil fuel energy sources and solar, wind and hydropower technologies (SWH) by 2050.

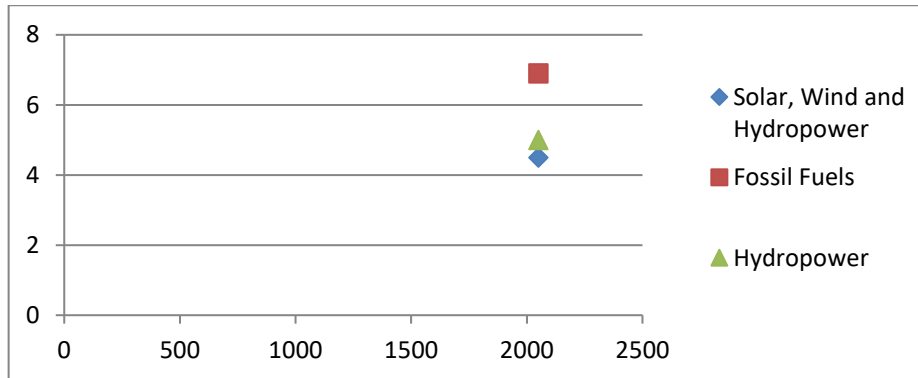


Figure 3 Projected Electricity Costs by 2050

Source: Data from Stanford University (The Solutions Project)

The projected electricity costs in USD/KWh are represented on the y-axis, while years are represented while on the x-axis. For the non-renewable energy sources (coal, oil, gas, and others), external costs could be added and could significantly increase their prices on the power market and even to be more expensive than the three selected renewable energy sources (solar, wind, and hydropower).

4. Electricity Cost Scenarios, Energy Storage and Transport

4.1 Electricity Costs

The trading of electricity either in the whole country or the city is regulated by the National utility company (SNEL), the only institution with the mandate of generation, transmission, distribution, and trading of power. In 2014, the Electricity Regulation Authority was set up with a mission of supervising the protection of consumer interests and facilitating the private sector participation in the energy sector development, in particular, electricity [10]. But unfortunately, the regulatory authority has not established yet consistent regulations to face the unfair competition of the National utility company which still has much power on the latter. Locally, the internal balance requires the electricity price to not be less than the cost price, while the external balance states that the more distant consumers are located in remote areas, the higher is the electricity cost. This principle is applicable to all energy providers operating in the whole country. In 2018, the average electricity price in the entire country was assessed at 0.05 USD/KWh which is currently considered as one of the lowest in the world [17]. Despite this low rate of electricity cost in the capital city, there are over one million people who are still not connected to the grid; often due to their low purchasing power. But the analysis and evaluation of the future electricity costs in the city-province are focused on two different scenarios which could be a turning point in the decentralization of the power sector for the millennium objectives of a smart and green city. The first scenario is focused on three alternative energy sources, in particular solar, wind, and hydropower in which the study findings have projected to cost lower than fossil fuel energy sources and thus, they exclude any external costs that could be added in the generation,

transmission, distribution, and consumption. These external costs could include, for example, damage associated with health concerns and the environment as well as other related to this type. Given these circumstances, their prices are projected to be between 0.04 USD/KWh and 0.05 USD/KWh even lower than the current average electricity stated above. This amount considered lower than the current average electricity price can be explained by the fact that energy audits and energy efficiency measures such as preventive maintenance, monitoring and control, insulation, heating, cooling, and lighting justification, and other related [18] would be much implemented in buildings and industries. Additionally, smart technologies using electric sensors could also be implemented within the city to help consumers to well save electricity, to control and monitor it at any time of use. Furthermore, significant tax and import exonerations shall be applied to companies operating or those intending to operate in the renewable energy sector. The second scenario, on the contrary, is focused on the future costs of fossil fuels for electricity generation and supply in buildings and much more in industries. Given these circumstances, their prices are projected to range between 0.069 and 0.075USD/KWh. And this could be normal because costs associated with pollution, damage caused often to health and the environment, global warming and any other of this type during or after the generation, transmission, distribution, and consumption could be, however, added as externalities [19].

4.2 Transport

This sector would require the city to be redesigned with more infrastructures to build principally based on the goal set which is to supply all Kinshasa municipalities with 100% renewable electricity by 2050 or earlier if possible. The increase of the population in this megacity has, however, created other social issues, in particular, overcrowding and anarchic constructions. To come up with, the city should be redesigned with a new urbanization plan that includes new infrastructures in the transport sector such as roads, highways, and railways. Besides, the city should also expect to see today's fuel vehicles to be replaced by electric vehicles. However, this would require the latter to install electric car charging stations in all corners of the city for the ease of supply of consumers and also achieve fully the vision by 2050 or earlier if possible.

4.3. Energy Storage

The current issue that the energy industry is facing about renewable energy is the integration to the grid which means that some of the renewable energy sources are intermittent (solar and wind). For example, solar and wind energy are intermittent in nature when compared to other renewable sources but possess a huge energy potential which is available everywhere on the Earth planet. Although in some corners of the globe insulation and wind speeds remain lower than the energy potential of the other renewable sources but there still exist possibilities to exploit both. Solar and wind technologies generate electricity one while the sun is shining in the day time and the other while winds are blowing in a given area. In order to keep supplying the grid and avoiding power interruptions during the supply, it is necessary nowadays to use batteries [20] capable to store that energy and use it for the supply when the intermittency problem occurs in one of them. This means one in the night time especially while the sun is

shining and the other while winds are not blowing. These storage technologies would be essential for PV systems, CSP and other related solar technologies and their use by 2050 would allow improving the power quality and providing electricity for both infrastructures and services without any interruption on the network.

5. Energy Policy and Future Challenges

5.1 Policy

A couple of years ago, the National government set a goal to increase access to electricity and bring the electrification rate up to 60% by 2025 in the whole country and over this value in the city-province of Kinshasa by using renewable energies [21] [22]. But unfortunately, this goal has been seen by many of energy experts to not be achieved by 2025 insofar as there still no policy to foster the rapid development of other renewable energy sources, such as solar and wind which have also an enormous energy potential once implemented in the city-province [23] [24] [25]. And the current policy established in 2009 is highly focused on the implementation of large scale hydropower plants. Meanwhile a certain number of studies around the world show that the reliance on hydropower has not been a source of achievement for economic growth in many countries around the world, the government continues to centralize all the local electricity supply on this source of energy which, besides, has dramatically been considered as one of the causes of power outages in the city due to its endless completion and sometimes its current poor infrastructures in a state of collapse and also a break for the socio-economic development of local communities [26] [27] [28]. But until now, only Norway keeps being prosperous with that dependency when compared globally to countries with the high electricity reliance on hydropower as it is the case now for the Democratic Republic of the Congo and its megacity [10] [29] [30] [31] [32]. Based on a series of investigations conducted on the ground, there are no clear plans that have been established to achieve this goal through the roadmap 2025. Also, due to difficulties to access easily to data, very often from public institutions and sometimes from private enterprises, the study suggests further research on the ground about plans established at the local level to achieve the roadmap goal 2025.

5. Constraints, Obstacles, and Opportunities

5.1 Constraints

Constraints can be classified into two categories (technical and economical). The first constraint is linked to any technical problem occurring either in the power plant or other related infrastructures mostly in the generation, transmission, and distribution. These technical constraints are often due to the lack of regular maintenance of turbines and some components of dams as well as in other electric compartments of dams such as power lines, distribution networks, and transformers, most certainly in a state of collapse. Whereas the second constraint is linked to a low rate of financial support from both, the National government and its foreign partners, low purchasing power of the population, and sometimes there exists a high reliance on foreign investments, difficulties on the management of the State-owned company (SNEL) often caused by the high level of corruption starting on the top from governing bodies [33] [34]. Low rates of

investments have been observed in the power sector since the beginning of the twenty-first century due to a certain number of factors among which can be quoted political uncertainties and instabilities including also the devaluation of the local currency on the stock market which recently affected the socio-economic development of many of residents in the city-province.

5.2 Obstacles to the Decentralization

This subsection provides a broad list of problems susceptible to constitute obstacles to the decentralization of the power sector in the city-province of Kinshasa before or by 2050. These problems include high rates of taxes and imports, the devaluation of the local currency, political uncertainties and instabilities, insecurity, lack of skilled workforce in the domain, high rate of corruption from governing bodies and the lack of adequate infrastructures to allow enterprises to have the ease of operating. Furthermore, the National utility company still possesses around 94% of all electricity generation [11] and this monopoly on the power market has been considered nowadays as one of the main causes of energy issues facing the city and the country in the electricity sector. In order to prevent them from occurring before or by 2050, a certain number of elements need to be fulfilled; for example, allow local or foreign investors to have the ease of doing business in the sector by restoring new anti-corruption measures aiming to sanction these practices, exempting companies from high rates of taxes and imports as it is the case nowadays for other products, capacity building in the sector for local professionals through seminars and vocational training, safety investment measures and other related. Another alternative in addition to the above potential solutions would require decentralizing the power sector for more privatization in the city in order to face the unfair competition of the State-owned company, SNEL.

5.3 Opportunities

Nobody can currently deny the benefits linked to the use of renewable energies in a green city. For example, fossil fuels release huge amounts of greenhouse gas emissions, they participate in Global warming, they pollute water and air, and they create political instabilities in some countries. Additionally, they are currently considered to be one of the causes of some diseases, in particular, asthma, chronic obstructive pulmonary, and cancer to name a few. Although they can create jobs to local communities and transform their cities, this is just for a short period of time. But unfortunately, all these problems cannot be associated with the use of alternative energy sources which are clean, renewable and sustainable for a very long period of time [34] [35] [36] [37] [38] [39] [40] [41]. This is the reason why the research study attempts to show their benefits in order to help actors to get committed and pave the road for their full adoption and implementation by 2050 or earlier if possible. In terms of opportunities, based on the research findings of recent projections, it is expected to see over one million jobs to be created in the city-province directly or indirectly by 2050. The study findings revealed that these jobs would probably include the design, installation, maintenance of solar panels and wind turbine components as well as the construction of power plants by including also hydropower. And this is a piece of good news for the city to get more committed for their full adoption, integration, and deployment simply because it would boost the

economy by bringing more investments and revenues. As enough electricity will be generated from solar and wind to cover the future energy demand of the city by 2050, the latter shall use hydropower much more for industrial purposes; for example, supplying industries in close and remote areas. On the contrary, solar and wind shall be used for electricity supply in homes, commercial and public buildings or other related in order to minimize the electricity transmission line costs as though power plants will be close to consumption centers. Additionally, the city will be given the possibilities to export enough electricity generated from hydropower plants in competitive prices to some neighboring countries, in particular, the Republic of the Congo and this will serve to reduce the cost of transmission lines.

6. Recommendations

The present paper has selected a broad list of recommendations to take into account to speed up the decentralization of the power sector that would be resulted by a full adoption of renewable energies principally solar and wind aiming to connect new power plants to remote zones to the grid (wind and solar) and increase the electrification rate up to 100% renewable. These recommendations imply setting clear targets at the local level to achieve access to clean, sustainable and affordable electricity by 2050 or earlier if possible, creating a peaceful environment that supports and provides safety to investments, installing smart sensors in homes, industries, commercial and public buildings to help customers have the ease of monitoring and controlling themselves their daily energy consumption as well as managing the cost to pay so that they can use it efficiently and smartly. These sensors should also be connected to the internet for the ease of control and monitoring everywhere they would be. This type of energy efficiency measures would serve to avoid energy losses during the consumption and the overuse as well.

7. Conclusion

References

- [1] A.S.A.Lateef, Max Fernandez-Alonso, Luc Tack, and Damien Delvaux, "Geological Constraints on Urban Sustainability, Kinshasa City, Democratic Republic of the Congo", *Environmental Geosciences*, V.17, NO.1, (March 2010), PP 17-35. Available (online): https://www.africamuseum.be/publication_docs/2010_Lateef-Kinshasa-PDF.pdf
- [2] Demographia World Urban Areas, Built Up Urban Areas or World Agglomerations, 15th Annual Edition, April 2019. Available (online) on: <http://www.demographia.com/db-worldua.pdf>
- [3] Kinshasa National Capital, Democratic Republic of the Congo, 2019. Available (online) on: <https://www.britannica.com/place/kinshasa> and <https://en.wikipedia.org/wiki/kinshasa>
- [4] DR Congo National Agency for the Promotion of Investments, "Energy", 2018. Available (online) on <https://www.investindrc.cd/en/sectors/energy>
- [5] Mark Z. Jacobson, Mark A. Delucci, Guillaume Bazouin, Zack A. F. Bauer, Christa C. Heavy, Emma Fisher, Sean B. Morris, Diniana J.Y. Piekutowski, Taylor A. Vencill and Tim W. Yeskoo, "100% Clean and renewable wind, water, and sunlight (WWS) all-sector energy roadmaps for the 50 United States",

- Energy Environmental Science, “Journal of Royal Society of Chemistry”, 2015. Available (online) on: <https://web.stanford.edu/group/efmh/jacobson/Articles/I/USStatesWWS.pdf>
- [6] Oxford County 100% Renewable energy plan, June 2018. Available (online) on: http://www.oxfordcounty.ca/Portals/15/Documents/Renewable%20Energy/OC_100RE_20180627.pdf
- [7] K. Kusakana, “A review of energy in the Democratic Republic of the Congo”, Conference paper, June 2016
- [8] Nicholas M. Odhiambo, “Energy consumption, prices and economic growth in three SSA countries: A comparative study”, Journal, January 2010, Available from https://ac.els-cdn.com/S0301421509009963/1-s2.0-S0301421509009963-main.pdf?_tid=af84253e-9b8d-4740-8f7c-3c9f9b5d9f71&acdnat=1544959271_a7ac055dc0d386c3d0b2ba4334241bdb
- [9] Société Nationale d’Electricité (SNEL) 2013 “Overvue of the electricity sector in the Democratic Republic of Congo” Available (online) on <http://www.usea.org/sites/default/files/event-/Democratic%20Republic%20of%20Congo%20Power%20Sector.pdf>
- [10] Lighting Africa Policy Note: Democratic Republic of Congo, March 2011, Available (online): https://sun-connect-news.org/fileadmin/D/ATEIEN/Dateien/New/27_FINAL-August-2012-x_LM.pdf
- [11] Green Climate Fund, Democratic Republic of Congo (DRC) Green Mini-Grid Program, 2018. Available (online) on: https://www.greenclimate.fund/documents/20182/574760/Funding_Proposal_-_FP096_-_AfDB_-_Democratic_Republic_of_Congo.pdf/f8a8f0b8-cce7-10ae-9838-cf704ac4e6e5
- [12] USAID and ICF-DRC Report (2017), “Conceptual plan for Enhancing Transmission Infrastructure to Expand Electricity Access in the Democratic Republic of Congo (DRC). Available (online) on: https://pdf.usaid.gov/pdf_docs/PA00SX8K.pdf
- [13] M.S. Kasemuana, Helio International (2010), Energy Systems: Vulnerability-Adaptation-Resilience (VAR): Democratic Republic of Congo. Available (online) on: www.helio-international.org/wp-content/uploads/2013/12/VARRDC.En_.pdf
- [14] J.M. Lukamba Muhiya and E. Uken, “Electricity Supply Industry in the Democratic Republic of the Congo”, Journal, available (online) on: http://www.erc.uct.ac.za/sites/default/files/image_tool/images/119/jesa/17-3jesa-lukamba.pdf
- [15] FAO, Democratic Republic of the Congo, Bioenergy and Food Security Approach, 2013. Available (online) on: www.fao.org/3/a-aq170e.pdf
- [16] 100% Democratic Republic of Congo, “2050 Projected Energy Mix”, Data from Stanford University, available (online) on : <https://thesolutionsproject.org/why-clean-energy/#/map/countries/location/COD>
- [17] Democratic Republic of the Congo, Electricity Prices, June 2018. Available on: <https://www.globalpetrolprices.com/Democratic-Republic-of-the-Congo/electricity>
- [18] Efstratios N. Pistikopoulos, Michael C. Georgiadis, and Vivek Dua.: Energy Systems Engineering. 1st Edition. WILEY-VCH Verlag GmbH & Co, Weinheim (2008)
- [19] Pramod Jain.: Wind Energy Engineering. 1st Edition. McGraw-Hill, New York (2011)
- [20] FRANCIS M. VANEK, LOUIS D. ALBRIGHT, and LARGUS T. ANGENENT.: Energy Systems Engineering: Evaluation and Implementation, 3rd Edition. McGraw-Hill, New York (2006)
- [21] REN21, Renewables 2018 Global Status Report, P213 Available (online) on: http://www.ren21.net/wp-content/uploads/2018/06/17-8652_GSR2018_FullReport_web_final_.pdf
- [22] Kate Davidson, Congo’s Energy Divide, Hydropower for Mines and Export Not for the Poor, Greenspace, International Rivers, Berkeley, California (2013). Available (online) on: https://www.internationalrivers.org/sites/default/files/attached-files/inga_factsheet_eng_dec13.pdf
- [23] Democratic Republic of the Congo, Current State of Play, https://learn.tearfund.org/~media/files/tilz/climate_and_energy/2018-odi-tearfund-pioneering-power-country-report-drc-en.pdf?la=en
- [24] Democratic Republic of the Congo, Cost-effectiveness of decentralised renewables available (online) on https://learn.tearfund.org/~media/files/tilz/climate_and_energy/2018-odi-tearfund-pioneering-power-country-report-drc-en.pdf?la=en
- [25] KPMG International Cooperative, Democratic Republic of the Congo, Report (2014). Available (online) on: <https://assets.kpmg/content/dam/kpmg/pdf/2014/09/democratic-republic-congo-mining-guide.pdf>
- [26] Reegle, Democratic Republic of the Congo, Energy Competition. Available (online) on: <http://www.reegle.info/policy-and-regulatory-overviews/CD>

- [27] Augustin Nguh, Corruption and Infrastructure Megaprojects in the DR Congo, A Failure for Recipe, Paper, International Rivers (2013). Available (online) on: https://www.internationalrivers.org/sites/default/files/attached-files/corruption_in_the_drc_.pdf
- [28] Jeroem Warner, Sarunas Jomantas, Eliot Jones, Md. Sazzad Ansari and Lotje de Vries, the Fantasy of the Grand Inga Hydroelectric Project on the Congo River, Water, Article (2019). Available (online) on: <https://res.mdpi.com>
- [29] IEA-ETSAP& IRENA, Hydropower Technology Brief, February 2015. Available (online) on: https://www.irena.org/-/media/Files/IRENA/Agency/Publication/2015/IRENA-ETSAP_Tech_Brief_E06_Hydropower.pdf
- [30] IRENA & Global Commission on the Geopolitics of the Energy Transformation, A New World, The Geopolitics of Energy Transformation, Report (2019). Available (online) on: [geopoliticsofenergy.org/assets/geopolitics/Reports/wp-content/uploads/2019/01/Global_commission_renewable_energy_2019.pdf](https://www.geopoliticsofenergy.org/assets/geopolitics/Reports/wp-content/uploads/2019/01/Global_commission_renewable_energy_2019.pdf)
- [31] The Hydropower Sector's Contribution to a Sustainable and Prosperous Europe, Main Report (2015). Available (online) on: <https://www.verbund.com>
- [32] Ministry of Petroleum and Energy, The History of Norwegian Hydropower in Five Minutes. Available (online) on: <https://www.regjeringen.no/en/topics/energy/renewable-energy/the-history-of-norwegian-hydropower-in-5-minutes/id2346106/>
- [33] USAID, Energy Sector Overview, Democratic Republic of Congo, Review (2013). Available (online) on: https://www.usaid.gov/sites/default/files/documents/1860/DRC-_November_2018_Country_Fact_Sheet_0.pdf
- [34] Leon Freris and David Infield: Renewable Energy in Power Systems, 1st Edition. A John & Sons, P205-206, West Sussex (2008).
- [35] David Pimentel: Biofuels, Solar and Wind as Renewable Energy Systems, Benefits and Risks, Pimentel Ed. Springer, NY, USA (2008)
- [36] Intergovernmental Panel on Climate Change, Global Warming of 1.5°C, Report (2018). Available (online) on: https://report.ipcc.ch/sr15/pdf/sr15_spm_final.pdf
- [37] Banking on Climate Change, Fossil Fuel Report Card 2018. Available (online) on: https://www.ran.org/wp-content/uploads/rainforestactionnetwork/pages/19540/attachments/original/1525099181/Banking_on_Climate_Change_2018_vWEB.pdf?1525099181
- [38] United Nations Environment Programme, Emissions Gap Report 2018. Available (online) on: https://wedocs.unep.org/bitstream/handle/20.500.11822/26879/EGR2018_ESEN.pdf?sequence=10
- [39] John Talbert and Daphne Wysham, Fossil Fuel Risk Bonds, Center for Sustainable Economy, 2016. Available (online) on: <https://sustainable-economy.org/wp-content/uploads/2016/06/Fossil-Fuel-Risk-Bonds-May-25.pdf>
- [40] Healthy Babies, Dirty and Dangerous: Damages to Health from Coal-Fired Power Plants, <https://hbbf.org/sites/default/files/documents/2018-10/Dirty-and-Dangerous-science-summary.pdf>
- [41] Health and Environment Alliance, Hidden Price Tags, How Ending Fossil Fuel Subsidies Would Benefit our Health, 2018. Available (online) on: https://www.env-health.org/wp-content/uploads/2018/06/hidden_price_tags_report.pdf

A Comprehensive Sustainability Investigation of Solar Hydrogen Production Options

Canan Acar ^[0000-0002-5808-7888]

¹ Faculty of Engineering and Natural Sciences, Bahcesehir University
Çırağan Caddesi No: 4 – 6 34353 Beşiktaş, İstanbul, Turkey
Canan.Acar@eng.bau.edu.tr

Abstract. In this study, a comprehensive life cycle assessment of solar hydrogen production options is conducted. The selected clean hydrogen production options are steam methane reforming, conventional electrolysis, photoelectrochemical cells, PV electrolysis, and photocatalysis. A complete source to service approach is taken when evaluating the environmental and technical performance of the selected hydrogen production options. Greenhouse gas (GHG) emissions, resource use, fossil fuel use, water use, energy and exergy efficiencies, and cost of hydrogen are the selected sustainability performance criteria. In the first part of this study, the selected hydrogen production options are compared based on these performance criteria. In the next part, the performance evaluation results of each option are normalized and ranked in 0-10 range where 0 gives the least sustainable manner and 10 is the hypothetical ideal case where there is no negative impact on the environment, zero resource and water use, and 100% energy and exergy efficiencies, and zero cost. The results show that in terms of GHG emissions, resource use, fossil fuel use, and water use, PEC are the most advantageous. Steam methane reforming has the highest energy and exergy efficiencies and the lowest cost compared to the other selected options. When all of the selected performance criteria are taken into account together, the average normalized rankings show that PEC have the highest rankings (5.24/10) and steam methane reforming has the lowest rankings (3.24/10).

Keywords: Hydrogen; energy; exergy; solar; sustainability.

1 Introduction

Hydrogen has a key role during the transition to clean energy systems for a sustainable future. When produced from clean and renewable resources like solar energy and water, hydrogen can provide safe, reliable, affordable, efficient, clean, and efficient energy to a wide variety of end users. This is especially important in terms of energy security in supply and demand. Therefore, the recent literature shows that there have been numerous studies towards more efficient, clean, and cheap solar hydrogen production.

The first step towards truly sustainable energy systems via hydrogen is the production. For that reason, solar hydrogen has to be produced in affordable, reliable, environmentally benign, and efficient manners with zero or minimal resource depletion [1].

In the literature, there are different studies focusing on different aspects of solar hydrogen production. For instance, Wang et al. [2] have focused on photocatalysis and photoelectrochemical cells (PEC). The authors have reviewed the recent progress of black TiO₂ for photocatalytic hydrogen evolution and PEC water splitting, along with detailed introduction to its unique structural features, optical property, charge carrier transfer property and related theoretical calculations. Lee et al. [3] have provided a review of advanced hydrogen passivation applied on p-type, n-type and upgraded metallurgical grade crystalline silicon solar cells, respectively. Acar et al. [4] have examined photocatalytic hydrogen production as a clean energy solution to address challenges of climate change and environmental sustainability. The authors have taken social, environmental and economic aspects of hydrogen production into account while assessing photocatalytic production methods and different types of photocatalysts. De Crisci et al. [5] have highlighted some of the methods of eliminating hydrogen sulfide pollution via partial oxidation, reformation and decomposition techniques and approaches. The authors have proposed an approach to convert hydrogen sulfide to sulfur, water and, more importantly, hydrogen. With their approach, hydrogen is produced with zero GHG emissions and the proposed method also helps to lower and eventually eliminate hydrogen sulfide.

In the literature, there is a need for studies comprehensively investigating solar hydrogen production systems from environmental, technical, and economic perspectives quantitatively based on their life cycle performances. For this reason, in this study, the impact of solar hydrogen production systems on the environment is quantitatively investigated by comparing their life cycle GHG emissions, fossil fuel use, water use, and resource use together with their energy and exergy efficiencies and cost. The life cycle term used in this study follows the source-system-service approach and includes all energy and material source harvesting and processing into account as well. Steam gas reforming (SMR), conventional electrolysis (CE), PEC, PV electrolysis (PE), and photocatalysis (PC) are the selected hydrogen production options for comparison purposes. For a better and clearer insight on the true sustainability of the selected options, the environmental, economic, and technical performance results of each option are normalized and ranked to highlight their strengths and weaknesses and provide future directions.

2 Sustainability Investigation of Hydrogen Production Options

The sustainability investigation of the selected clean hydrogen production options include GHG emissions, resource use, fossil fuel use, water use, energy and exergy efficiencies, and cost. All of the sustainability performance criteria values are calculated based on the life cycle performance of the selected hydrogen production options, from the source to the end user, by using the GaBi software. It should be noted that life cycle results sum up all of the energy and emissions associated with the process inputs, including upstream. Energy and emission adjustments associated with by-products are not included. In GHG emissions category, the following are considered:

- CO₂ emissions
- SO_x emissions

- NO_x emissions
- CO emissions
- CH₄ emissions
- Particulate matter (PM₁₀ and PM_{2.5}) emissions
- Volatile organic compound (VOC) emissions
- Primary organic carbon emissions
- Black carbon emissions

All emissions are given in units as kg emissions per kg hydrogen produced. Resource use indicates the amount of resource energy used (MJ) per kg hydrogen produced. This resource energy can be natural gas, grid electricity (conventional electrolysis), or solar energy (PEC, photocatalysis, or PV electrolysis). Fossil fuel use indicates the amount of fossil energy used (MJ) per kg hydrogen produced. And water use is the total amount of water usage per kg hydrogen production. It should be noted that the life cycle includes the preparation of resources, distribution, transportation, processing, waste handling, and the hydrogen production process itself. That is why the selected options have fossil fuel use despite the fact that the production processes alone do not involve any fossil fuel use. Cost indicates the life cycle cost of the selected options. The energy efficiency of the hydrogen production options are calculated based on the following equation:

$$\eta = \frac{HHV_{H_2}}{\text{Resource use} \left(\frac{MJ}{kg H_2} \right) + \text{Fossil fuel use} \left(\frac{MJ}{kg H_2} \right)} \quad (1)$$

Here, η is the energy efficiency and HHV_{H_2} is the higher heating value (also known gross calorific value or gross energy) of a hydrogen which is defined as the amount of heat released by one kg hydrogen (initially at 25°C) once it is combusted and the products have returned to a temperature of 25°C. HHV_{H_2} takes into account the latent heat of vaporization of water in the combustion products. And the exergy efficiency of the selected hydrogen production options are calculated as

$$\psi = \frac{ex_{H_2}^{ch}}{\text{Exergy content of the resource} \left(\frac{MJ}{kg H_2} \right) + \text{Exergy content of the fossil fuel} \left(\frac{MJ}{kg H_2} \right)} \quad (2)$$

In this equation, ψ is the exergy efficiency and $ex_{H_2}^{ch}$ is the chemical exergy content of one kg hydrogen. For comparison purposes, all chemical exergies are calculated at standard state, which is 25°C and 1 atm. And the hydrogen cost is gathered from the recent literature.

In the next step, for a more comprehensive investigation, the environmental, economic, and technical performance results are normalized and ranked within the range of 0 – 10 where 0 indicates the least desired performance and 10 is given to a hypothetical ideal case. 0 is given to the highest GHG emissions, resource use, fossil fuel use, water use, and cost and 0% energy and exergy efficiencies. On the other hand, 10 is assigned to a non-existing ideal situation where the hydrogen production option has zero emissions, cost, resource use, fossil fuel use, and water use and 100% energy and exergy efficiencies. Given these conditions, the normalized rankings of the GHG emissions, resource use, fossil fuel use, water use, and cost are calculated based on:

$$\text{Rank}_i = \frac{\text{max}-i}{\text{max}} \times 10 \quad (3)$$

Here, Rank_i is the rank of the selected hydrogen production option (i.e., SMR, CE, PEC, PVE, or PC). And max is the maximum GHG emissions, resource use, fossil fuel

use, water use, or cost among the selected options while “ P ” is the GHG emissions, resource use, fossil fuel use, water use, or cost of the selected hydrogen production option. And the energy and exergy efficiency rankings of the selected hydrogen production options are calculated from the following equation:

$$Rank_i = efficiency_i \times 10 \quad (4)$$

Here, since the energy and exergy efficiencies of each option is within the range of 0-1, the efficiency data are normalized by simply multiplying them with 10. The comprehensive performance investigation results are presented and discussed in detail in the next section with some possible future directions.

3 Results and Discussion

In this section, comprehensive sustainability analysis results of the selected hydrogen production options are given and the GHG emissions, resource, fossil fuel, and water use, energy and exergy efficiencies, and the hydrogen production costs of the selected options are discussed in detail.

In Figure 1, GHG emission of the selected hydrogen production options are compared and the results show that steam methane reforming has the highest emissions (about 9 kg GHG/kg H₂ produced), followed by conventional electrolysis, which is around 7 kg GHG/kg H₂ produced. The lowest GHG emissions come from PEC (less than 0.5 kg GHG/kg H₂ produced). PV electrolysis has about 4 kg GHG emissions and photocatalysis has 0.6 kg GHG emissions per kg hydrogen production.

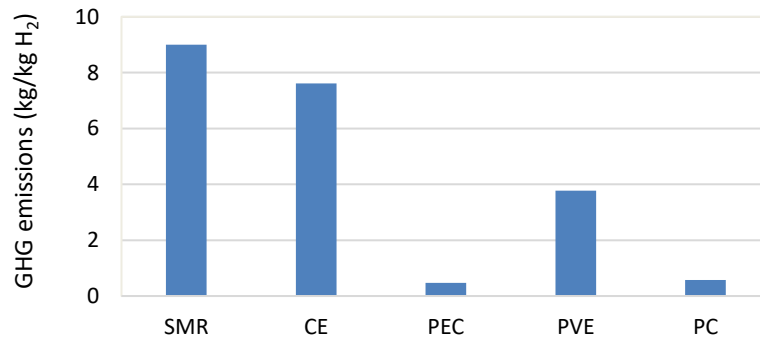


Fig. 1. GHG emissions of the selected hydrogen production options.

Figure 2 shows the resource use comparison of the selected hydrogen production options. Here, it can be seen that steam methane reforming has the highest resource use (about 251 MJ/kg H₂), followed by conventional electrolysis (around 128 MJ/kg H₂). PEC has the lowest resource use, which is around 100 MJ/kg H₂.

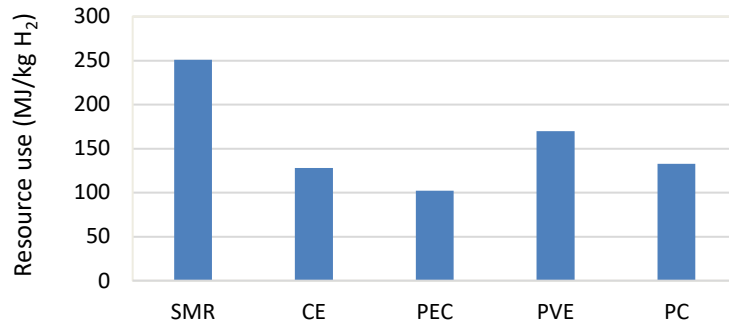


Fig. 2. Resource use comparison of the selected hydrogen production options.

The life cycle fossil fuel use performance of the selected hydrogen production options are shown in Figure 3. The highest fossil fuel use happens to be in steam methane reforming (251 MJ/kg H₂). The second highest fossil fuel use belongs to conventional electrolysis (110 MJ/kg H₂) which is due to the high fossil fuel contribution in the grid electricity mix. PEC has the lowest fossil fuel use of about 20 MJ/kg H₂. PV electrolysis and photocatalysis have similar fossil fuel use of around 30 MJ/kg H₂.

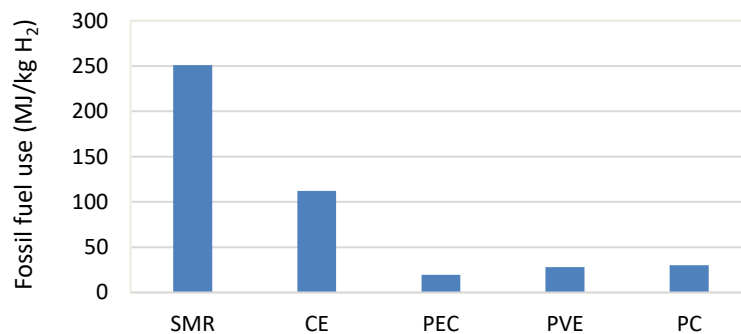


Fig. 3. Fossil fuel use comparison of the selected hydrogen production options.

Figure 4 shows that steam methane reforming has the highest water use which is around 140 L/kg H₂, followed by conventional electrolysis which is almost 30 L/kg H₂. PEC has the lowest water consumption of around 15 L/kg H₂, followed by PV electrolysis and photocatalysis (about 20 L/kg H₂).

Hydrogen production costs of the selected hydrogen production options are calculated by taking the life cycle approach and the results are presented in Figure 5. Here, it can be seen that PEC, due to its early R&D stage and smaller scales, has the highest cost, which is around 9 USD/kg H₂. Following PEC, PV electrolysis and photocatalysis have the second highest production cost of about 6 USD/kg H₂. The lowest production cost belongs to steam methane reforming (less than 1 USD/kg H₂), followed by conventional electrolysis (almost 3 USD/kg H₂).

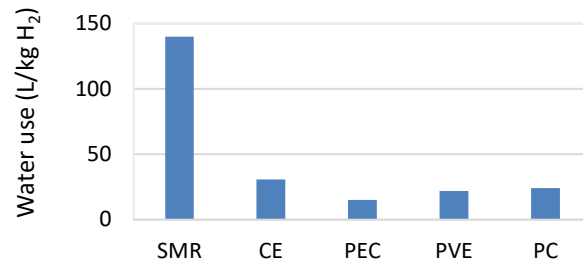


Fig. 4. Water use comparison of the selected hydrogen production options.

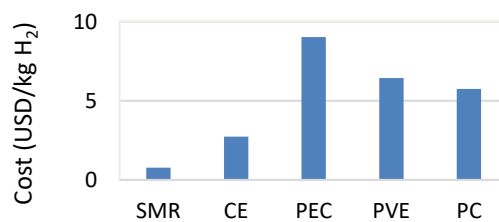


Fig. 5. Hydrogen production costs of the selected hydrogen production options.

The last category is energy and exergy efficiencies of the selected hydrogen production options and the results are presented in Figure 6. Steam methane reforming has about 84% energy efficiency and 52% exergy efficiency. The energy and exergy efficiencies of conventional electrolysis are 53% and 25%, respectively. Photocatalysis has the lowest efficiencies among the selected options with 3% energy efficiency and 2% exergy efficiency. With 18% energy and 12% exergy efficiency, PEC has a higher performance than PV electrolysis, which has 12% energy and 7% exergy efficiency.

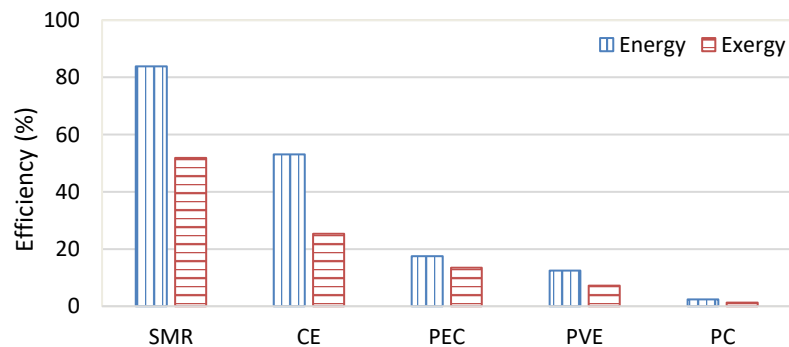


Fig. 6. Energy and exergy efficiencies of the selected hydrogen production options.

After performing the environmental, energetic, exergetic, and economic performance of the selected hydrogen production methods, the results are normalized and ranked based on the procedure explained in Section 3. The results presented visually in Figure 7. The overall comparison shows that PEC has advantages in terms of its low emissions and use of energy and material resources. Steam methane reforming has the highest performance in terms of energy and exergy efficiencies and hydrogen

production cost. On the other hand, steam methane reforming has the lowest performance in terms of emissions, resource use, fossil fuel use, and water use. PEC has the lowest performance in cost criteria while photocatalysis has the lowest performance in energy and exergy efficiency categories. When the averages of the normalized performance rankings are taken, it is seen that PEC has the highest normalized average ranking of 5.24 out of 10 which is immediately followed by photocatalysis with 5.02. The third highest normalized average ranking belongs to conventional electrolysis that is 4.94. Among the selected options, steam methane reforming has the lowest average normalized ranking (3.24) and PV electrolysis has 4.45.

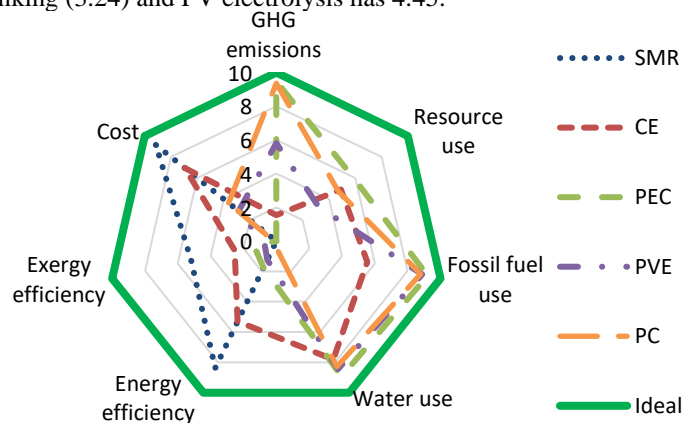


Fig. 7. Normalized performance rankings of the selected hydrogen production options.

In this study, for the first time in the literature, a comprehensive quantitative comparison approach is taken to evaluate the environmental, economic, thermodynamic, and technical performances of the solar, conventional, and fossil fuel based hydrogen production options. This study takes GHG emissions, resource use, fossil fuel use, water use, energy and exergy efficiencies, and cost into account to provide a better insight about the cleaner hydrogen production methods. The results not only show a clear picture of the current status of these options, but also provides potential future directions to guide researchers, policy makers, and industries in the field of hydrogen energy systems.

4 Conclusions

In this study, the GHG emissions, resource use, fossil fuel use, water use, energy and exergy efficiencies, and cost of hydrogen via five different production methods are investigated in detail from a life cycle perspective. The results are then comparatively evaluated by normalizing and ranking the environmental, energetic and exergetic, and economic performances of the selected hydrogen production options. Steam methane reforming, conventional electrolysis, photoelectrochemical cells, PV electrolysis, and photocatalysis are the selected hydrogen production options. This study is one of the first attempts to thoroughly investigate the life cycle environmental and economic impacts of sustainable hydrogen production. And the results show that:

- In terms of GHG emissions, steam methane reforming has the highest emissions (9 kg GHG/kg H₂) and PEC has the lowest emissions (0.47 kg GHG/kg H₂).
- Steam methane reforming has the highest resource consumption (251 MJ natural gas energy/kg H₂) and PEC has the lowest resource consumption (103 MJ solar energy/kg H₂).
- Fossil fuel consumption data shows that steam methane reforming has the highest fossil fuel consumption (251 MJ fossil fuel energy/kg H₂) and PEC has the lowest resource consumption (20 MJ fossil fuel energy/kg H₂).
- Steam methane reforming has the highest water consumption (140 L water/kg H₂) and PEC has the lowest water consumption (15 L water/kg H₂).
- Steam methane reforming has the highest energy and exergy efficiencies, which are 83% and 52%, respectively and photocatalysis has the lowest energy and exergy efficiencies, which are 2% and 1%.
- Cost comparison shows that steam methane reforming has the lowest cost (0.76 USD/kg H₂) while PEC has the highest cost (9.02 USD/kg H₂).
- When all selected performance criteria are taken into account, the overall normalized performance ranking comparison shows that PEC has the highest average normalized ranking (5.24/10) and steam methane reforming has the lowest average normalized ranking (3.24/10).

References

1. Acar, C., Dincer, I. (2019). Review and evaluation of hydrogen production options for better environment. *Journal of Cleaner Production*, 218, 835-849.
2. Wang, B., Shen, S., Mao, S. S. (2017). Black TiO₂ for solar hydrogen conversion. *Journal of Materiomics*, 3(2), 96-111.
3. Lee, S. H., Bhopal, M. F., Lee, D. W., Lee, S. H. (2018). Review of advanced hydrogen passivation for high efficient crystalline silicon solar cells. *Materials Science in Semiconductor Processing*, 79, 66-73.
4. Acar, C., Dincer, I., Naterer, G. F. (2016). Review of photocatalytic water-splitting methods for sustainable hydrogen production. *International Journal of Energy Research*, 40(11), 1449-1473.
5. De Crisci, A. G., Moniri, A., Xu, Y. (2018). Hydrogen from hydrogen sulfide: towards a more sustainable hydrogen economy. *International Journal of Hydrogen Energy*, 44(3), 1299-1327.